KU LEUVEN

FACULTEIT INGENIEURSWETENSCHAPPEN

Design, model, benchmark and optimisation of a continuous photochemical reactor for europium recovery from rare earth mixtures

Glen Meir

Thesis submitted for the degree of
Master of Science in
Chemical Engineering, option
Chemical and biochemical process
engineering

Thesis supervisor:
Prof. dr. ir. T. Van Gerven

Assessors:
Prof. dr. ir. C. Clasen
ir. S. Formenti

Mentor:
Dr. ir. M. E. Leblebici

Academic year 2016 – 2017

Preface

I would like to take this opportunity to express my appreciation towards all of the people who supported me while I was working on this master thesis.

First of all, I would like to thank my promotor; Prof. Dr. Ir. Tom Van Gerven for providing me this fascinating research topic and guiding me through the project with his knowledge and enthusiasm. The monthly meetings encouraged me to keep researching and inspired me for new leads in the project.

My sincerest gratitude goes out to my mentor; Dr. E. M. Leblecici, who encouraged me to keep trying, even though experimental results where disappointing and inspired me to think about improvements and explanations for experimental results. He helped me construct the experimental set-ups and showed how the analysis of experiments was conducted. Without his experience, knowledge and support, I would not have been able to write this thesis.

A special thank you is directed to Bart Van den Bogaert who helped me to understand the reaction mechanism and who was always available to answer my questions. Furthermore, I would like to thank all the people who assisted me in the lab, in particular Tom Vander Hoogerstraete for giving me advice about TXRF.

In addition, I am grateful to my friends at CIT and my residence for their friendship to make my time in Leuven an unforgettable experience.

Last but not least, I would like to thank my family for their support and being able to always rely on them. A special thanks goes to my parents and my brother Kristof, for constantly supporting me and being there whenever I needed them. Without them, I wouldn't been able to get to the point where I am now.

Glen Meir

Contents

Abstract

The Rare Earth Elements (REEs), including europium and yttrium, are classified as critical materials with a large supply risk. Therefore, it becomes important to recycle end-of-life products containing these elements to close the loop. Photochemical recycling in organic and aqueous media is studied before in batch reactors, but was not yet fully optimized to be used in a continuous manner that is more aimed towards industrial applications.

An assessment of separation of Eu and Y was done in methanol using dibuthylphosphate. The aim was to use a two-stage process for the separation whereby the first step includes the photoreduction of Eu(III) and the second step deals with the precipitation of Y that could be separated in space using two separate reactors. This assessment did not yield favourable results for this principle and alternatives in the separation such as the use of extractants, selective crystallisation or selective precipitation were not suitable for Eu/Y separation.

The two-stage procedure as explained before could not be used as photochemical reduction and precipitation in aqueous media are inherently connected in the principle, which means that clogging in the reactor should be avoided.

A model for photochemical reactors was derived, making it possible to determine the outflow of the reactor based upon the feed concentration as well as determining the reaction rate at each point in the reactor and optimizing the reactor for best light distribution and utilisation. The model is used to estimate the conversion in the continuous flow reactor. The reactor was build using a low-pressure mercury lamp (LPML) which was used to asses the separation of Eu and Y. Separation was achieved faster up to a factor 40 for space-time and space-time yield for removal up to 50% of the available Eu in solutions containing no Y. The reactor was constructed as such that the light was used more efficiently as the photochemical space-time yield (PSTY) is 20 times better at 50% removal of Eu. The model as derived before matched the results seen in the continuous flow reactor well up to 50% recovery of Eu, after this point, deviations started to occur as the model did not account for solid particles, gas bubbles and dark spots in the reactor. Only 75% conversion was achieved in the current reactor with a possibility to achieve a higher conversion at higher retention times, but with large deviations compared to the model.

Reducing the amount of dark spots in the reactor by pulsing the feed did not yield an increase in conversion, but by seeding the reactor an increase from 33% to 42% conversion was seen at the same residence time.

Separation of Eu/Y solutions was assessed as well. Artificial YOX solutions

(having the same composition as YOX, but with lab-grade chemicals) were introduced into the reactor, but separation was poor as only 25% conversion was observed with a decrease at higher residence times due to clogging of the reactor. Reaction rate was higher compared to batch results, but this was not truly comparable as no near full conversion could be achieved. As YOX was introduced in the reactor, no conversion of Eu was measured, batch results did already confirm difficult separation as an increased induction time was seen. It is likely that the induction time was longer than the residence time of the YOX in the reactor. YOX separation was more difficult than recovery of Eu from solutions without Y. Y does not react or interfere with the reactions, but altered the reaction rate of the unwanted oxidation of $EuSO_4$ and the solubility of $EuSO_4$. Thus, an increase in induction time and a reduced reaction rate of the photochemical reduction is expected and seen in the results.

List of Figures and Tables

List of Figures

List of Tables

List of Abbreviations and Symbols

Abbreviations

A/V	Area over volume
CFL	Compact fluorescent lamp
CRT	Cathode Ray Tube
CT-band	Charge transfer band
DBP	Dibutylphosphate (basic form)
EDTA	Ethylenediaminetetraacetic acid
FL	Fluorescent lamp
FWHM	Full width at half maximum (for a filter)
HCl	Hydrochloric acid
HDBP	Dibutylphosphate (acid form)
HDEHP	Di-(2-ethylhexyl)phosphoric acid, a common extractant for REEs
HREE	Heavy Rare Earth Element
IPA	Isopropanol
kW	kilowatt
LED	Light emitting diode
LP	Scaled lamp power
LPML	Low-pressure mercury lamp
LREE	Light Rare Earth Element
LVREA	Local Volumetric Rate of Energy Absorption
MeOH	Methanol
MPML	Medium-pressure mercury lamp
MREE	Medium Rare Earth Element
NaDBP	Sodium dibutylphosphate
NTA	Nitrilotriacetic acid
PFA	Perfluoroalkoxy alkanes

ppm	Parts per million
PSTY	Photocatalytic space-time yield
PTFE	Polytetrafluoroethylene
REE	Rare Earth Element
REO	Rare Earth Oxide
RT	Residence time
SEM	Scanning Electron Microscopy
STY	Space-time yield
TXRF	Total Reflection X-ray Fluorescence
UV	Ultraviolet
UV/Vis	Ultraviolet-visible
v/v%	Volume over volume percent
wt.%	Weight percent
XRF	X-ray Fluorescence
YOX	Europium-doped yttria (Y_2O_3:Eu^{3+})

Symbols

# coils	Number of reactor coils	
A	Absorbance	
a_0	Ionic radius	m
α	Separation factor	
c	Concentration of absorbent species in solution	$mol.L^{-1}$
c_{in}	Feed concentration of Eu	$mol.m^{-3}$
c_{light}	Speed of light	$m.s^{-1}$
D	Distribution ratio	
d	Diameter	m
D_{cooler}	Outer diameter of cooler	m
d_{in}	Inner diameter of reactor	m
d_{out}	Outer diameter of reactor	m
E_0	Standard redox potential	V
ε	Specific absorptivity (different for each wavelength)	m^2/mol
$\varepsilon_{Eu,220-240}$	Specific absorbance of Eu-solution (220-240 nm)	$m^2.mol^{-1}$
$\varepsilon_{Eu,240-270}$	Specific absorbance of Eu-solution (240-270 nm)	$m^2.mol^{-1}$
$\epsilon_{R,220-240}$	Specific absorbance of reactor solution (220-240 nm)	m^{-1}
$\epsilon_{R,240-270}$	Specific absorbance of reactor solution (240-270 nm)	m^{-1}
F_L	Limiting settling velocity factor	
g	Gravitational accelleration	$m.s^{-2}$
γ	Activity coefficient	
h	Planck constant	$J.s$

I	Intensity of the light after absorption by a species	$W.m^{-2}$
I_{abs}	Absorbed intensity	$W.m^{-2}$
$I_{in,220-240}$	Irradiation at reactor wall (220-240 nm)	W/m^2
$I_{in,240-270}$	Irradiation at reactor wall (240-270 nm)	W/m^2
I_{in}	Incoming intensity produced by the UV-lamp	$W.m^{-2}$
I_0	Incoming light intensity	$W.m^{-2}$
I_s	Ionic strenght	$mol.L^{-1}$
L	Length of reactor	m
l_{wall}	Path-length of the light (through the reactor wall)	m
λ	Wavelength	m
M_w	Molecular weight	$g.mol^{-1}$
μ_{fluid}	Viscosity of the fluid	$Pa.s$
μ_{PFA}	Attenuation of of PFA tubings	m^{-1}
n	Amount of mol of a substance	mol
N_A	Number of Avogadro	mol^{-1}
p	Pressure	Pa
ϕ	Photon flux	$mol.L^{-1}.s^{-1}$
π	The number pi	
Q	Flowrate	$m^3.s^{-1}$
$Q.E.$	Quantum efficiency (ratio of efficiently used photons to absorbed photons)	
R	Gas constant	$J.mol^{-1}.K^{-1}$
$R_{cooling\ jacket}$	Radius of the cooler	m
Rc	Reaction rate	$mol.m^{-3}.s^{-1}$
Re	Reynolds number	
Re_s	Particle Reynolds number	
rho	Density	$kg.m^{-3}$
S	Projected surface area of reactor	m^2
S_g	Specific gravity of dry solids	
σ	Standard deviation	
T	Transmittance of a material	
t	Time	s
τ	Residence time in the reactor	s
τ_{ind}	Induction time in the reactor	s
Θ	Temperature	℃
V	Volume of the reactor	m^3
v	Velocity	$m.s^{-1}$
v_C	Critical velocity for particles settling in tubes	$m.s^{-1}$
x	Distance	m
z	Relative charge of ion	

Chapter 1

Introduction

The rare earth elements (REEs) are a group of elements in the periodic table containing the lantanides, yttrium (Y) and scandium (Sc). Contrary to their name, these elements are not that rare and quite abundant in the earth's crust. [1] These elements are of high interest by industry since they are used in lots of applications such as light sources and magnets. [2, 3] The demand in REEs has shifted from readily available REEs such as lanthanum (La) and cerium (Ce) to less abundant elements such as europium (Eu) and gadolinium (Gd). [4, 3] Therefore the recovery of these highly demanded elements from end-of-life consumer products is becoming a real opportunity, especially as the REEs are classified as critical elements. [5] An interesting waste streams that is viable for recovery are lamp phosphors.

Lamp phosphors are found in the coating of fluorescent lamp as they have the purpose of converting UV-light, created by the arc, into visible light. Several types of lamp phosphors capable of producing different colours in lamps are present in lamps. A red lamp phosphor called YOX (Y_2O_3:Eu^{3+}) is available in the coating of the fluorescent lamps. This lamp phosphor is fairly common, has a high value due to its presence of yttrium and europium and for this reasons has a potential for recycling. [6]

This work considers the recovery of Eu from these YOX waste streams via a continuous process to meet the rising demand of REEs and create an alternative source of REEs to reduce the balance problem of REEs and the monopoly concerning the production of REEs.

1.1 Problem statement and aims

As the demand for REE is increasing and prices of REEs are rising, an alternative source by urban mining has great potential. The YOX waste as described before, is of great interest for recovery of Eu for its relative high concentration (9 m/m%) and low complexity (only Y is present as matrix).

Already a lot of research has been done in the field of recycling YOX by Van den Bogaert [7, 8, 9], Van Meerbeeck [10], Haveaux [11], Gheeraert [12] et al. It was

aimed at the separation by selective precipitation via selective reduction in aqueous media and organic media. This research was done in batch reactors.

Separation in aqueous media was tackled by the use of additives (including sulphates) to achieve photochemical reduction of Eu^{3+} to Eu^{2+} and forms $EuSO_4$ which immediately precipitates due to its poor solubility. [8] The use of shorter wavelenghts to achieve the charge transfer compared to separation in organic media makes the method slightly more energy consuming. This method was only performed in batch with very long residence times (hours), making it unattractive for industrial applications.

Separation in organic media was performed via the use of organic solvents which have a low solubility for the reaction products, therefore after photochemically reducing Eu^{3+}, $EuCl_2$ could be separated as it exceeded its solubility [12]. The solubility in methanol however was too large for precipitation to occur. Organic solvents where used rather than aqueous media as the absorption band for the reduction of europium is positioned at longer wavelengths, reducing the energy per photon and energy consumption. Recent work aimed at recycling of YOX as well showed promising results in the separation of mixtures containing Sr^{2+} (mimicking Eu^{2+}) and Y^{3+} by the use of dibuthylphosphate for precipitation of Y^{3+}. [13] Combining both platforms could yield a stepwise separation of Eu and Y.

The current state of the art concerning Eu recovery from YOX, as shown above, is by the use of batch reactors with medium power lamps (range of hundred watts) with very high residence times (sometimes up to days). These long residence times and the batch process is unattractive for industrial applications as they tend to implement continuous processes. Therefore, this thesis aims towards developing a continuous separation technique for Eu and Y via photochemical reduction of Eu followed by precipitation in a tubular reactor which builds on the knowledge developed by Van den Bogaert et al. as mentioned before. A mathematical model for photochemical reactors will be developed in parallel to aid the development of the tubular reactor. An overview of the aims is given below:

1. Assess the selective precipitation of Y^{3+} in the presence of Eu^{2+} by the use of Van Puyvelde's previous work. [13] Assess its potential for use in a continuous separation using a two step process involving a photochemical reduction step and a selective precipitation step in two separate unit operations. Results from this assessment can be found in Appendix D.

2. Develop a model for photochemical reactors to estimate the conversion, space-time yield, photochemical space-time yield of the reactor in this thesis and optimal design in terms of size of a photochemical reactor for Eu recovery. The model and its derivations can be found in Chapter 4.

3. Develop a continuous reactor for recovery of Eu from YOX waste by the use of separation of Eu and Y in aqueous environment and assess its performance with laboratory solutions of Eu and artificial YOX and YOX-waste samples, this can be read in Chapter 5.

4. Intensify the previously mentioned reactor by means of reducing the deviation between the mathematical model and reducing the induction time to increase productivity. Results of this intensification are found in chapter 6.

Summarising, a platform for industrial recycling of YOX will be aimed by the development and optimisation of a continuous process and model for photochemical reactors by the aid of a mathematical model.

1.2 Scope

This thesis focusses towards on the design of a continuous reactor for photochemical reduction and separation of Eu from YOX waste streams. In a first step an assessment is made for a possible separation rout in methanolic environment and in the next stage, the reactor is designed and a separation strategy is implemented using the aid of a mathematical model.

A preliminary assessment is made towards the feasibility of using selective precipitation of Y^{3+} with dibuthylphosphate in a continuous process in methanolic environment as it enables the process to be split up in two process operation units. As dibuthylphosphate poses too many difficulties in its use for selective precipitation, alternatives in the form of selective extraction, precipitation and crystallisation are investigated, but they all had its shortcomings.

For the design of the photochemical reactor, a mathematical model is derived based upon the law of Lambert-Beer for light absorption. The model is implemented in Matlab and can be used to determine the conversion and productivity of a photochemical reactor for Eu recovery. The developed model can be used to design photochemical reactor for alternative applications.

The photochemical reactor for Eu recovery is assembled once the assessment of separation in methanolic environment was done to select the separation technique. The separation of Eu from Y is performed in aqueous media using a tubular reactor and a low pressure mercury lamp. The reactor is benchmarked and compared to the mathematical model and previous batch results, yielding a reduction of residence time of a factor of 41, an increase in productivity of a factor 49 and a increase in photochemical space-time yield of a factor 20. Separation of artifical YOX and waste YOX indicated that side reactions reduced the yield significantly.

The model pointed two possible routes for optimizing and intensifying the process. The reduction of ‘dark zones’ in the reactor did not yield improvements, but seeding of the feed solution increased productivity by 42% at a relatively low residence time.

The thesis ends with the conclusion and propositions for future work.

1.3 Outline

This thesis is divided in eight chapters and one chapter in appendix. An outline of these chapters is given below. Chapter 1 gives the problem description, scope

and aims of this thesis. It summarizes the objectives of this theses and as well as an outline. Chapter 2 includes the current state of the art about the REEs concerning their properties, applications, production history and separation methods. The last part of Chapter 2 handles about the application of light for the separation of europium from waste components and how the light can be implemented in a reactor. Chapter 3 provides the equipment and methods which are used in this thesis. These range from analysis methods to the reactors used in experiments. Appendix D reports the results concerning the separation of Eu from Y in organic media. Herein, separation was assessed by selective reduction of Eu followed by selective precipitation of Y (the other waste component). None of these methods were viable to be used in a continuous separation process for Eu and Y. Chapter 4 describes a model concerning the light consumption and reaction rate that is verified in further experiments. Chapter 5 deals with separation of Eu and Y in aqueous media via a continuous tubular reactor. Separation was undertaken via selective reduction of Eu following by precipitation as $EuSO_4$. Using the model in Chapter 4, the performance is compared and the model predictions are tested. Chapter 6 aims at increasing the conversion of the reactor from chapter 5 via process intensification tools including pulsating the feed stream to enhance solid behaviour and seeding the feed stream to reduce the induction time (time needed to build up supersaturation). Chapter 7 investigates further routes for research to improve the working of the tubular reactor in Chapter 5. Chapter 8 provides the conclusion of this work.

Chapter 2

State of the art

2.1 Rare earth elements

As this work is mainly focussing on the separation of rare earth elements (REEs), therefore these REEs are explained in the upcoming sections by explaining what they are and where they are used for.

2.1.1 What are Rare earth elements (REE)

The International Union of Pure and Applied Chemistry classifies Rare earth elements (further abbreviated as REEs) as a group of 17 elements in the third group of the periodic table of elements. This group of 17 elements can be seen in Figure 2.1 and consists of the lanthanides and two additional elements: scandium and yttrium with an atomic number (Z) of 21 and 39 respectively. Of this group, promethium usually isn't included as it is radioactive and doesn't occur in nature.

These REEs can be further divided in light rare earth elements (LREEs) and heavy rare earth elements (HREEs) according to the United States Geological Survey (USGS) [14]. The LREEs include the elements La up to Sm, as the HREEs contain the elements europium (Eu) to lutetium (Lu) as well as yttrium (Y) and scandium (Sc), shown in Figure 2.1. According to Kingsnorth, a 3rd group exists as well; the medium rare earth elements (MREEs) [3]. In this vision, the classes are shifted slightly. Including lanthanum (La) to neodymium (Nd) to the LREE, praseodymium (Pm) to gadolinium (Gd) to MREEs and terbium (Tb) to lutetium (Lu) and yttrium (Y) to the HREEs and excluding scandium (Sc) from the REEs at all. [4, 3]

Contrary to their name, REEs are not that rare. The orgin of the term 'rare earth elements' dates back to the 1800s when the elements were discovered. The term "rare" refers to the fact that these elements were strange and extraordinary at the time that they were found. [3]

REEs are relatively common. The REEs have an abundance margin of 0.1 up to 100 ppm relative to silicium (Si). When this is compared to rock-forming elements (think about silicates) their abundance is a lot lower, but when compared to elements with an atomic number larger than 25, their abundance is normal. Of all elements,

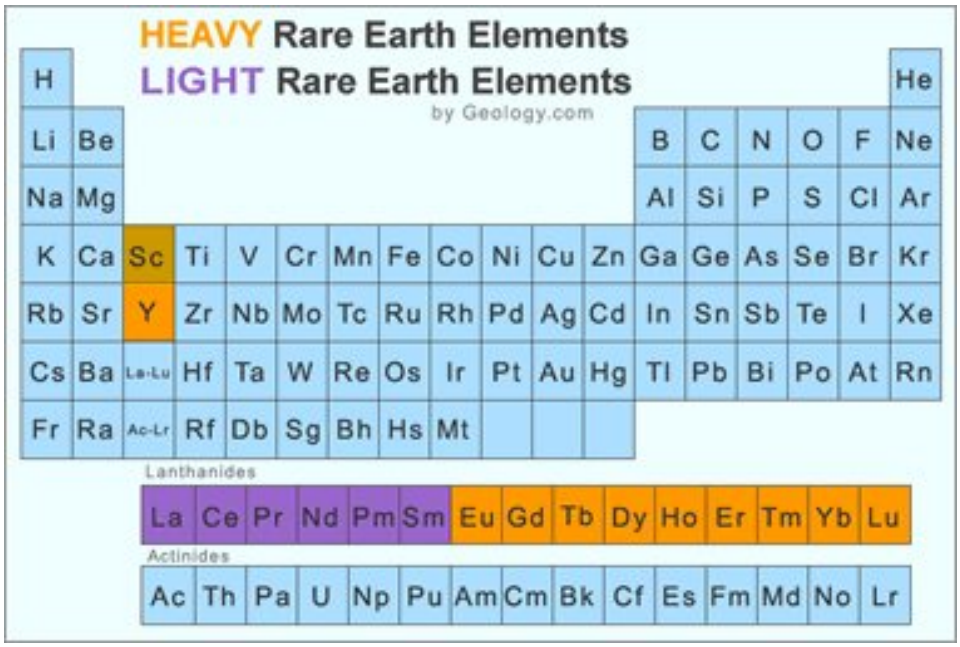

Figure 2.1: Situation of the REEs in the periodic table, the REEs can be divided in LREEs and HREEs. [4]

the precious metals (Au, Pt, Ir, Os, Rh, Pd, Ru, Ag) are the least common elements of all, around 10000 times less abundant than REEs, as shown in Figure 2.2. [4, 15] In the region of REEs, it can be seen that elements with an odd atomic number have a lower abundance than elements with an even atomic number, this is called the rule of Oddo-Harkins and is due to the stability of the element when it has been formed by fusion [15, 16].

The only problem with REEs is that they are difficult to mine as the concentration of any REE in minerals are very low (e.g. only 0.1% of the mined minerals in Mountain Pass Mine (Mine in US) contain REE). It results in the excavation of a lot of material for just a little of REE and a lot of effort is necessary to concentrate the elements. [4]

2.1.2 Applications of REE

REEs are used in lots of applications and play a critical role in the world as they are vital for some applications. Most of the demand for rare earth oxides (REOs) can be explained by the use of permanent magnets for electric motors and lamp phosphors (shown in Table 2.1).

As rare earth elements are used in lots of applications, only a few of them will be further explained in this section. As the main aim of this work is to recycle Eu and Y, its practical uses will be illustrated further.

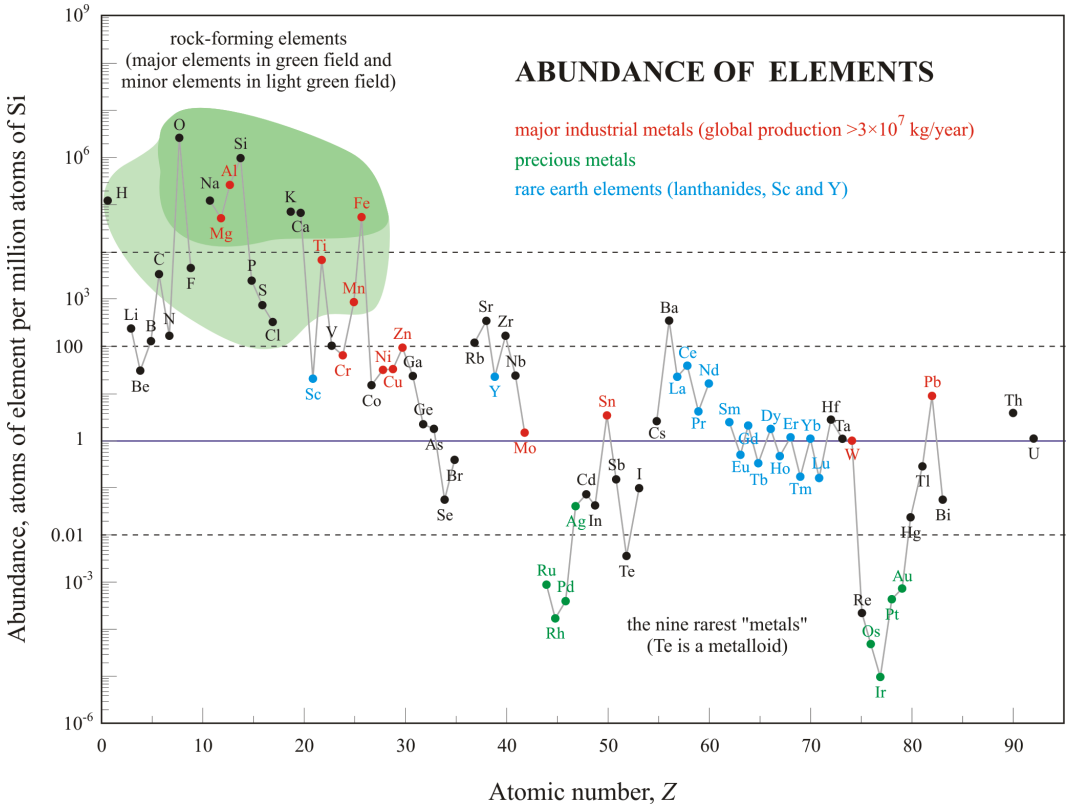

Figure 2.2: Abundance of elements from the periodic table in the earth's crust compared to 1 million particles of silicium (Si). The y-axis is logarithmically. [1]

Europium (Eu) is mainly used in phoshors for its phosphorescence abilities in its 2+ or 3+ oxidation state [2]. For the application, it's usually used as dopant in these lamp phosphors. A commonly used phosphor is Y_2O_3:Eu^{3+} which results in a red phosphor. But other lamp phosphors are also used such as $Sr_5(PO_4)_3Cl$:Eu^{2+} and $BaMgAl_{11}O_{17}$:Eu^{2+} which are blue phosphors [2, 3]. Some applications of these phosphors include TL-lamps, flat screens and televisions [2]. A second application involves radiation shielding in nuclear industry and it is also used in control rods in nuclear reactors to absorb neutrons [17].

Yttrium (Y), which is the second element of interest to this work, is used in more diverse applications. The most common applications include alloys (with Mg, Cr, Mo, Zr) and lamp phosphors. As mentioned before, Y is present in lamp phosphors from which Y_2O_3:Eu^{3+} is an example. Another lamp phosphor is YVO_4:Eu which is also a red lamp phosphor. [2, 3] Y_2O_3 is used to make glass heat and shock resistant for cameras. Ceramics do contain Y_2O_3 to make them stronger and tougher, they have the benefit that the sintering temperature of the ceramic is reduced by adding the oxide [17]. Yttrium is also used in radars and lasers for the crystals to produce the electromagnetic waves, Y-Fe (YIG) and Y-Al (YAG) for

radars and lasers respectively. [2, 3] Other applications range from superconductors ($YBa_2Cu_3O_{7-9}$) up to increasing the strength of alloys (decreases crystal grain size) [2].

In order to give a general idea of which elements are used for which applications, Table 2.1 is shown.

Table 2.1: Volume share of REEs in various applications [3].

Applications	La (%)	Ce (%)	Pr (%)	Nd (%)	Sm (%)	Eu (%)	Gd (%)	Tb (%)	Dy (%)	Y (%)
Permanent magnets			23	69			2	1	5	
Lamp Phosphors	9	10				5	2	5		69
Battery alloy	50	34	3	10	3					
Fluid catalytic cracking	90	10								
Ceramics	17	12	6	12						53
Glass additives	24	66	1	3						2
Polishing powders	31	65	4							
Auto catalysts	5	90	2	3						
Metallurgy	26	52	5	17						

Table 2.1 shows the volume share of REEs in various applications. The applications with the highest share in value are permanent magnets (38%), lamp phosphors (32%) and metal alloys (13%) [17].

2.1.3 Production history and market situation of REEs

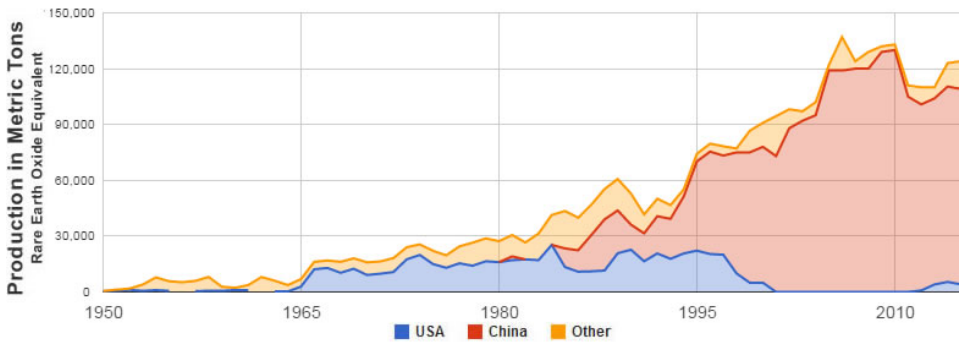

Figure 2.3: Production of REEs from 1950 up to 2014 expressed in metric ton [4]

Before 1965, demand for REEs was very low (shown in Figure 2.3) and production came from South Africa and a small part from the USA (Mountain Pass Mine) [18]. The Mountain Pass Mine is a mine situated in the Mojave Desert in California and produces mainly bastnäsite which contains $(Ce,La,Nd,\ldots)CO_3F$ [18, 17].

Up till the 1980s, the situation was stable. Around 1985, China started to produce REEs at a very high capacity. China exploits 2 mines; the Bayan Obo Mine (Mongolia) and one situated in Southern China. The capacity increased throughout the 1990s and 2000s due to higher demand for color television etc. Other mines couldn't compete against the low prices of Chinese mines and quit entirely (also the Mountain Pass Mine) as their mines weren't profitable any more, shown in Figure 2.3. [18]

As the United States now only depends on the import of Chinese REEs, the REEs supply is not optimal. In the first place, the US is about to lose its long-lasting leadership in some areas concerning REEs technology. Secondly, as technology becomes more and more dependant on REEs, it becomes increasingly important to have a reliable source of REEs at an affordable price. Thirdly, the availability of REEs isn't constant and depends heavily on China in term of the relationship between the US and China and on China's politics and economy and of course their own needs for REEs. [18]

Later, China began to restrict the output of REEs mostly for their own use, such that the prices rose as well. In 2010, when prices had risen 500%, manufacturers in the USA, India, Australia began to reconsider earlier projects and started to produce REEs again [4]. As shown in Figure 2.3. Around 2012, most of them were fully operational again. The prices of REEs are shown in Figure 2.4. It is very clear that China regulates the price from around 2011 as it is the major producer of REEs. The prices multiplied by factor 20 for dysprosium. [3]

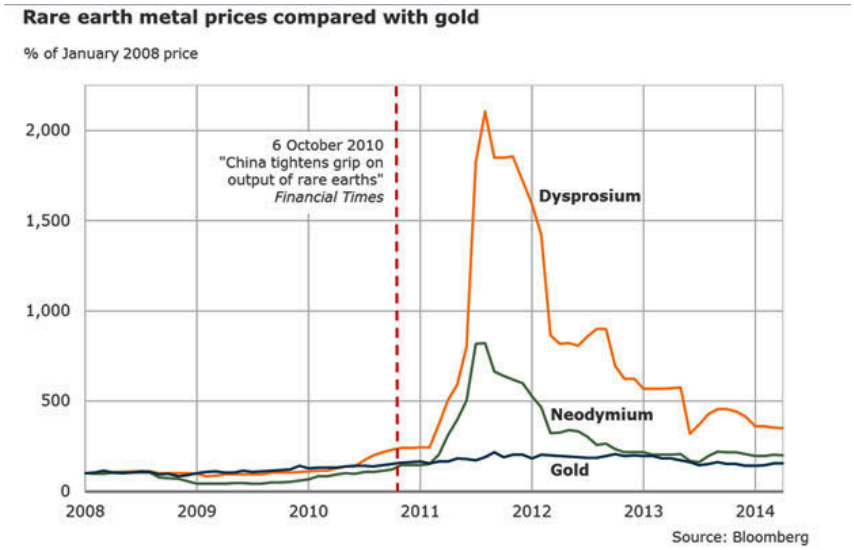

Figure 2.4: Prices of some REEs between 2008 and 2014 compared to gold and relative to the price of each element at the start of 2008. The situation of the other REEs that are not depicted here are similar, they all show a large increase in price between 2011 and 2012. [19]

As can be seen on Figure 2.4, the last 15 years, China had almost a monopoly on

the production of REEs. It not only means that they can determine the price (since there are almost no competitors) but they could also determine whether they would export it or not. [4]

In the future, demand for REEs will continue to rise as the production of rechargeable batteries, consumer electronics, energy-efficient lighting, and catalysts will increase as well. Therefore these LREEs and HREEs are critical materials (by the European Commission) with a high supply risk (unstable supply by china). [5, 20]

2.1.4 Balance problem and recycling

As REEs mainly come from complex minerals as bastnäsite, it is possible that when demand for one element rises, the production rises as well, but a lot of unused elements are left over. In the 1960s, demand for mixed rare earths was common, where mostly La and Ce were needed for e.g. polishing powder, battery alloys, etc. Nowadays, the industry has moved towards more specialised applications that demand more rare elements present in lower concentration in the ore such as Nd, Sm (for magnets used in motors), Y, Eu, Tb, La, Ce, Gd (for phosphors for lamps, Cathode Ray Tubes (CRTs) and X-ray intensifying screens). [15]

The high demand for Nd leads to a massive excess in Ce, Pr and Sm which are stockpiled at the mines, which is the case for the LREEs-segment. The HREEs market is mainly driven of its demand for Eu, Tb, Dy and Y and is smaller than the LREEs demand. It indicates that the market is not in balance due to the excess in production of those 3 elements (Ce, Pr and Sm). When the market would be in balance, the price of all REEs would drop to its lowest as the production cost of mining is shared by all the elements instead of just the ones with a high demand whilst the excess is stockpiled at the mine. To reach the balance will be very difficult as ores have mostly a fixed composition, but the market demand changes from time to time due to changes in applications. [15]

One way to reach the balance is to recycle Nd and Dy to reduce overproduction of Ce, Sm and other elements. In the HREEs segment, the problem can be reduced by recycling Eu, Tb and Y from lamp phosphors [15]. This work is attempting to recycle Eu and Y.

In order to restore the balance in the REEs mining, it is important to recycle the elements which are heavily requested by the market, these are Eu, Tb, Y, Nd, Dy and La. These elements can be recovered from waste products as lamp phophors (Eu, Tb, Y, Gd, La and Ce), permanent magnets (Nd, Pr, Tb and Dy) and nickel metal hydride batteries (La, Ce and Ni). [21] Only 1% of the REEs were recycled in 2011, which means there is a lot of work still to be done in the future. The reason why the number is so low, is that the technology fully developed, the REEs aren't collected sufficiently and a lot of initiative is still missing [21].

The two most interesting waste streams containing REEs are the magnets and lamp phosphors (they will be discussed in the next subsection). [21]

2.1.5 Lamp phosphors

(Compact) fluorescent lamp waste

Since the phase out on incandescent lamps in 2011, the customer was given 2 alternatives instead: compact fluorescent lamps (CFLs) (and the bigger tl-lamps) and light emitting diodes (LEDs). Since the LEDs weren't fully optimized a few years ago, CFLs became the first alternative to incandescent lamps.[22]

In order to produce these CFLs (light bulbs, not electronics), certain basic products are necessary as shown in Table 2.2. When these lamps are recycled, the mercury inside the lamp is recycled as well, preventing the release to the atmosphere of the toxic component [6].

Table 2.2: Composition of a CFL without electronics [6]

Material Composition	mass fraction (wt. %)
Glass	88
Metals	5
Plastic	4
Lamp phosphor powder	**3**
Mercury	0.005

Most of these materials are commodity materials such as glass, metals and plastic and mercury. But REEs are speciality chemicals which constitute the lamp phosphor powder. The amount of lamp phosphor powder used in every lamp is small (3 wt. %), but it is vital to convert the light produced by the arc to visible light. [23, 6]

It was already introduced that compact fluorescent lamps and fluorescent lamps do contain lamp phosphors that are vital to produce the correct colors for a 'natural light'. The working principle is shown in Figure 2.5. Electrodes introduce energy into the lamp that is taken up by the mercury in the lamp. Mercury becomes energetically excited and falls back to its ground state by emitting a UV-photon in the process. These UV-photons are absorbed by the phosphors in the lamp and emitted again as visual light. [24]

Different types of lamp phosphors

The composition of the lamp phosphors commonly used in compact fluorescent lamps is shown in Table 2.3. Most of the shown lamp phosphors do contain REEs from which some of them are highly requested elements with a high value. [26]

As some of the lamp phosphors, shown in Table 2.3, contain highly requested REEs, it is advisable to recycle this waste stream. Recycling can be done in various ways, direct re-use of those elements is a first method. It is very simple in use and needs no chemicals, but only works if only 1 type of lamp phosphors are used as they cannot be separated and the lamp phosphors that are recycled via direct re-use deteriorate as time progresses. [21]

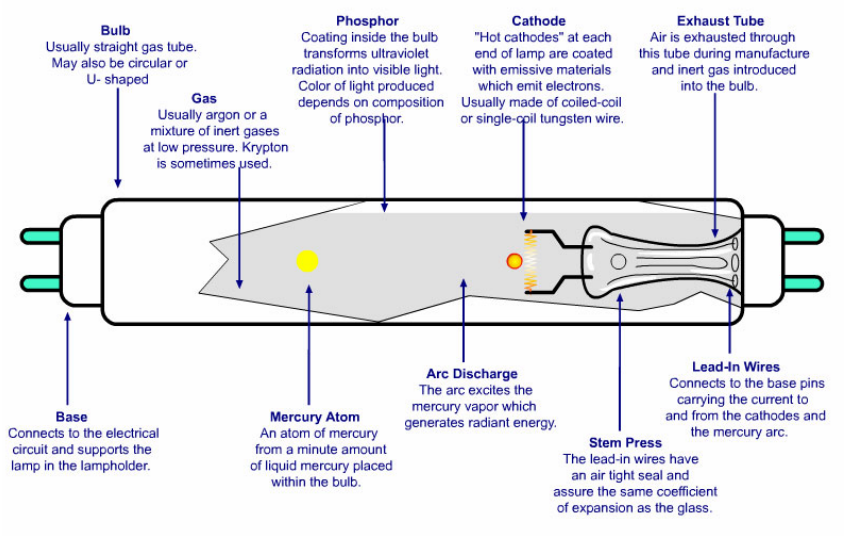

Figure 2.5: Fluorescent lamp [25]

Table 2.3: Lamp phosphor fraction composition found in CFL and FL [6]

Emission color	Composition	Name	value
red	Y_2O_3:Eu^{3+}	(YOX)	high
green	$LaPO_4$:Ce^{3+},Tb^{3+}	(LAP)	high
	$GdMgB_5O_{10}$:Ce^{3+},Tb^{3+}	(CBT)	N/A
	(Ce,Tb)$MgAl_{11}O_{19}$	(CAT)	high
blue	$BaMgAl_{10}O_{17}$:Eu_2^+	(BAM)	low
	$(Sr,Ca,Ba,Mg)_5(PO_4)_3Cl$:$Eu^{2+}$	N/A	less common
white	$(Sr,Ca)_{10}(PO_4)(Cl,F)_2$:$Sb^{3+}$,$Mn^{2+}$	HALO	low

A second method of recycling is by separation the lamp phosphors. Separation is done by techniques as floatation, pneumatic separation or gravity separation in dense medium. The method doesn't need chemicals to work, but the quality of the lamp phosphors deteriorates as well as the particle size may change and still it's very difficult to get the pure phosphor fractions. [21]

As a third method, the separation can also be done by the aid of chemicals which results in pure REOs by acid and alkali decomposition and extraction. The method produces large amounts waste and a large consumption of chemicals. [21]

In order to separate the lamp phosphors from the fluorescent lamps, one more problem has to be tackled. Each lamp is filled with mercury in vapour form, as the substance is toxic to the environment, it's important to extract it from the lamp as much as possible. Europe has already agreed to reduce the amount of Hg to 3.5

mg/lamp for lamps with a power of 50W and lower. Hg itself settles in the phosphor layer (85% of the total Hg content) at the end of its lifetime, making it easier to remove. Mercury is extracted from the phosphor layer and from the rest of the crushed lamps by thermal treatment at 400-600 ℃ for several hours in vacuum and full removal is only achieved at 800 ℃Ṫhe removal of the mercury is very energy consuming. [21]

An example of the entire process can be seen on Figures A.1 and A.2 in Appendix A which is used at Rhodia which is a company belonging to Solvay [27, 28]. In the first step, the phosphor from lamps are chemically attacked to dissolve the waste products, the REEs and other components will stay in the solid fraction. The solid fraction undergoes liquid-solid extraction whereby more waste products are extracted from the solid phosphors. The powder that is left after extraction is sent to Rhodia's second plant to undergo purification. There the powders undergo thermal treatment followed by re-suspension to remove more waste products. The REOs are then chemically attacked by nitric acid to produce rare earth nitrates which are separated further by a battery of mixer-settlers with specialised solvents. After separation, the powders are fractionated in La, Ce, Eu, Tb, Gd and Y, all in nitrate form. These can be converted in oxide form by calcination. [27, 28]

Some of these elements (e.g. Europium) are produced quasi only in Chinese mines. [15] Thus by recycling lamp phosphors and extracting the necessary elements as seen on figures A.1 and A.2, it's not only good for the environment as these elements are not dumped on landfills, but also provides an alternative source of these elements to reduce the so called 'balance problem'. [21]

2.2 Conventional separation of REEs

The REEs have very similar chemical properties which can be explained by their electronic configurations and their ionic radii.

The **electronic configurations** of the REEs have some similarities. Sc, Y and La are similar by the fact that they have a fully filled s-orbital and 1 electron in their d-orbital, which is the same as $ns^2(n-1)d^1$ with $n = 4$, 5 and 6 respectively. Ce to Lu have the following electron configuration; $6s^25d^14f^{(n-1)}$ or $6s^24f^n$. The reason for 2 common electron configurations is that the 5d and the 4f orbitals have similar energies.

The REEs all have oxidation state 3+ which is also the most stable. Some elements (e.g. Eu) have also 2+ as stable oxidation state, explained by the stability created of an half filled f-orbital. Also 4+ is a stable state for some elements, the most common one is Ce, its stability is explained as Ce^{4+} acquires the electron configuration of Xe, Pr and Tb share the 4+ oxidation state because of different reasons (half filled f-orbital for Tb). The special stability of these 2+ and 4+ states

is of great importance for further separation techniques. All electron configurations are shown in Table 2.4. [29]

Table 2.4: Oxidation states of the REEs. The states in bold are the most common and also the most stable states found in nature of these elements. The states in brackets are not stable. [2]

La	Ce	Pr	Nd	Pm	Sm	Eu	Gd	Tb	Dy	Ho	Er	Tm	Yb	Lu
		(2)	(2)		2	2			(2)	(2)		(2)	2	
3	**3**	**3**	**3**	**3**	**3**	**3**	**3**	**3**	**3**	**3**	**3**	**3**	**3**	**3**
	4	4	(4)					4	(4)					

Furthermore, looking at the **atomic radii** of these elements are shown in Figure 2.6, it can be seen that the radii decrease with increasing atomic number due to imperfect shielding of the nucleus by the electrons in the f-orbital because of its shape. The decrease in ionic radii is also called the lanthanide contraction. The chemistry of the REEs is predominantly ionic (most of it by its 3+ state) and it can be explained by the size of the ion. Yttrium is divided into the HREEs because it has roughly the same ionic radii as the HREEs thus ending up in the HREEs fraction when the ore is separated. [29]

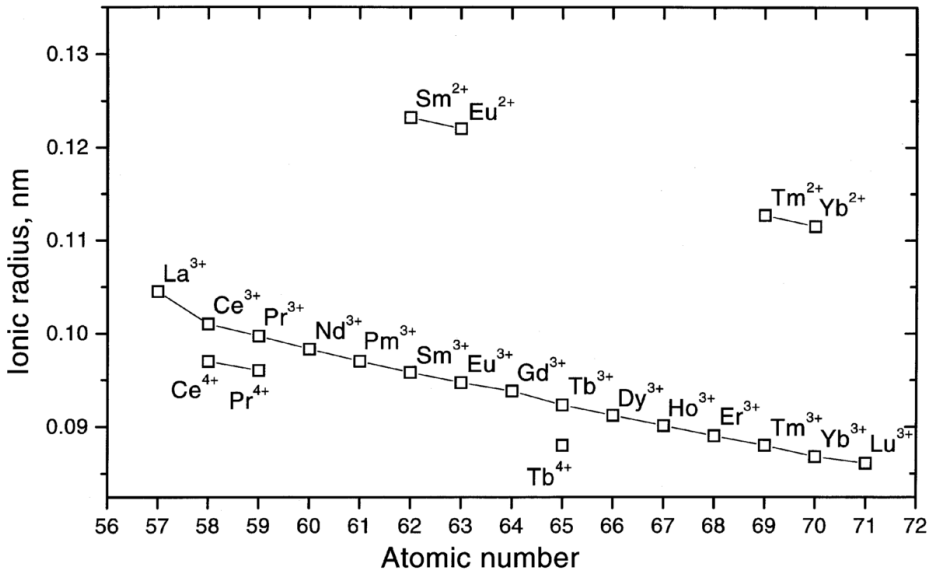

Figure 2.6: Ionic Radii of REEs [29]

Another important issue that is exploited in some separation methods is the difference in **basicity** of the REEs. Basicity determines when cations hydrolyse in water, how soluble certain salts are, the ease of breakup of oxyanions when they're heated and the stability of complex ions. Basicity is directly related to their ionic

size which is shown in Figure 2.6. The order of strength in basicity is the following [29], going from most to least basic:

$$La^{3+} > Ce^{3+} > Pr^{3+} > Nd^{3+} > Pm^{3+} > Sm^{3+} > Eu^{3+} > Gd^{3+} > Tb^{3+} > Dy^{3+} > Ho^{3+} > Y^{3+} > Er^{3+} > Tm^{3+} > Yb^{3+} > Lu^{3+} > Sc^{3+}$$

The 4+ ions (e.g. Ce^{4+}) are less basic than the 3+ ions and the 2+ ions (e.g. Eu^{2+}) are more basic than the 3+ ions. The difference in basicity is the basis for some separation techniques that include; fractional crystallisation, fractional precipitation, ion exchange and solvent extraction. Other techniques indirectly use the basicity difference in elements as there is the selective oxidation or reduction of a species.

As the difference in basicity increases, the separation is easier to achieve, therefore separating e.g. La^{3+} from Lu^{3+} is easy. But the separation of 2 adjacent elements (e.g. La^{3+} and Ce^{3+}) is more difficult because of the small difference.
[29]

After the mined ore is separated from the uninteresting rock, it can be further separated into its elementary components which can be used in all sorts of applications.

2.2.1 Selective oxidation

In a mixture of REEs, Ce can be easily removed by selectively oxidising it from its 3+ to 4+ oxidation state, the oxidation can be done by heating the substance in air at 650 ℃ or by drying REE hydroxides in air at 120-130 ℃ . The removal of Ce^{4+} can be done by selective dissolution of all trivalent species or by complete dissolution of all species followed by selective precipitation of tetravalent species. The method doesn't remove all tetravalent species.[29]

Although Pr(4+) and Tb(4+) also form tetravalent species, they are not stable in water and can not be removed by the same method. [29]

2.2.2 Selective reduction

Sm, Eu and Yb can be separated by exploiting their divalent state. The separation of these elements must be done after they were concentrated first to make the method more effective. [29] The reduction could be done by a few methods. It can be done electrochemically by using mercury cathodes, lithium amalgam electrodes (separation Sm from Eu and Yb). An industrial method for recovering Eu is via the reduction of Eu^{3+} by zinc (Zn) to Eu^{2+} followed by precipitating $EuSO_4$ with the aid of sulphates. Zn will not reduce Sm and Yb. In solutions with limited amount of Eu, co-precipitation with $BaSO_4$ is used and later the Eu is redissolved leaving the $BaSO_4$ as precipitate. [29]

Even photochemical reduction of Eu can be done. Eu can be reduced and precipitated as divalent europium as a sulphate or chloride as they both are sparingly

soluble (using concentrated HCl for the chloride). Photochemical reduction involves the light coming from a low pressure mercury lamp at 185 nm, or a lamp with a filter at 254 nm or an ArF excimer laser at 193 nm. The solutions that were illuminated contained lanthanide perchlorates (0.01M), 0.05M of K_2SO_4 in 10% isopropanol. Photochemical reduction will be fully explained and illustrated in Section 2.3.[29]

2.2.3 Fractional crystallization

Fractional crystallization works by either changing the temperature of the solution or by evaporation a saturated solution of salt. It only works if the solubility of the components in the solution differ. Using fractional crystallization, the lesser soluble component gets removed by crystallization, the more soluble component is enriched in the liquor. [29]

For fractional crystallization, salts and double salts are used. An example of these double salts are the double ammonium nitrate salts ($RE(NO_3)_3 \cdot 2\,NH_4NO_3 \cdot 4\,H_2O$) which are used to remove La and separate Pr and Nd. The method is extremely slow for HREEs and must be repeated many times to yield a pure product. [29]

2.2.4 Fractional precipitation

Fractional precipitation works by the addition of a chemical reagent which forms new less soluble species which precipitate. The remaining REEs can be fully precipitated in a second step as oxalate or hydroxide.

Some salts that can be used for fractional precipitation include double sulphates, double chromates (to separate REEs from Y). Hydroxide precipitation is used to remove La. Double sulphates ($RE_2(SO_4)3 \cdot Na_2SO_4 \cdot nH_2O$) are used to mainly precipitate La, Ce, Pr, Nd as these are sparingly soluble, the other elements form more soluble double salts. [29]

2.2.5 Ion exchange

Ion exchange uses a resin which can be compared to an ionic salt whereby one end of the salt is fixed to an insoluble matrix. For REEs, an cation exchanger is used. When the column is loaded with a salt solution, it is possible that the counter ions of the column are displaced by the ions of the salt solution. Some rules apply, an ion with a higher charge replaces one with a lower charge. When both have the same charge, the ion with largest radius replaces the one with the smallest radius. And lastly, the replacement occurs according to the law of mass action.

The affinity towards the exchanger is given by its distribution coefficient, defined as follows for a substance A distributed in phase 1 (e.g. on the exchanger) and phase 2 (e.g. the solvent):

$$D_A = \frac{C_{A1}}{C_{A2}} \tag{2.1}$$

Equation 2.1 shows the distribution of a component A over two phases, the concentration to fill in in the equation should have the same units (e.g. mol/L). For a

substance B, the same equation as 2.1 is applied (but than with index B). To see if both ions would be separated in a particular exchanger column using a particular solvent, the ratio of the distribution coefficients, also called separation coefficient, is described al follows:

$$\alpha_B^A = \frac{D_a}{D_B} \tag{2.2}$$

Separation is well if α is either very large or very small. When α approaches unity, separation is poor. [29]

Separation of REE by ion exchange can be done, but it relies on the difference in size of the hydrated ion, which is directly linked to the ionic radius (shown in Figure 2.6). A decrease in affinity was observed from La(III) to Lu(III), implying that separation adjacent elements is difficult for their small difference in affinity, thus small separation coefficient, towards the resin. Separation of two elements further apart in the periodic table, Y(III) and Gd(III), was already successful in 1893. The introduction of complexing agents (citric acid, nitrilotriacetic acid (NTA), etc.) lead to an increase in separation coefficient for REEs. Several mixtures of REEs could be separated well via these complexing agents. Using Ethylenediaminetetraacetic acid (EDTA) for band displacement whereby the state of the resin is changed to a special cationic state results in better separation. Ion exchange with complexing agents (EDTA) could be commercialized as it could produce 99.99% purity in one pass with the biggest downside that ion exchange is an inherent batch system.

2.2.6 Solvent extraction

Solvent extraction is based upon the preference of some elements to distribute themselves between different phases, also seen in ion exchange. The same distribution coefficient and ratio are used as before and are shown in Equations 2.1 and 2.2. In solvent extraction, the 2 phases consist of liquids that are immiscible, meaning that they will separate and form a boundary layer in between them. The method has some advantages, but also some disadvantages compared to other techniques. One of the advantages is that high concentrations of rare earth oxides (REOs) can be used, up to 180 g/L. The high concentrations reduces the amount of liquid necessary thus the size of the plant. The disadvantages include the low separation facts for REEs as explained later.

In most cases, the 2 phases consist of an aqueous and an organic phase. The organic phase is composed of 2 or more substances. Most of the times an extractant is used as organic phase, but these are usually too viscous thus it has to be dissolved by a more suitable solvent (e.g. kerosene or aromatics). A schematic of the process is shown in Figure 2.7 as it is applied to the ores coming from Mountain Pass Mine (USA).[29]

In practice, it it difficult to separate REEs by solvent extraction. It requires a large amount of mixer settler tanks to do so, it is not fully clear in Figure 2.7. Referring back to Figure A.2, it can be seen commercially, that the last separation step is performed by solvent extraction to produce REOs.

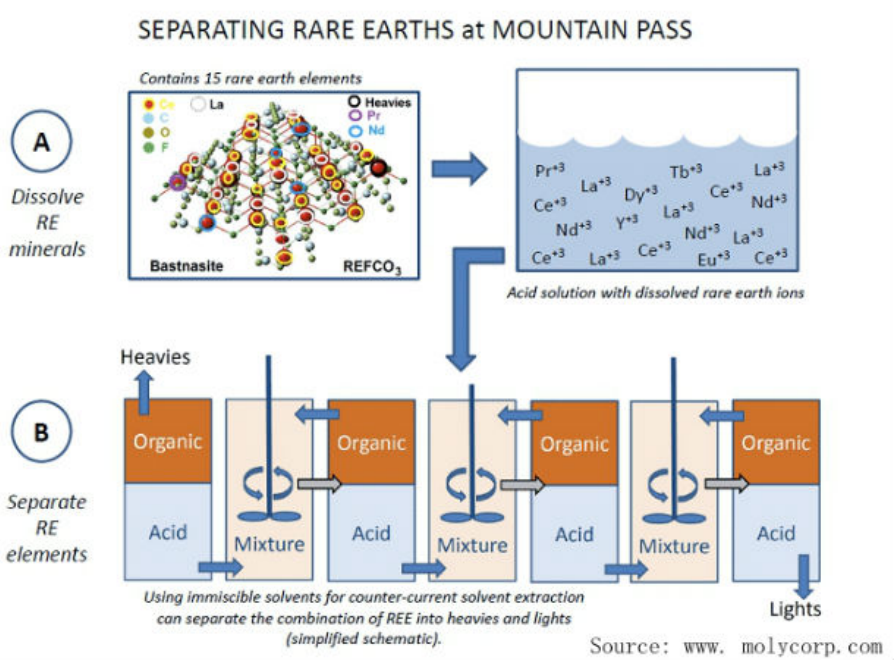

Figure 2.7: Solvent extraction of REEs coming from Mountain Pass (USA), Molycorp is the company that owns and exploits Mountain Pass [30]. The inlet for the acid and organic phase in the bottom part of the scheme are neglected for simplicity.

An example to illustrate the difficulty of extraction, is the use of a system containing REE(III)-HCl-HDEHP, the system is capable of separation REEs, but with a different degree of difficulty. It is difficult to separate successive elements (also seen in ion exchange) resulting in separation coefficients ranging from 1.03 up to 4.86, thus resulting in a difficult separation. Separating non-successive elements is easier with separation factors ranging up to 425 for La(III)-Lu(III) separation. [29]

2.3 Photochemical separation

Photochemical separation usually requires UV-radiation as it requires a certain amount of energy (energy of the photon) to break bonds in a molecule and UV-radiation is powerful enough to do so [31, 32]. In this work and previous works [9, 12, 8, 10, 11], Eu^{3+} is photochemical reduced by UV-radiation to Eu^{2+}. The reduction is very selective since only Eu^{3+} is targeted. The reaction mechanism is based on a ligand-to-metal charge transfer between Eu^{3+} and its ligand. [12] This principle is explained further in more detail. Once Eu^{2+} is formed, a difference in chemical properties is exploited to separate europium from yttrium (the yttrium is present in YOX-waste streams which will be the main scope of this work). The actual separation depends on the solvent that will be used as different separation mechanisms can be used in each of them. [12]

2.3.1 Photochemical separation in organic media

The state of photochemical separation in organic media for Eu will be explored. The mechanism for separation in organic media is described by Van den Bogaert and Gheeraert [9, 12] and shown below. Precipitation of trivalent ions by the addition of dibutylphosphate is included as well as a possible step for precipitation which is further explored in this work. [13]

Reaction mechanism

The reaction mechanism consists of a four-step process which include the following steps in subsequent order: dissolving and complexing, photoexitation, electron transfer and precipitation. A fifth step describes the destruction of all the radicals that are formed in those four previous steps.

Step 1: Dissolving and complexing. The first step in the mechanism is the dissolution of the $EuCl_3$. It is shown in in Equation 2.3. $EuCl_3$ is present in the leachate of the lamp phosphors after separation into each lamp phosphor fraction. [12]

$$EuCl_3 \cdot 6\,H_2O_{(s)} + 3\,R_2CHOH_{(l)} \longrightarrow EuCl_3 \cdot 3\,R_2CHOH_{(l)} + 6\,H_2O \tag{2.3}$$

with R as a side chain (e.g. H for methanol) [9]. Some of the water molecules from the hydrated salt will be replaced by the solvent. $EuCl_3{\cdot}6\,H_2O$ has 2 absorption bands when dissolved in methanol: one is situated at 228 nm, which can be linked to the charge transfer from methanol to Eu^{3+}-ion. The second one is situated at 272 nm that can be assigned to the charge transfer of Cl^-. [12]

Step 2: Photoexcitation. Two cases are possible for the photoexcitation step; either a Eu^{3+}-MeOH -complex is exited and a charge transfer will occur later on (Equation 2.4), or a Eu^{3+}-Cl^- -complex is exited [9] (Equation 2.5) [12]:

$$EuCl_3 \cdot 3\,R_2CHOH \xrightarrow{228nm} Eu^*Cl_3 \cdot 3\,R_2CHOH \tag{2.4}$$

$$Eu^{3+} - Cl^- \xrightarrow{272nm} [Eu^{2+} - Cl]^* \tag{2.5}$$

The exited complexes are indicated with an asterisk. These have absorbed a photon with the energy that's indicated in the reaction. The exited complexes could lose their energy by emitting light, heat or use it to react to a different species. The latter is the desired one. The electron transfer is already included in the reaction 2.5 as can be observed. [12]

Step 3: Electron transfer. The electron transfer, also called charge transfer, is the process in which the exited complex consumes its energy by transferring an electron from its ligand that could be chloride or methanol. The charge transfer

reactions are shown below, reaction 2.6 is based on methanol (builds on reaction 2.4) and reaction 2.8 is based on chloride (builds on reaction 2.5). [12]

$$Eu^{*}Cl_3 \cdot 3\,R_2CHOH \longrightarrow EuCl_2 + 2\,R_2CHOH + \text{organic oxidation products} + HCl \tag{2.6}$$

The organic oxidation products could consist of ordinary products like methanal (CH_2O), formic acid, CO_2 up to more complex polymers when methanol is used as solvent [33].

$$[Eu^{2+}{-}Cl]^{*} \longrightarrow Eu^{2+} + Cl^{\bullet} \tag{2.7}$$

The reaction products of both reactions consist of radicals ($Cl^{\bullet}$ and organic oxidation products). These radicals are not stable and will immediately react to form a more stable component. There are lots of possibilities which will not be explained in detail since these are by-products of the reactions. [9]

Step 4: Precipitation of $EuCl_2$ Gheeraerts deduced that by using ethanol, isopropanol or mixtures of the two, precipitation of $EuCl_2$ occurs. The solubility is dependent on the type of solvent used. Higher solubility is seen in ethanol compared to isopropanol. It was also observed that no precipitation of $EuCl_2$ occured when methanol was used as solvent for concentration up to 500 mM. The precipitation reaction can be written as follows:[12]

$$Eu^{2+} + 2\,Cl^{-} \xleftrightarrow{K\_sp=f(solvent,water)} EuCl_{2s} \tag{2.8}$$

Step 5: Destruction radicals and reduction of Eu^{3+}. Looking back to reaction 2.8 it is shown that $Cl^{\bullet}$ is formed. $Cl^{\bullet}$ is a radical and tends to be very reactive, as such the following reaction will occur [9]:

$$Cl^{\bullet} + R_2CHOH \longrightarrow HCl + R_2C^{\bullet}OH \tag{2.9}$$

The HCl formed in reaction 2.6 and 2.9 will dissociate and form H^{+}. The formed $CH_2C^{\bullet}OH$ is a very unstable radical since the C is not stabilized by e.g. methyl-groups (like e.g. ethanol is) as such it will be capable to perform the following reaction [12, 9]:

$$R_2C^{\bullet}OH + Eu^{3+} \longrightarrow Eu^{2+} + R_2CO + H^{+} \tag{2.10}$$

The reduction reaction via the $CH_2C^{\bullet}OH$ radical is very advantageous since it's an extra reducing agent for Eu^{3+}. Y^{3+} will not be reduced by the radical as it is not stable in aqueous environments in other oxidation states than 3+. [12]

Precipitation of trivalent metals. When methanol is used as solvent, a mixture of Eu^{2+} and Y^{3+} is left in solution after the reduction of Eu^{3+}. In order to separate them, selective precipitation can be assessed. Dibutylphosphate was selected as it selectively precipitates Y^{3+} in a mixture with Sr^{2+}. Sr^{2+} resembles Eu^{2+} as it has

similar charge densities. The precipitate can be easily centrifuged and separated from the solution. The dibuthylphosphate precipitation was not yet tested with Eu^{2+} in solution. [13] The principle is further assessed in Appendix D.

Photolysis of methanol

Methanol isn't completely resistant to UV-radiation, shown in Figure 2.8.

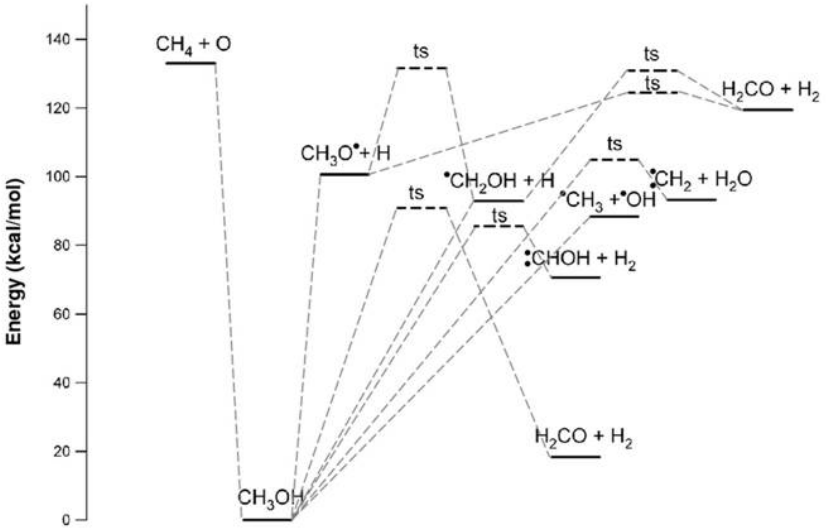

Figure 2.8: Photolysis of methanol. The 'ts' indicates an intermediate form. [34]

The energy on the left axis can be converted to wavelength since E=hν. (e.g. to form the intermediate to $H_2CO + H_2$ light of 317 nm (based upon 90 kcal/mol) is required). [34]

Most of these reaction products will be formed in reaction 2.10 since other radicals can also be the basis of that reaction, thus creating other, more oxidised, products as well. The formation of these other radicals by UV-light doesn't interfere with the reduction of Eu(III), if the formed radicals have a tendency to reduce Eu(III) as well. If they have the tendency to oxidise Eu(II), a reduction in overall reaction speed will be observed.

2.3.2 Photochemical separation in aqueous media

The photochemical separation of Eu was also studied in aqueous media by Van den Bogaert, Van Meerbeeck and Haveaux in previous works. [8, 10, 11] The mechanism is based on the charge transfer (CT) in a $[Eu^{3+}-SO_4^{2-}]$ complex. [8]

Reaction mechanism

The principle reaction mechanism of the reduction of Eu(III) in water is similar to the mechanism in organic media, but with different chemicals that perform the reduction of Eu(III) and a different Eu-salt ($EuSO_4$) is formed.

Step 1: Dissolving and complexing. Step one consists of the dissolution of $EuCl_3 \cdot 6\,H_2O$, since the solvent is water and $EuCl_3 \cdot 6\,H_2O$ is an hydrated salt, a different reaction will occur in this stage. Since sulphate (which will be dissolved as $(NH_4)_2SO_4$) and water will coordinate the Eu^{3+}, the chlorides surrounding it will be dissolved in the water and mostly water and some sulphate molecules will remain. The reaction isn't of big importance and since the exact distribution of sulphate to water molecules surrounding the Eu(III) is not known, the reaction is not described here. [7, 8]

Step 2: Photoexcitation and charge transfer. The next step consists of the excitation of Eu. Since two coordination species are available (water and sulphate), also two reactions will occur. The first one (Equation 2.11 consists of the excitation and reduction via a CT-band of water:

$$[Eu(H_2O)_n]^{3+} \xrightarrow{188nm} [Eu(H_2O)_{n-1}]^{2+} + OH^{\bullet} + H^{+} \tag{2.11}$$

However, a wavelength of 188 nm is very difficult to achieve since the mercury lamps can produce it, but the quartz glass surrounding it in a set-up will totally absorb all wavelengths shorter than 200 nm, other materials can be considered for this purpose.

The second reduction reaction is a couple of 2 redox reactions. Sulphate in solution can break down into a radical and donate the released electrons to a substance that's in the neighbourhood and can reduce. Therefore, the sulphate ions must be in the coordinating sphere of the Eu(III)-ions as they are able to accept the electrons and reduce to Eu(II). It is shown in the couple of redox reactions in Equation 2.12. [7, 8]

$$\begin{aligned} SO_4^{2-} &\xrightarrow{240nm} O^{\bullet}SO_3^{-} + e^{-} \\ Eu^{3+} + e^{-} &\longrightarrow Eu^{2+} \end{aligned} \tag{2.12}$$

Step 3: Precipitating Eu(II). The reduced Eu^{2+} must be separated from the Y^{3+} which is also present in YOX waste streams. Eu^{2+} will undergo precipitation by the sulphate ions in solution by the reaction 2.13.

$$Eu^{2+} + SO_4^{2-} \rightleftharpoons EuSO_{4,(s)} \quad K_{sp} = 1.5 \cdot 10^{-9} \tag{2.13}$$

Since the solubility product of $EuSO_4$ is relatively low, a low concentration of Eu^{2+} will remain in solution as an excess of SO^{2-} is added. [7, 8]

Step 4: Destruction of the radicals and side reactions. A $O^{\bullet}SO_3$ molecule is formed in the reduction step of Eu. The molecule is not at all stable and will react with a water molecule when it encounters one as seen in Equation 2.14.

$$O^{\bullet}SO_3 + H_2O \longrightarrow HSO_4^- + OH^{\bullet} \tag{2.14}$$

These $OH^{\bullet}$ radicals are highly unwanted since they can cause the following reaction:

$$[Eu^{2+*} - {}^{\bullet}OH] \longrightarrow Eu^{3+} + OH^- \tag{2.15}$$

In order to eliminate unwanted oxidation of Eu^{2+}, other organic products are added. Mostly, either isopropylalcohol or formic acid are used as radical scavenger [7, 8]. With **isopropylalcohol** (IPA) the following reactions occur:

$$(CH_3)_2CHOH + OH^{\bullet} \longrightarrow (CH_3)_2C^{\bullet}OH + H_2O \tag{2.16}$$
$$(CH_3)_2C^{\bullet}OH + Eu^{3+} \longrightarrow Eu^{2+} + H^+ + (CH_3)_2CO \tag{2.17}$$

IPA will capture the $OH^{\bullet}$ radicals and will form a radical that will reduce Eu. Via this mechanism, one photon will result in the reduction of 2 Eu^{3+} molecules.

The use of **formic acid** gives rise to the following reactions:

$$CHOOH + OH^{\bullet} \longrightarrow C^{\bullet}OOH + H_2O \tag{2.18}$$
$$C^{\bullet}OOH + Eu^{3+} \longrightarrow Eu^{2+} + H^+ + CO_2 \tag{2.19}$$

But formic acid has a special property compared to isopropylalcohol, it dissociates under the influence of light (Equation 2.20):

$$CHOOH \xrightarrow{260nm} C^{\bullet}OOH + H^{\bullet} \tag{2.20}$$

The two radicals each have their own purpose, the $C^{\bullet}OOH$ is capable of reducing Eu^{3+} and the $H^{\bullet}$ radical can act as radical scavanger for $OH^{\bullet}$, which is formed in Reaction 2.14, shown in Reaction 2.22.

$$H^{\bullet} + OH^{\bullet} \longrightarrow H_2O \tag{2.21}$$
$$2\,H^{\bullet} \longrightarrow H_2 \tag{2.22}$$

The formed H_2 can cause some problems in as large concentrations are formed as hydrogen is extremely flammable and can cause explosions.

Based on all these equations, the use of a scavenger is necessary to avoid that Eu^{2+} is oxidised by the formed $OH^{\bullet}$ radicals. Isopropylalcohol is commonly used as it can be used in more neutral environments (e.g. pH 4) whereby formic acid requires more acidic conditions for it to work (pH 1 and lower). Formic acid acts as a secondary reducing agent for Eu^{3+} which can increase the reaction speed. [7, 8] However the use of formic acid has some drawbacks as well, Eu^{2+} isn't stable in acid environments which will be explained in the next section.

Oxidation reactions of Eu^{2+} The formed Eu^{2+} can re-oxidise to Eu^{3+} in a number of ways, some are already mentioned. Oxidation can occur due to a low pH as H^+ is capable because of its redox potential:

$$Eu^{3+} + e^- \rightleftharpoons Eu^{2+} \quad E_0 = -0.35V \tag{2.23}$$

$$2\,H^+ + 2\,e^- \rightleftharpoons H_{2(g)} \quad E_0 = 0.00V \tag{2.24}$$

But oxidation by H^+ can also be aided with light with a wavelength of 366 nm:

$$2\,Eu^{3+} + 2\,H^+ \xrightarrow{366nm} 2\,Eu^{2+} + H_2 \tag{2.25}$$

Thus a wavelength of 366 nm must be avoided if a lamp with multiple emission lines is used (e.g. a medium pressure mercury lamp (MPML) if possible. And lastly, oxidation via $OH^\bullet$ radicals is possible as well and explained before.

Stability of Eu in aqueous environments

A Pourbaix diagram indicates the stable region of a specific element and what species can be found in aqueous environment. For Eu, it can be seen that the species that is formed in both reaction schemes is only stable in neutral environment (pH 5 to 9) and in very reducing media (in oxygen-free environments) (Figure 2.9). But when the pH is increased to about 7.5, the formation of $Eu_2(CO_3)_3$ kicks in (if enough CO_3^{2-} is present in solution, followed by hydrolysis and formation of $Eu(OH)_3$. It indicates that Eu^{2+} is only stable around pH 5.8 up to 7.5 and in the absence of oxygen. [35]

Kinetics of the overall reaction in batch set-up

Earlier tests done by Van den Bogaert et al. have shown that the light intensity is an important factor to the reaction speed. His results are shown in Figure 2.10.

As shown in Figure 2.10, the irradiance has two effects. One on the induction time, which is the time in which the concentration of Eu in solution remains nearly 100%. In that region, the Eu^{2+} is rising until supersaturation is reached such that crystal formation can start. The second phase will also influenced by the irradiance. The intenser the light, the faster the crystals grow, it is also observed by the slope of the graph. The slope in the second region is nearly linear for all tested irradiances, it implies that a 0th order reaction is taking place at these conditions. The reason for it, is that the reaction is limited by the photon flux, which is relatively constant, resulting in a constant reaction speed.

2.4 Reactor design for solid producing reactors by light

2.4.1 Light efficiency benchmarks in photo-catalytic reactors

For reactors and in particular for photochemical reactors, it is important to indicate some benchmarks which indicate the efficiency and productivity of the reactor.

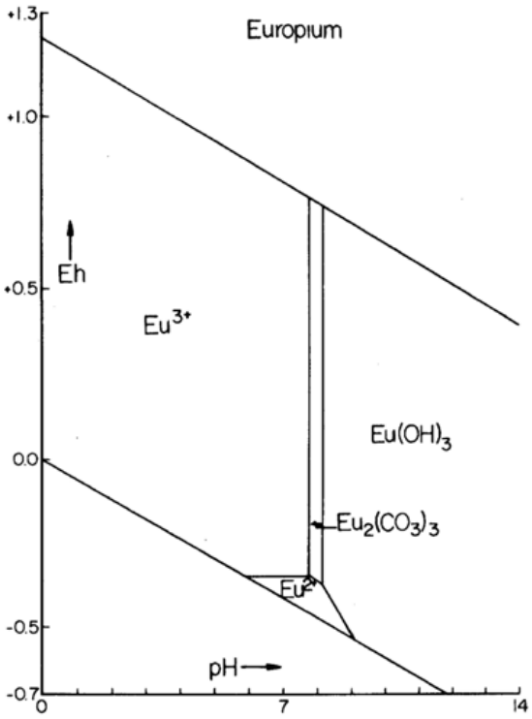

Figure 2.9: Pourbaix diagram of Eu [35]

One of these benchmarks is the **apparent first-order reaction rate constant**, k (min^{-1}), it give a fast indication of the speed at which the reaction occurs. But of course, it is an approximation. If the reaction is photon limited, the order is approximates zeroth order, therefore this benchmark isn't sufficient. It also volume dependent, as such, the benchmark is difficult to use to compare a reaction in two different reactors. [36, 37]

A second benchmark, which is more aimed at photochemical reactors is the **photonic efficiency** which is also called the quantum yield. The formula for it, is the following:

$$Q.E. = z \cdot \frac{Rc}{\phi} \cdot 100 \tag{2.26}$$

With $Q.E.$ being the dimensionless photonic efficiency, z being the amount electrons that are exchanged per molecule that is degraded or converted, R ($mol \cdot L^{-1} \cdot s^{-1}$) is the reaction speed and ϕ is the photon flux ($mol \cdot L^{-1} \cdot s^{-1}$). $Q.E.$ only gives an indication of how efficient the reaction itself is with photons, but it gives no information about the efficiency on reactor basis. [36, 37]

A novel benchmark, introduced by Leblebici et al [36], takes the ratio of space-time yield (STY) over the lamp power (LP) supplied to the reactor and is called the **photocatalytic space-time yield (PSTY)**. The STY is the production capacitiy

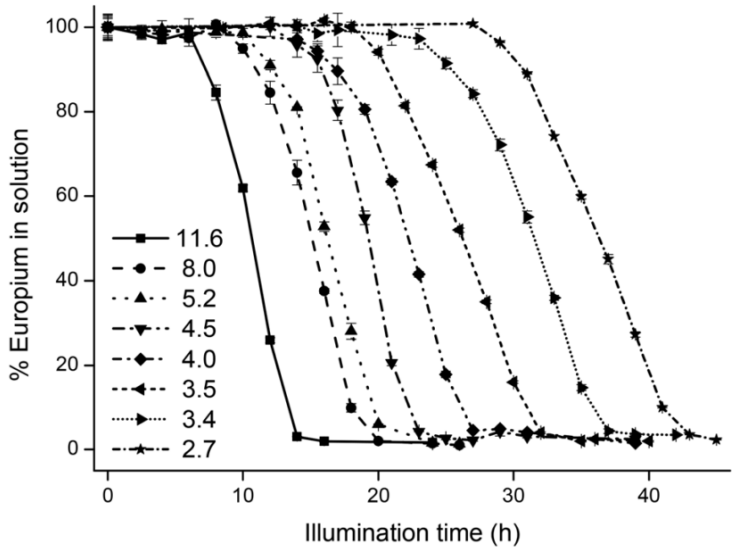

Figure 2.10: Europium removal in $EuCl_3$ (10mM) - $(NH_4)_2SO_4$ (50mM) solution with 20 v% isopropylacolhol in water vs illumination time at different irradiances expressed in $[mW \cdot cm^{-2}]$. The graph is valid for a batch type reactor. [7]

($kg \cdot L^{-1} \cdot day^{-1}$) of the reactor:

$$STY = M_w(\frac{dC}{dt}) \tag{2.27}$$

with M_w ($g \cdot mol^{-1}$) of the product and $\frac{dC}{dt}$ ($mol \cdot L^{-1} \cdot day^{-1}$) being the reaction rate per volume.

As the STY is volume scaled, the LP should also be scaled to a unit volume of the reactor. It is done as follows:

$$LP = P \cdot \frac{1L}{V} \tag{2.28}$$

with LP (W) being the standardized lamp power, P (W) the power of the lamp used in the reactor and V (L) the volume of the reactor.

The PSTY is the fraction of STY over LP which is:

$$PSTY = \frac{STY}{LP} \tag{2.29}$$

The newer benchmark takes the reactor set-up as well, which wasn't taken into account in the other benchmarks. As such, the PSTY can be improved by specifically irradiating the reactor with more efficient lightning more targeted at the wavelength needed in the reaction. The local volumetric rate of radiative energy absorption (LVREA) also affects the PSTY, it can be considered as the energy that is absorbed by the reactants in space dimensions. Furthermore, the outward photon flux, which can be influenced by the absorptivity of the reactants has a contribution in the

PSTY. The mechanism, which is also in the quantum efficiency, contributes to PSTY. And lastly, the presence of solids, which might disperse the light and reflect it back outwards, also have an influence. [36, 37]

2.4.2 Solid handling in tubes

For slurry transport, as it is called for liquid-solid transport, a few factors have to be considered to determine the flow regime such as the Pipe Reynolds Number (Re), the Particle Reynolds Number (Res), particle properties (shape, size, density, distribution), solid concentration and the direction of flow. Other aspects are the increase in viscosity with increasing concentration of solids. For solids particles larger than 50 μm they follow Newtonian slurries (constant viscosity as function of shear rate and stress) up to 25 v/v%. [38, 39]

The Reynolds Number for the tube and the particles are shown below:

$$Re = \frac{\rho_{fluid} \cdot u_{fluid} \cdot d_{tube}}{\mu_{fluid}} \tag{2.30}$$

$$Re_s = \frac{\rho_{fluid} \cdot u_{particle} \cdot d_{particle}}{\mu_{fluid}} \tag{2.31}$$

Very fine particles with $Re_s < 10^{-6}$ will not settle due to Brownian motion and is called a colloidal dispersion. For particles with $10^{-6} < Re_s < 0.1$ little turbulence is required to keep the particles suspended and is called homogeneous flow. For particles $0.1 < Re_s < 2$ more turbulence is required as they tend to settle even faster, segregation in horizontal tubes will be present in these regimes and is called pseudo-homogeneous flow regime. And lastly for particles with a $Re_s > 2$, segregation is larger and the regime is called heterogeneous flow, saltation will occur as velocity drops below the critical deposition velocity. Durand classifies homogeneous ($Re_s \leqslant 0.1$), pseudo-homogeneous ($0.1 < Re_s < 2$) and heterogeneous ($Re_s > 2$) flow behaviour for particle concentration below 25 v/v%. [38]

In order to keep the solids in the stream, the slurry velocity has to be higher than the settling velocity of the particles. The behaviour is shown in Figure 2.11. On the x-axis, the velocity of the slurry is shown and on the y-axis the pressure drop in manometric head. The minimum of the curves is indicated, it is the point on which the solids start to block the reactor by settling down due to the low flow rate. As the flow rate decreases even further, the entire tube is filled up even more as particles will clump together to form plugs (as seen in pneumatic transport) which will induce an higher pressure drop. High flow rates will disperse the particles well and the pressure drop will not deviate much from that of pure water.[38, 39]

The same source [39] indicates that as the diameter of the tube decreases, the critical velocity (whereby the solids settle) lowers. It can be explained by wall phenomena (shear flow by the wall which results in more turbulent flow). As the particle size decreases, the critical velocity decreases as well as their settling velocity decreases. Friction losses resulting in pressure drops are not considered here.[39]

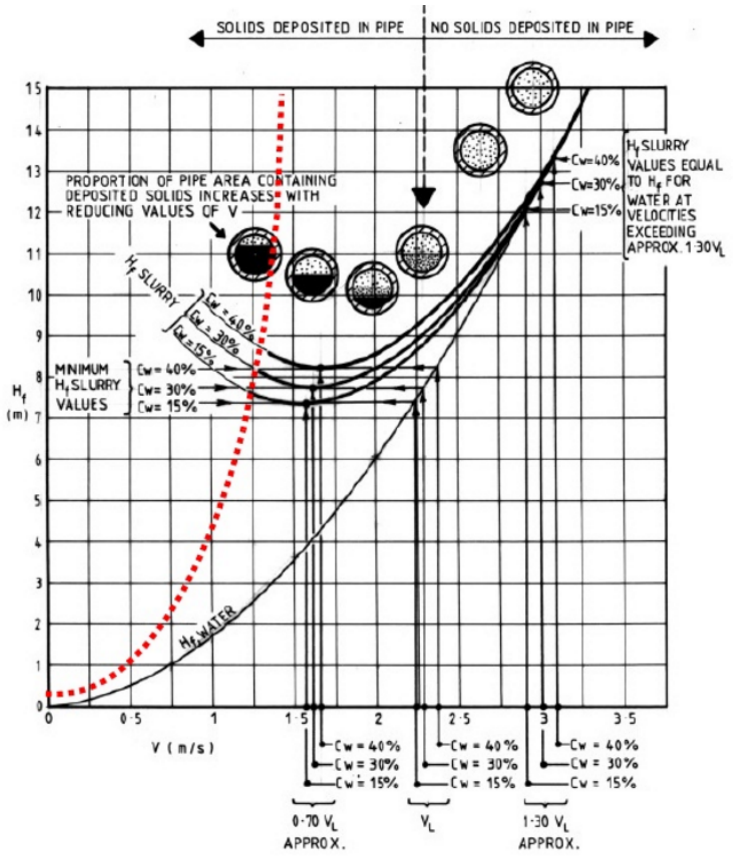

Figure 2.11: Slurry conveying in piping systems [39] On the x-axis, the velocity of the slurry is shown and on the y-axis the pressure drop in manometric head.

A formula was obtained to calculate the settling velocity of particles. The formula by Durand is the following [39]:

$$v_C = F_L \sqrt{2 \cdot g \cdot d \cdot (S_g - 1)} \tag{2.32}$$

Durands formula was later modified by Wasp to correct for the particle size, which results in the following equation [40]:

$$v_C = F_L \sqrt{2 \cdot g \cdot d \cdot (S_g - 1) \cdot (\frac{d_p}{d})^{1/6}} \tag{2.33}$$

with v_C the critical velocity (m/s), F_L limiting settling velocity factor as seen in Figure 2.12, g the gravity constant (9.81 $m \cdot s^{-2}$), d the diameter of the tube (m), S_g the specific gravity of dry solids ($\rho_{solids}/\rho_{water}$) and d_p the diameter of the particles (m). It is valid for sub mm size particles, but can give an indication for μm size particles.

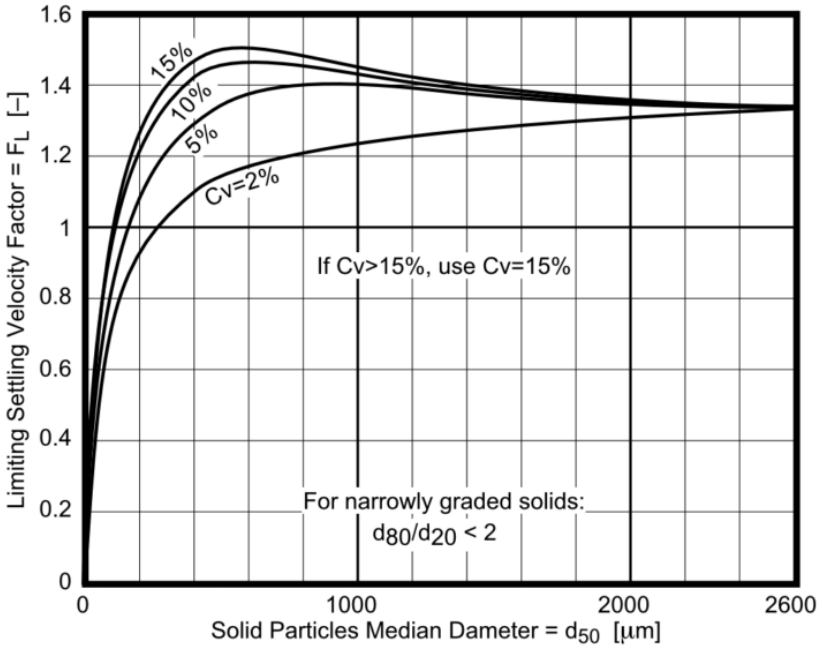

Figure 2.12: Durands limiting settling velocity graph for particles ranging from 0 up to 2600 µm in size with a very narrow particle size distribution and a concentration of 2 to 15 v/v%. [41]

2.5 Conclusions

The REEs are an important group in the table of Mendeljev that is overlooked most of the times. REEs have many applications, such as magnets, fluorescent lamps and applications in nuclear facilities.

Nowadays, China is a big producer of REEs, LREEs and HREEs, which implies that the US and EU are mostly dependent on China for supply of REEs. Chinas monopoly has created a supply risk for the US and EU that can have major implications. Also during the last decades a shift in demand from mixed REEs to a demand for very specific elements which has resulted in the 'balance problem'. The 'balance problem' can be reduced by recycling these specific elements for which demand is high in the various applications in which they are used, lamp phosphors is one of them.

Separation of REEs is very difficult since most REE(III)s have similar properties which result in exploiting the minor differences between the REEs. Various techniques can be used for separating REEs and solvent extraction is the most commonly used.

Photochemical separation is a technique for separation of Eu from mixtures of Eu and Y that is studied before by Van den Bogaert et al. The reaction scheme for separation in organic and aqueous media are based on a charge transfer from a ligand to Eu(III), resulting in the reduction of Eu(III) to Eu(II), followed by precipitation

of Eu as a salt.

In order to estimate how efficient photo-reactors use their light, several benchmarks are introduced, such as apparent first order rate constant (for the reaction rate), quantum yield (reaction level) and a novel one: photocatalytic space time yield (PSTY). All these parameters can be used to optimize a reactor geometry and feed concentration for optimal light utilisation.

Solid precipitation in tubes is dependent on the flow rate and a critical flow rate can be determined for which solids will start to deposit in the tube.

Chapter 3

Materials and Methods

In Appendix D and Chapter 5, two kinds of experiments can be found. In Appendix D, separation of Eu and Y was assessed in organic media, the method involved photochemical separation (as seen in Section 2.3.1) split up in two parts, a photo-reduction step of Eu and a precipitation step of Y. The principle was tested in a batch reactor. Further assessment, as can be read in appendix, showed that the principle is not usefull for the separation of Eu and Y.

Chapter 5 uses separation of Eu and Y in aqueous environment (as shown in Section 2.3.2). Batch results for this separation are already available, thus the focus shifts from a batch reactor to a continuous reactor to increase productivity and efficiency.

The materials and methods for experiments in organic media will be introduced first, followed by the materials and set-up used the aqueous media experiments. This section not only describes how these solution were prepared, but also their important characteristics, wherever needed. These characteristics are required to set up a model for photo reactors as seen in Chapter 4.

3.1 Materials for organic media experiments

$EuCl_2$, $EuCl_3$ and YCl_3 stock solutions The stocksolutions which are used in Chapter D are produced by dissolving an appropriate amount (10 mM) of $EuCl_2$, $EuCl_3 \cdot 6\,H_2O$ and $YCl_3 \cdot 6\,H_2O$ in pure methanol. The $EuCl_2$, $EuCl_3 \cdot 6\,H_2O$ and $YCl_3 \cdot 6\,H_2O$ are all from Sigma Aldrich and the methanol that is used has a quality of 99.99% and is purchased from Merck.

For further applications, the absorbence spectrum is required to use the correct light to perform the the desired reaction (reduction of Eu^{3+}). The spectrum is shown in Figure 3.1 for the 10 mM of $EuCl_3 \cdot 6\,H_2O$ dissolved in methanol without further additives as this is the solution which will be irradiated and a charge-transfer band is present which reduces Eu^{2+}. It is shown that the absorbance peak related to the CT-band is visible from 260 up to 290 nm with its maximum at 275 nm. The maximum absorbance for this particular solution at 275 nm is equal to 1.63.

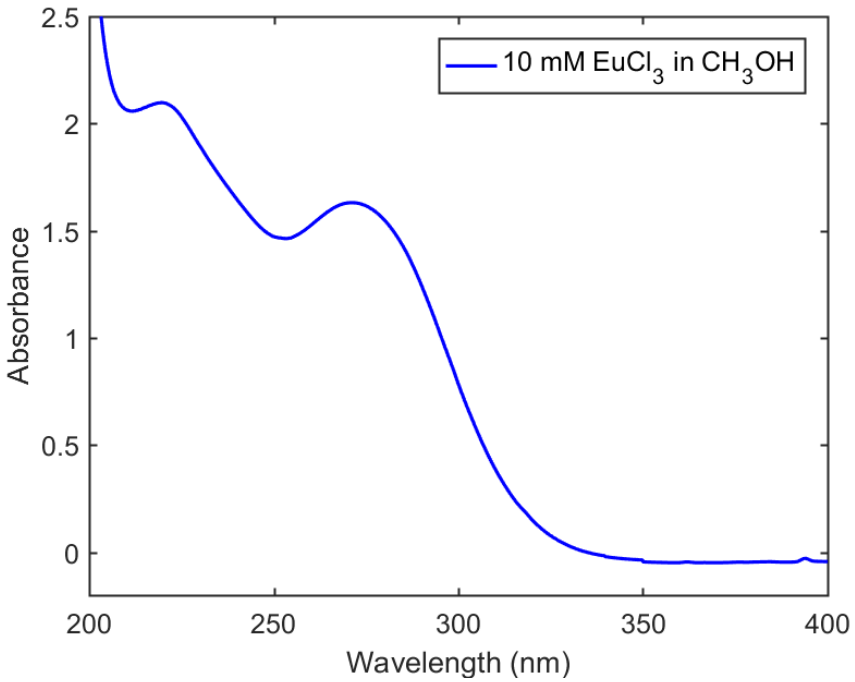

Figure 3.1: Absorbance of $Eu^{3+}-Cl^-$ in methanolic environment.

HDBP stock dibuthylphosphate (HDBP) is purchased from Sigma Aldrich and has a purity of 97%, it is used in several experiments to precipitate Y^{3+} from solution.

NaDBP NaDBP is produced by neutralising dibuthylphosphate (HDBP, 97% Sigma Aldrich) with NaOH (Sigma Aldrich) and carefully checking the pH with a pH meter. The addition of HDBP was stopped at pH 7. The solution was evaporated afterwards in an oven at 110 ℃ for a day. The crystals were later dissolved in MeOH to obtain a 1 M solution/dispersion.

3.2 Materials for aqueous media experiments

Eu stock solution For the aqueous experiments, the solutions used in the reactor contain slightly more additives. For a solution containing 10 mM $EuCl_3 \cdot 6\,H_2O$ (3.664 g/L $EuCl_3 \cdot 6\,H_2O$) (Sigma Aldrich), also 50 mM of $(NH_4)_2SO_4$ (6.607 g/L $(NH_4)_2SO_4$) (VWR) is added as well as 20 v/v% 2-propanol (Sigma Aldrich).

The $(NH_4)_2SO_4$ is dissolved in half the volume of water (milli-Q quality, resistance of 18.2 MΩ) necessary for the solution. The pH of the solution is adapted to pH 5 by adding a small quantity of HCl (Sigma Aldrich). The next step is to add the $EuCl_3 \cdot 6\,H_2O$ to the solution and mix well till everything is dissolved. The pH is checked once more and adapted to pH 4.0. and more milli-Q water is added and 20 v/v% of

the total volume of 2-propanol (Sigma Aldrich) is added. The solution is poured in a flask of appropriate volume and milli-Q water is added up to the mark.

Also for this solution, the absorbance spectrum is measured and shown in Figure 3.2. As compared to Figure 3.1, the wavelength to perform the charge transfer is shorter in this case (i.e. more energy per charge transfer is required). For aqueous Eu, the absorbance peak linked to the CT-band of Eu(III) is seen at 240 nm with an absorbance of around 0.9. As shown on Figure 3.2, it is the SO_4^{2-} ion in combination with Eu^{3+} that cause the absorption of light. The lower absorbance in the aqueous solution indicates that the methanolic reaction might be slightly more light efficient due to the higher specific absorbance.

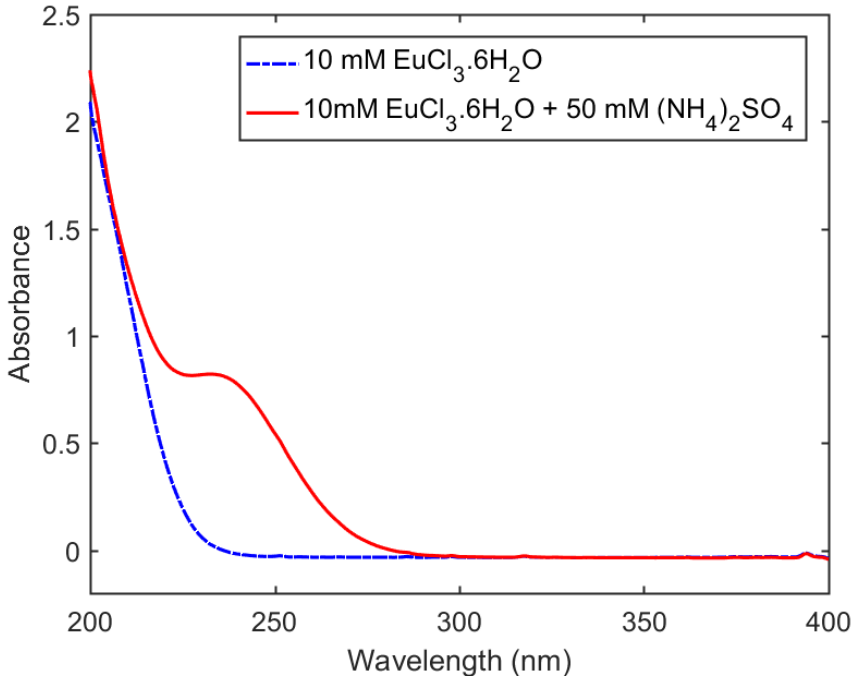

Figure 3.2: Absorbance of $Eu^{3+}-SO_4^{2-}$ in aqueous environment at pH=1 [8]

Artificial YOX stock solution YOX in the lab (supplied by Osram) has a composition of 9 m% Eu_2O_3 and 91 m% Y_2O_3. To produce artifical YOX with a composition similar to real YOX and a concentration of 10 mM Eu^{3+} (3.664 g/L $EuCl_3 \cdot 6\,H_2O$) (Sigma Aldrich), 212 mM Y^{3+} (64.38 g/L $YCl_3 \cdot 6\,H_2O$) (Sigma Aldrich) is required. To these two elements, 50 mM of $(NH_4)_2SO_4$ (6.607 g/L $(NH_4)_2SO_4$) (VWR) is added.

The preparation method is the same as for the Eu stock solution in that difference that the $YCl_3 \cdot 6\,H_2O$ is added to the mixture at the same moment as the $EuCl_3 \cdot 6\,H_2O$.

YOX stock solution As the YOX (Osram) has a composition of 9 m% Eu_2O_3 and 91 m% Y_2O_3, only 6.4302 g/L is required for a 10mM solution of Eu.

To prepare this solution, YOX is weighed and put in a small test-tube. To this tube, 4 M of HCl (Sigma Aldrich) is added (10/1 v/m ratio). The solution is shaken for 24 hours till the solution is clear and fully transparent. Excess HCl is neutralized by the addition of NaOH till pH 2. 50 mM of $(NH_4)_2SO_4$ (6.607 g/L $(NH_4)_2SO_4$) (VWR) is added. The pH is checked and adjusted by adding NaOH (Sigma Aldrich) until pH 4 is reached. More milli-Q water is added and 20 v/v% of the total volume of 2-propanol (Sigma Aldrich) is added. The solution is poured in a flask of appropriate volume and milli-Q water is added up to the mark.

3.3 Experimental set-up

Three types of experimental set-ups involving reactors were used. One containing a batch type of reactor for experiments in organic media, one containing a tubular reactor and one containing a modified tubular reactor, both for experiments in aqueous media. The reactor set-ups are constructed in a black box to prevent UV-light from escaping to the environment causing harm.

3.3.1 MPML batch set-up

A batch set-up is used in the experiments in organic media (methanol). The set-up consists of a quartz double walled reactor, cooled to 10 ℃, placed above a medium pressure mercury lamp which is cooled by a cooler set to 10 ℃. A filter is placed in between the reactor and lamp to prevent side reaction (oxidation of Eu^{2+} at 366 nm) from happening. The filter only transmits light at 270 nm (with a full width at half maximum (FWHM) of 10 nm). The spectrum of the lamp can be found in Figure 3.9 and the spectrum with the filter in between is seen in Figure 3.4. The reactor is placed 2 cm above the cooling of the lamp to have the highest intensity without having the risk of the reactor medium to warm up by the lamp or the filter (placed underneath the reactor) to be damaged. In total this distance is equal to 4.7 cm from the center of the lamp due to the cooling jacket around the lamp. The charge transfer of $[Cl^- - Eu^{3+}]$ (reduction reaction of Eu) takes place at 272 nm. The absorption of that specific wavelength is monitored by a spectrometer probe that is placed above the reactor. The set-up is shown in Figure 3.3. The cooling jacket and reactor were custom made by the university using quartz glass especially for this purpose.

3.3.2 LPML tubular reactor set-up

The second reactor type is a tubular reactor. The reaction that takes place is explained in Section 2.3.2. In this reactor Eu^{3+} will be reduced to Eu^{2+} by a charge transfer with SO_4^{2-} and immediately precipitate as $EuSO_4$. For this reason, it is important to use a material that is transparent to UV-radiation at 240 nm (CT-band). To prevent clogging, it might be usefull to have a sleek surface.

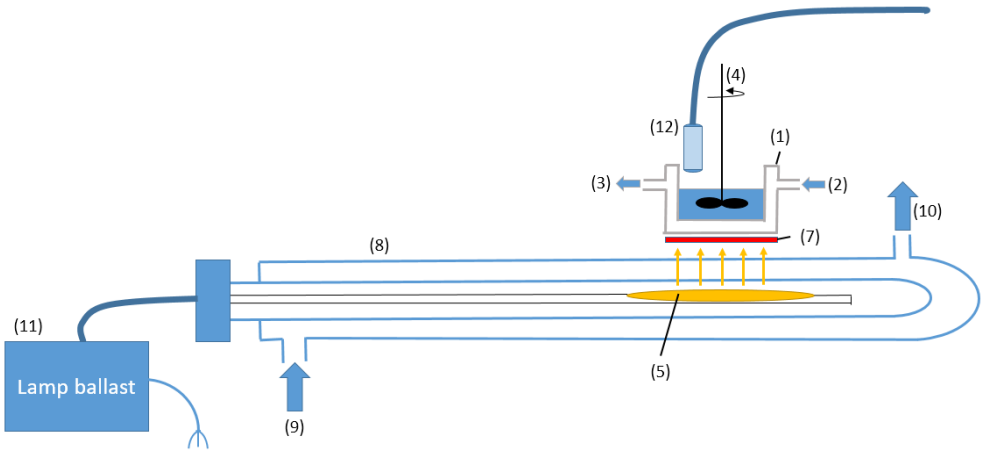

Figure 3.3: Reactor set-up for experiments with organic media. The reactor (1) is made up of quartz and liquid cooled (2) and (3), the content is mixed (4) at 50 rpm for the duration of the reaction. A medium pressure mercury lamp (5) powered by a lamp ballast (11), cooled as well (8), (9) and (10), is placed below and a filter (7) that only transmits 270 nm light is placed in between (showed in red). Above the reactor, a spectrometer (12) is placed to monitor the absorption of light by Eu.

Therefore the reactor material that was selected is the following; PFA, which stands for perfluoroalkoxy alkanes, and consists of PTFE (Polytetrafluoroethylene) copolymerized with perfluoroethers. The structure of this polymer is shown on Figure 3.5.

This material is reasonably transparent to UV-radiation, making it a suitable material. An alternative is quartz as it is fully transparent to radiation with a wavelength over 210 nm, but this is not so easy to handle and to make small tubes out of it.

In Figure 3.6, a sketch of the complete reactor set-up is shown. The construction consists of a tubular reactor (9.4 m in length, 3.0 mm outer diameter, 1.4 mm inner diameter and a wall thickness of 0.8 mm) coiled around a coiling jacket (34 mm in diameter) for the UV-lamp which is put inside the coiling jacket.

The LPML is U-shaped and consists of 2 tubes with a radius of 7.15 mm capped with a turn which has a major radius of 10.35 mm. The distance between the legs is equal to 6.4 mm. In total, the total length of the lamp is 242 mm and a width of 35 mm and a height of 14.3 mm.

In this configuration, the reactor is as close to the lamp as possible. It can also be observed that a lot of coils are made, this is done to maximize the use of the UV light emitted by the lamp. The coils are positioned without spacing in between them. The total width is 135 mm. The outer diameter of the cooling jacket is 68 mm and will be used to determine the light intensity. The total amount of coils is 44.

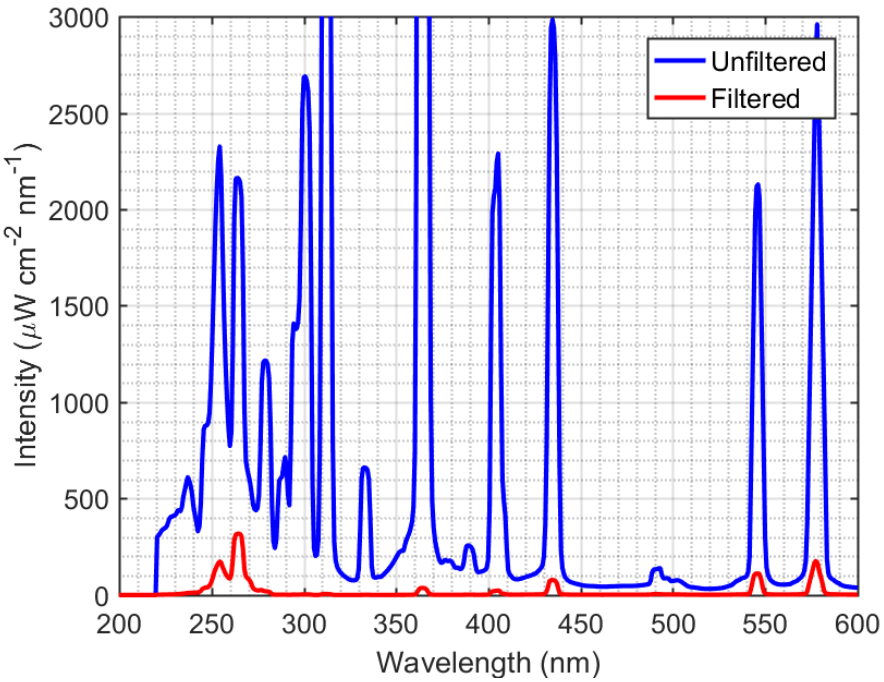

Figure 3.4: Overview of the spectrum of the MPML measured by the spectrometer as indicated on the sketch in the setup without reagent in the reactor. The spectrum is clipped at 600 nm as peaks with higher intensity are not observed. The spectrum is clipped at 3000 $\mu W cm^{-2} nm^{-1}$ to improve readability, the peak at 365 nm is the highest, peaking at 13400 $\mu W cm^{-2} nm^{-1}$. The maximal transmittance of the filter in the region of 270 nm is 17%.

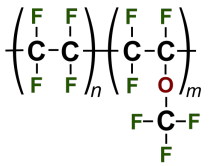

Figure 3.5: Structure of PFA [42]

3.3.3 LPML tubular reactor set-up in pulsed operation

Later on, some pulsed flow experiments will be performed with the setup described in Section 3.3.2. To do this, some adjustments were made regarding the pump. The power cable of the pump is split and the electric circuit that was build is shown in Figure 3.7.

The arduino in the scheme is an Arduino uno, the transistor is a pnp type and the relay is one that can handle 230V (AC) and is operated at 12V. The arduino uses a 'blink' program to switch the output from on to off and back again. This code

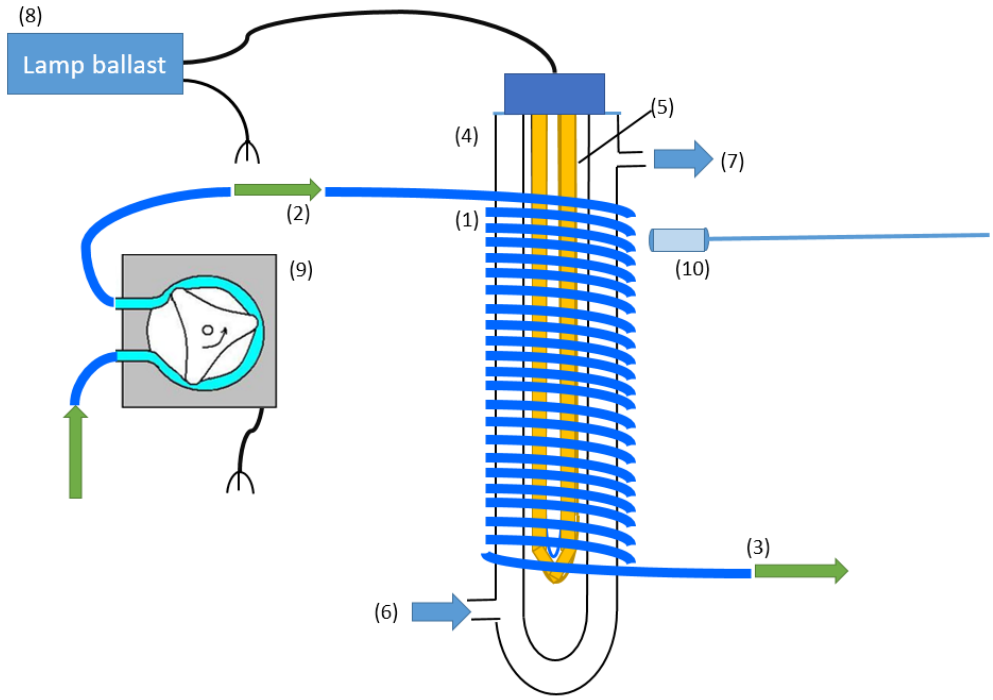

Figure 3.6: Set-up used for the aqueous experiments. In the middle, a lamp (5) (in yellow) connected to the lamp ballast (8) is shown, surrounded by a cooling jacket (4). The jacket is fed with cooling water (6 and 7) and the direction of flow is shown with blue arrows. The blue tubing around the tube is the reactor (1), it is fed from above (2 and 3), the direction of flow is shown by the green arrows. De flow is provided by a peristaltic pump (9). A spectrometer (10), indicated in the sketch can be used in some experiments and positioned where necessary.

is shown in Appendix B.1.

The time as seen in the code is in milliseconds and will be altered to obtain exactly the time required for the experiment. This time will however be different as the required time. Observations have determined that the pump functions longer than the on-time defined by the arduino, probably due to capacitors which load faster than they drain power. Therefore the pump flow rate will be measured and this calibration is used to set the appropriate time in the arduino code.

3.4 Experimental procedures

3.4.1 Experiments in methanolic media

As mentioned, the reactor is used in the organic media (methanol) experiments. Firstly, the cooling for the reactor has to be put on some time before to start the

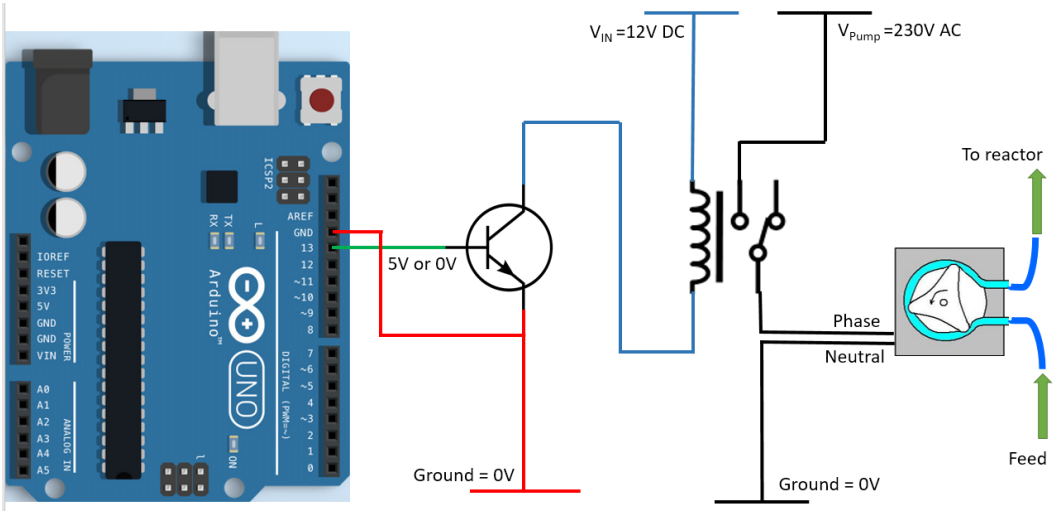

Figure 3.7: Electrical scheme of power supply to the peristaltic pump to achieve pulsed operation. The arduino uses the 'blink' program to make the pulse.

experiment in order to reach 10 °C which is the desired temperature for both the lamp cooler as the reactor cooler. This temperature eliminates methanol evaporation from the test solution. Next, 18.3 mL of 10 mM $EuCl_3$ is introduced in the batch reactor via a pipette. This amount of solution results in a liquid height of 15 mm. The liquid is stirred by a mixer at 50 rpm for the duration of the experiment. The rotor of the mixer is approximately two thirds of the diameter of the reactor. Next, the spectrometer is positioned right above the reactor to monitor the absorption of light. Once that has been done, the dark box is closed and the lamp is turned on for the specified time. After this time, the lamp is turned off and a sample is taken. To this sample, the necessary products (HDBP or others) were added to test the separation of Eu from Y (when it is present) in solution. Afterwards the modified sample is centrifuged at 4000 rpm for 3 minutes, the supernatans is decanted and prepared for analysis by TXRF. For this, the sample is diluted and internal standard (Sm) is added.

The results of the experiments in methanolic media presented in Appendix D.

3.4.2 Experiments in aqueous media: Continuous flow experiments

This reactor is used for the separation of Eu and Y in aqueous environment. These tests are explained in Chapter 5. The reactor is operated by cooling the reactor by process cooling water in this case which has a temperature dependent on the weather and is equal to 10-20 °C. Next, the solution is prepared which has to be pumped through the reactor which is described in Section 3.3.2. This solution is put into a beaker and put next to the peristaltic pump. Once everything is prepared, the dark box, containing the lamp and reactor, is closed and the lamp is turned on. The

pump is set to the correct setting (rpm) and started. From here on, three retention times is waited until steady state is achieved. Afterwards, a sample is taken on the outlet of the reactor which is centrifuged immediately at 4000 rpm for 3 minutes. The supernatans is decanted and analysed by TXRF using Sm as internal standard afterwards.

3.4.3 Experiments in aqueous media: Pulsed flow experiments

The reactor in pulsed operation is operated in the same way as described in Section 3.3.2, but the arduino program has to be correctly programmed to achieve the correct pulsation. Afterwards, samples are taken in the same manner as in the aqueous experiments and analysed by TXRF afterwards.

3.5 UV-Lamps

UV-light is essential for the photoreduction of Eu^{3+} to form Eu^{2+} which is further used in either one of the reaction schemes, the organic scheme can be found in Appendix D but led to unsatisfying results and the scheme in aqueous media is found in Chapter 5. For the UV-lamps, two sources are used, each with different purposes. These are the low pressure mercury lamp (LPML) and medium pressure mercury lamp (MPML), these lamps are used in the set-ups explained in Section 3.3. The MPML will be used in the reactor for the assessment of separation of Eu and Y in methanolic media. The LPML will be used in the set-up for separation in aqueous media as it is more selective in its output of 254 nm. The main difference between these two are the light intensity and the spectrum. Both lamps are supplied by UV Technik Speziallampen GmbH.

3.5.1 Low pressure mercury lamp (LPML)

One type of low pressure mercury lamp (LPML) was used in further experiments. This is a 60 W U-shaped lamp. The lamp has a length of 242 mm (225 mm without the U-bend). The diameter of the tube is 14.3 mm and the 2 legs of the U-shaped tube have a total width of 35 mm (distance between the two legs is 6.4 mm).

The LPML has 2 main output lines, one at 185 nm and one at 254 nm. The first output line is cut off since the lamp is constructed from a type of quartz glass. This quartz permits the 254 nm light to pass though. The lamp is hooked up with a ballast which can power 40 up to 150 W lamps also from UV-Technik. The irradiance output of the lamp is shown on Figure 3.8, this is measured at 37 mm from the central axis of the lamp.

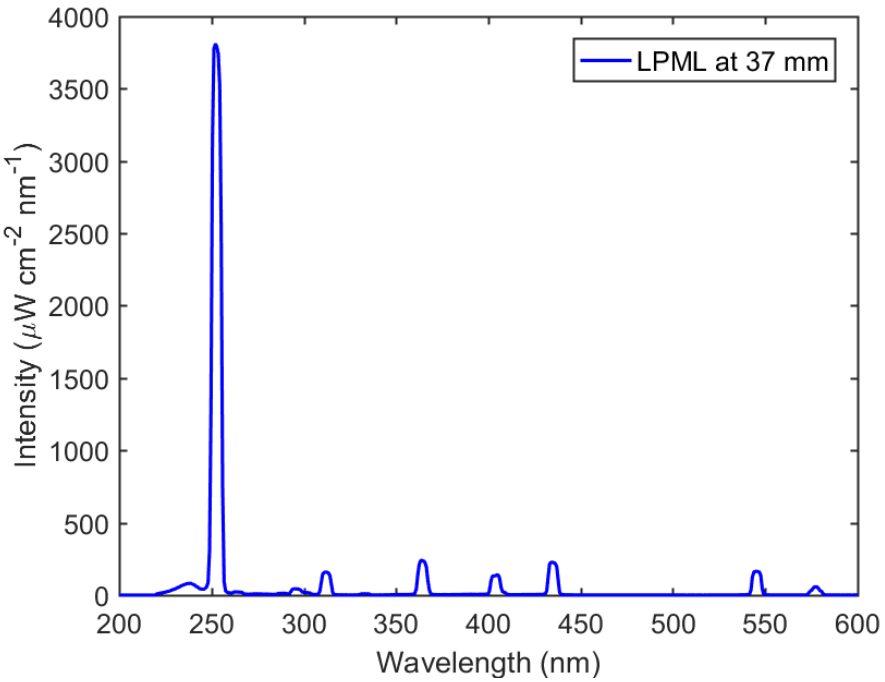

Figure 3.8: Irradiance of LPML measured at 37 mm

This lamp is used for the reactor set-up used in Chapter 4 and described in Section 3.3.2 and is for this purpose surrounded by a cooling jacket to avoid heating the lamp and the reactor.

3.5.2 Medium pressure mercury lamp (MPML)

A second lamp used in this work is a medium pressure mercury lamp (MPML). This type of lamp has a lamp output of 700 W and is of type TQ 700. The lamp glass is made of 99.9% quartz of type RQ 200 which is comprised of a very viscous type of quartz. This makes sure the lamp can handle the very high energy output in terms of light and heat.

The main output of this lamp is at 366 nm and has multiple other output lines. The lamp is surrounded by a quartz cooling jacket to prevent it from overheating. The spectrum of the lamp source can be found in Figure 3.9, the spectrum was measured at 37 and 47 mm from the lamp axis and when the lamp was surrounded by its cooling jacket.

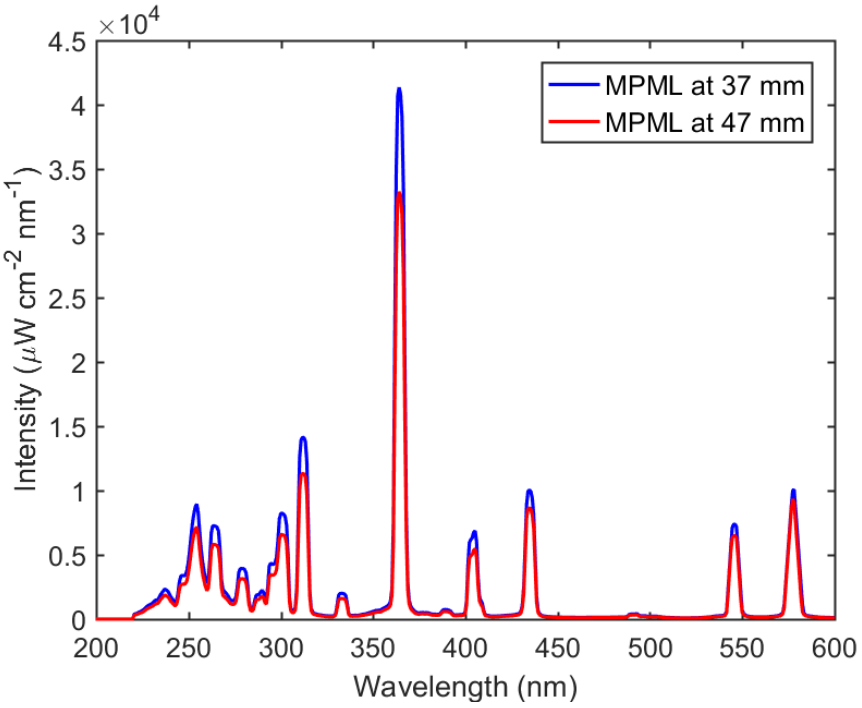

Figure 3.9: Irradiance of MPML measured at 37 and 47 mm

This lamp is used in early experiments in conjunction with a filter that only permits light of a wavelength of 272 nm to pass (with a FWHM (full width at half maximum intensity) of 10 nm).

3.6 UV-VIS spectrometry

UV-Vis spectrometry refers to the measurement in absorbance or transmittance of a certain solution or material. For this, light from the visible up to near infra-red as well as the ultraviolet region is used as both can be important to certain applications.

For the purpose of this thesis, it is important to indicate the position and magnitude of the absorbance bands of Eu in different environments (methanol or water with additives) that are linked to the CT-band.

3.6.1 Principle

A scheme of a spectrometer is shown in Figure 3.10. The spectrometer consists of two lamps, one able to produce UV light (a deuterium lamp in most cases) and the other able to produce visible light (a tungsten lamp). A collimated part of the light is obtained by sending it through a slit. The light is split into its constituent wavelengths by a grating or a monochromator. A half mirror splits the beam and sends it to a reference cuvette to determine the intensity where no absorption occurs

(I_0) and a second fraction is sent to the sample cuvette to determine the light intensity after absorption (I). This is done for all wavelengths possible, this is for 200 nm up to 400 nm in UV region and 400 nm up to 800 nm in the visible region and near infra-red. [43]

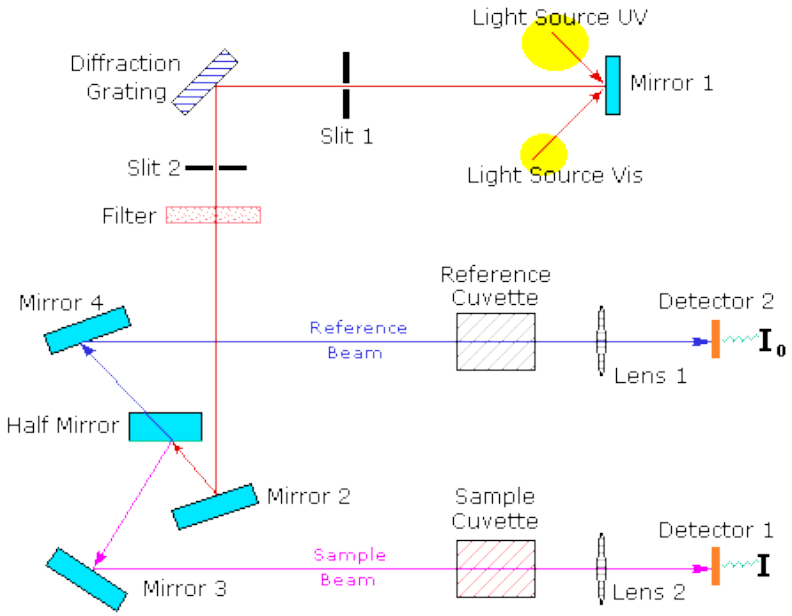

Figure 3.10: Scheme of a spectrometer [43]

The principle on which UV-Vis is based upon is energy absorption, more specifically about energy absorbtion by σ-, π-electrons or non bounding electrons which can jump to different energy positions. The less energy an electron requires to jump between different energy states, the higher the wavelength is. [43]

The law of Lambert-Beer permits to determine the concentration in a certain solution if the molar absorptivity and pathlength are known. This law is presented in Equation 3.1 [44, 45]:

$$A = \log_{10} \frac{\phi_e^i}{\phi_e^t} = -\log_{10} T = \log_{10} \frac{I_0}{I} = \varepsilon \cdot l \cdot c \tag{3.1}$$

With A the absorbance, Φ_e the light flux (i incoming, t transmitted) and T being the transmittance of the material. I_0 the incoming light intensity, I the intensity of the light leaving the solution, ε ($L.mol^{-1}.m^{-1}$) the specific absorbance of the species in solution, l (m) the length of the path the light travels and c ($mol.L^{-1}$) the concentration of the absorbent species in solution. This absorbance is in most cases wavelength (or frequency) dependent. [43]

3.6.2 Procedure

UV-Vis spectroscopy is used in this work to define the position of the CT-bands of Eu in different complexes (in water and methanol). The equipment used, is a Varian Cary 50 UV/Vis spectrophotometer. This equipment is limited to absorbances of 2, more than this will lead to large errors since it means that 99% of the incoming light is absorbed. Dilution is required if the absorbance is higher than 2.

The sample is put into quartz cuvettes with a pathlenght of 1 cm. The absorbance is measured and a quartz cuvette with ultrapure water is taken as reference.

3.7 Total reflection X-Ray Fluorescence (TXRF)

Total Reflection X-ray Fluorescence (TXRF) is mostly used in this thesis to measure the concentration of europium and yttrium in certain experiments. TXRF is capable of measuring the concentration of all elements in solution starting from sodium (z=11). [46, 47]

3.7.1 Internal standards in TXRF

For the measurement to be accurate in TXRF, an internal standard is necessary since the sample preparation has a high influence. Therefore, the measured intensity of the fluorescent rays emitted by the sample are compared to another element introduced in the sample. For this purpose, gallium (for yttrium) and samarium (for europium) are used.

Gheeraerts et all. previously determined that samarium is a good internal standard to measure europium since the mass attenuation coefficient (μ/ρ) are quite similar as shown in Figure 3.11. Gallium is more adequate for measurements of yttrium. [12]. The mass attenuation coefficients as depicted in the figure are similar to specific absorbances in UV-Vis spectrometry, but with the main difference being the type of radiation. The absorption edges as they are called are located at the exact energy required to eject an electron from a specific shell (K,L,M,N...). Photons with energies below the minimal energy for ejection are not absorbed by the electron of the specific shell. Photons having a slightly higher energy are absorbed and the difference between the photon energy and minimum ejection energy is used as kinetic energy of the ejecting electron. [48]

3.7.2 Principle

For TXRF analysis, a S2 Picofox from Bruker is used. An x-ray tube is mounted in the device to produce x-rays of a specific wavelength and energy. The target of the tube is composed of molybdenum. A multilayer monochromator is used to select a specific x-ray line. TXRF is slightly different from XRF in the manner of it use of x-rays. The incident angle of the x-rays is very low compared to XRF. In TXRF the angle is set at about 0.05°. The very low angle has the advantage that not too

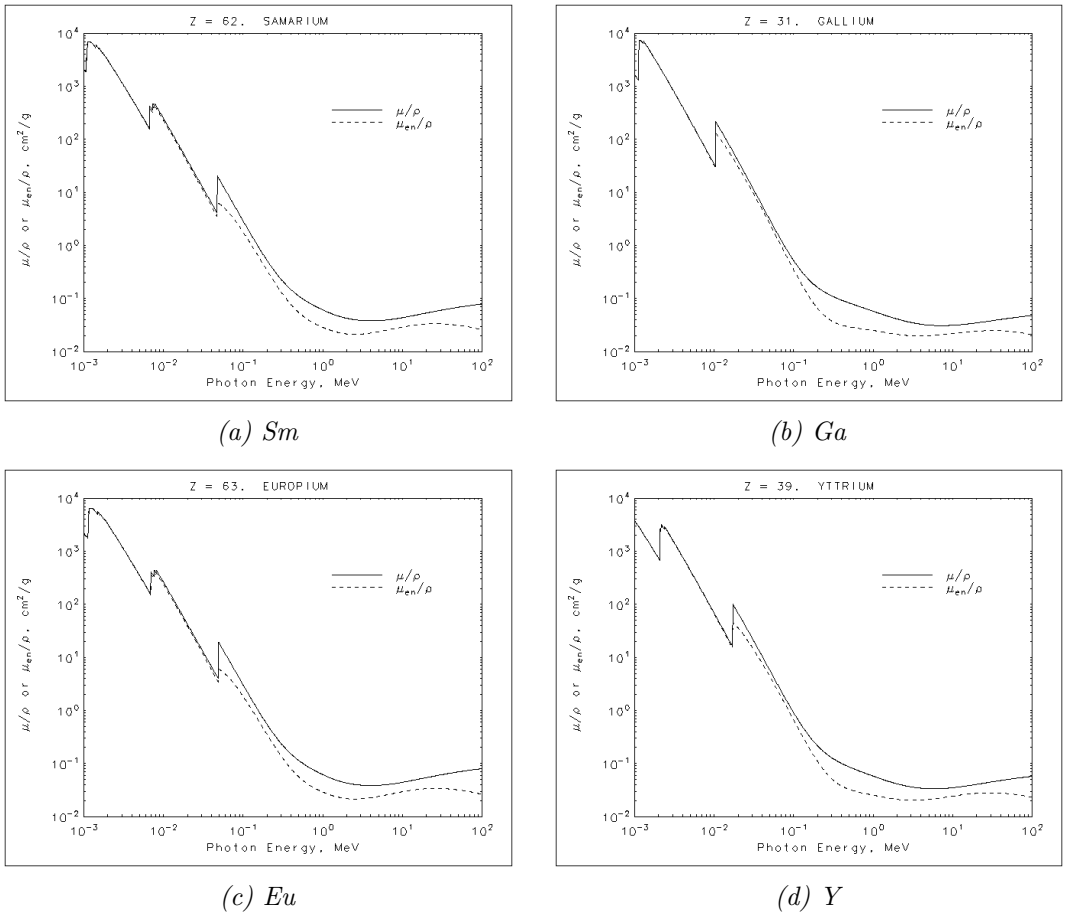

(a) Sm *(b) Ga*

(c) Eu *(d) Y*

Figure 3.11: Mass attenuation coefficients for Sm, Ga and Eu [49]

much of the target x-rays (from the molybdenum target) reaches the detector. The principle of this technique is shown in Figure 3.12.

The identification occurs due to the fluorescent waves emitted by the elements in the samples. The sample elements absorb x-rays and eject electrons from either their K, L or another shell. After the ejection of the electron, an empty place in that orbital is present which has to be filled with an electron from a higher shell. The displacement of an electron from a higher to lower (the empty place) shell goes along with the emission of an x-ray with an energy being the difference between the two states. [48]

3.7.3 Sample preparation

The samples have to be prepared in a certain way to be analysed by TXRF. Samples from either reactor experiments or other experiments have to be diluted and internal standard has to be added.

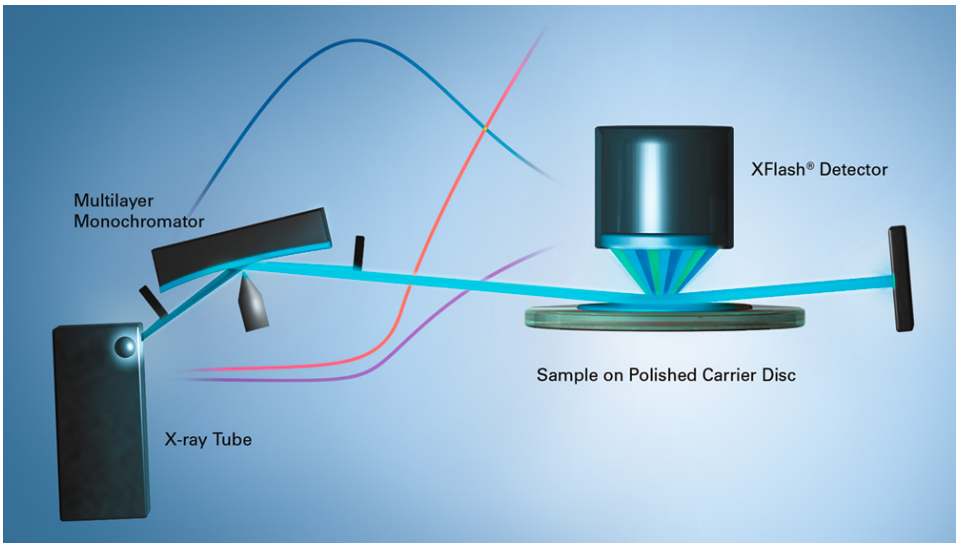

Figure 3.12: Principle of a TXRF [50]

A rule of thumb for these measurements is that the concentration in ppm of the internal standard cannot be more than double or less than half than the element that needs to be analysed in the sample. As such, the sample preparation is dependent on the elements that needs to be measured but the steps are generally the same. A test-tube is filled with 100 µL of sample, 100 µL of internal standard (Ga of Sm of 1000 ppm) and diluted with 800 µL of 2 vol% HNO_3 dissolved in milli-Q water. Dilution ratios may vary dependent on the sample, but are still in the same boundary of half up to double the to be analysed element concentration and in the neighbourhood of 100 ppm.

Once the samples are properly diluted and internal standard(s) are added, they are ready to be used in TXRF. For this, polished quartz carriers are coated with 8 µL of Serva-solution and placed in an oven at 60 ℃ to be dried. This solution makes the surface hydrophobic as such that the sample solution will form a round droplet on the carrier. For this, the sample solution (made before) is mixed by a vortex-mixer and 7 µL is put on the carrier and the carrier is left to dry in the oven at 60 ℃ for 30 minutes. The Serva-solution made sure that all of the analyte is dried at the position where the droplet was put to enhance measurement detection by the TXRF equipment. The carriers are put into the TXRF equipment to be analysed. Three samples are measured to determine the standard deviation.

3.8 Irradiance measurements

3.8.1 Principle of a spectrometer

The spectrometer used to measure the irradiance is from Ocean Optics and the type is QE65 Pro. The device is able to measure wavelengths from 200 up to 1000 nm.

It is able to measure the spectral irradiance as seen in Equation 3.3. The probe itself has a diameter of 3.9 mm, indication that the measurement will be the average intensity in that area of measurement.

The irradiance (or light flux, E_e);

$$E_{\mathrm{e}} = \frac{\partial \phi_{\mathrm{e}}}{\partial A_{probe}} \tag{3.2}$$

where ∂ stands for the partial derivative, Φ_{e} for the radiant flux and A_{probe} is the area of the probe. A spectrometer measures the intensity at each wavelength, which looks like the following:

$$E_{\mathrm{e},\nu} = \frac{\partial E_{\mathrm{e}}}{\partial \lambda}, \tag{3.3}$$

with λ being the wavelength.

The spectrometer is equipped with a cosine corrector (to collect light from all directions) [51]. The light then channels through a glass fibre to the spectrometer where it is split by a monochromator and measured by a photo-detector. The use of the spectrometer probe is already shown in Figure 3.6.

3.8.2 Procedure

The spectrometer probe is placed at the position at which the spectrum has to be measured, the device is turned on and coupled to a computer for data analysis. The measurements are done in a black box to avoid contamination from other light sources. For this measurement to be accurate, a dark spectrum is taken before the start of the experiment to correct for any stray light.

Chapter 4

Modelling reactor and lamp source

Since the reduction of Eu^{3+} in the mechanism described in Section 2.3 will use light as a reagent, it will be very important to know the light intensity in the reactor that will be used. As such that it will be the driving force of the reaction. This was described earlier in Section 2.3.2. In this section, the model is derived for continuous photochemical reactor and applied to the reactor for the reduction of Eu (III) in aqueous media. Only the aqueous media is modelled as the results concerning separation in organic media, as shown in Appendix D, did not yield favourable results.

4.1 Reactor Design

The reactor that will be used is a tubular reactor. These reactors are relatively easy to operate as they work stationary in place domain, meaning that the same conditions apply at a certain point in the reactor in time at steady state.

The complete set-up is shown in Section 3.3.2. In short, a tubular reactor (made of PFA) that is transparent to near UV-radiation is coiled around the cooling jacket with a low pressure mercury lamp in there. The UV-lamp has a high output in the region of 254 nm which is right in the region of the CT-band of $[Eu^{3+}{-}SO_4^{2-}]$. A scheme of the setup can be found in Figure 3.6 in Section 3.3.2.

4.1.1 Dimensions and materials used

The reactor and its dimensions are described in Section 3.3.2, but some calculations necessary for the model are placed here.

The volume of the tubular reactor can be calculated as follows, with $R_{cooling\ jacket} = 34\ mm$ and $r_{in} = 0.70\ mm$:

$$V_{reactor} = 44 \cdot 2 \cdot \pi \cdot R_{cooling\ jacket} \cdot \pi \cdot r_{in}^2 = 14.47mL \tag{4.1}$$

Lastly, one factor which will be required for the model in the next section, this is the projected area, i.e. the area perpendicular to the direction of light and available

for light absorption. This area is equal to the following:

$$S_{projected} = 44 \cdot 2 \cdot \pi \cdot R_{coolingjacket} \cdot \ 2 \cdot r_{in,reactor} = 0.0132m^2 \tag{4.2}$$

PFA has a certain contribution towards the workings of the reactor. It is not completely transparent to UV light. In order to check for the specific absorbance of the tubings, the intensity of the light was measured with and without the tubings in between them, Intensity in (I_{in}) and out (I_{out}) respectively. The measurements are shown in Table 4.1.

Table 4.1: Absorbance measurements of PFA. The path-length of the light was calculated to be 1.76 mm (slightly thicker than the double the thickness of the tubing due to the curvature of the tube).

Wavelength range (nm)	I_{in} ($\mu W/cm^2$)	I_{out} ($\mu W/cm^2$)	Absorbance	Specific absorbance (1/m)
220 - 240	857	286	0.477	271
240 - 270	20716	2581	0.905	514

4.1.2 Light source

As described before, a low pressure mercury lamp (LPML) is used in this setup. But it is difficult to determine the average light intensity in the reactor without a model due to the U-shaped legs.

The LPML is U-shaped and consists of 2 tubes with a radius of 7.15 mm capped with a turn which has a major radius of 10.35 mm. The distance between the legs is equal to 6.4 mm. In total, the total length of the lamp is 242 mm and a width of 35 mm and a height of 14.3 mm. These measurements are used to make a model in COMSOL multiphysics 5.2a.

The output measured at the center of the lamp at a distance of 37 mm is shown in Figure 3.8 in Section 3.5.1 to give an indication of the output received by the reactor. The distance is about the distance where the reactor will be positioned, but this is not accurate enough.

In order to determine the accurate intensity of the light received by the reactor, a COMSOL model is made. The geometry of the lamp is described before and used as input for COMSOL. The reactor is made up of a helix with a diameter of 1.4 mm (internal diameter of the reactor) and an axial pitch of 3 mm (outer diameter of the reactor). The reactor starts at 89 mm and ends at 215 mm measured from the top of the lamp.

To determine the intensity, an empirical formula by Pareek et al. was used to describe the intensity as a function of distance and position relative to a linear source of light in air. [37] The formula is the following:

$$G_\lambda = \frac{K_\lambda}{4 \cdot \pi \cdot r} \cdot (arctan\frac{z+L}{r} - arctan\frac{z-L}{r}) \tag{4.3}$$

Herein, G_λ is the intensity (W/m^2) of a given wavelength (λ) or range of wavelengths (G). K_λ is the radiation power of the lamp per unit length of the lamp (W/m), r is the radial distance from the center axis of the lamp (m), z is the distance from the lamp center (m) and L is the length of the lamp (0.225 m).

This empirical formula was put into COMSOL by using the mathematical plugin for determining the wall distances. r could be easily determined by calculating the distance from the point to the wall of the lamp and adding the radius of the lamp (7.15 mm) to that value. Determining z was slightly more challenging, for this, a 0.1 mm thick section was created in the middle of the lamp. The distance from any point to this thin section was set to be z. A figure of the setup is shown in Figure 4.1.

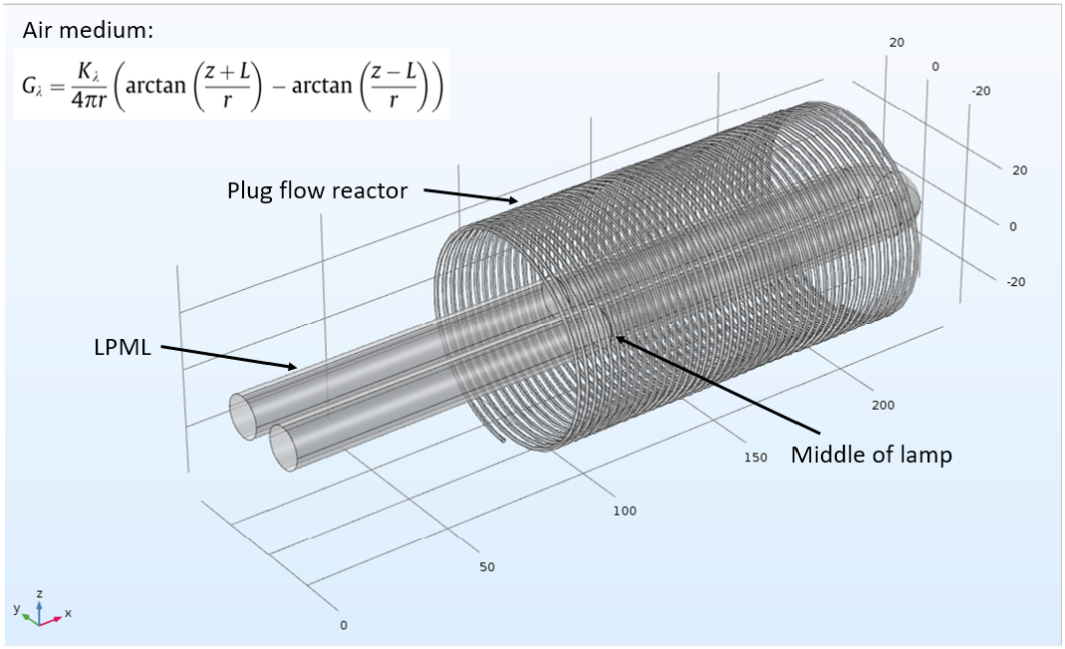

Figure 4.1: Setup of LPML with tubular reactor modelled in COMSOL using Pareek et al. equation.

Only one value remains to be set, which is K_λ. This is a fitting parameter which has to be determined by practically measuring the intensity at a given point by a spectrometer and setting the K_λ to match the measured intensity. In practice, this means that a spectrometer probe is positioned in COMSOL at the exact position relative to the lamp as where the measurement is obtained. In order to have a reliable calibration, the intensity of the lamp is measured for different distances from the lamp as is shown in Figure 4.2. On this graph the selected K_λ-value (determined by COMSOL) with its model-intensity is shown as well. For the 220-240 nm region a K_λ-value of 0.776 W/m is used and for the 240-270 nm region this value is equal to 18.6 W/m.

In order to determine the average received intensity by the reactor, a boundary

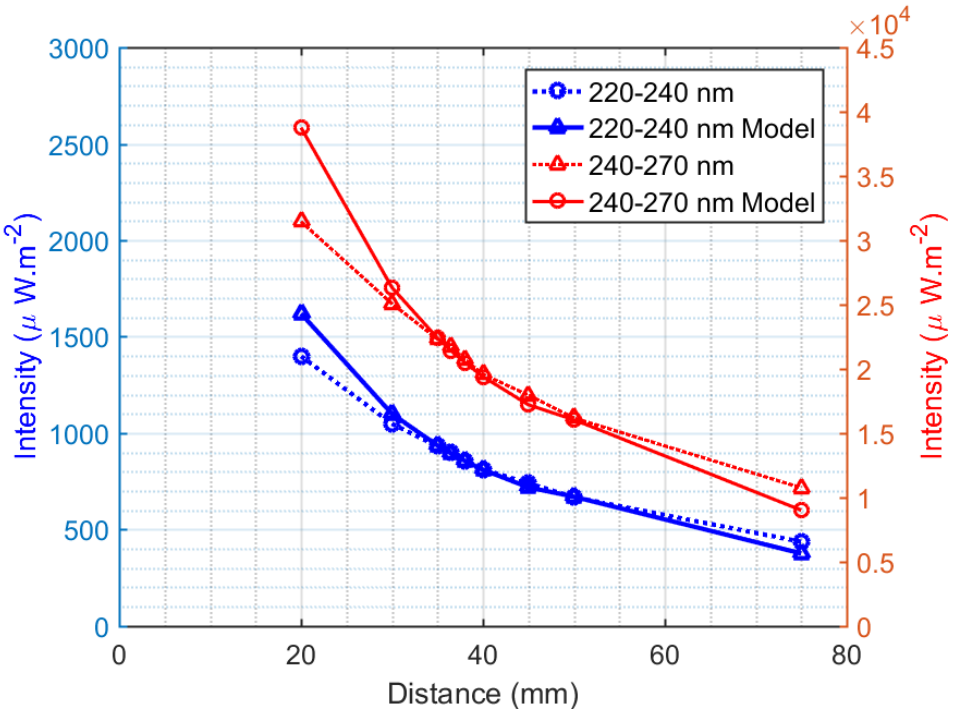

Figure 4.2: Calibration of COMSOL model, graph of measured irradiances compared to predicted irradiances by COMSOL for different distances which are measured along the z-axis perpendicular to the center of the lamp as described in Figure 4.1. A fit is obtained in the 35-40 mm distance area which is the position of the reactor.

probe is used. The probe is bound to the inner surface of the reactor wall and set to show the average of the entire surface facing the light source. The probe data provides an average intensity of 9.54 W/m^2 in the region of 220-240 nm and 228.26 W/m^2 for the 240-270 nm region.

4.1.3 Inlet concentration

The inlet concentration is one more variable to choose. This mixture will contain europium in all of the mixtures described in Section 3.2. In the beginning, the solution will only contain europium and additives. In later stages, artificial YOX and real YOX-mixtures will be used.

In order to determine how much light is used for the desired reaction (reduction of Eu to have it precipitate), it is important to understand that the light that is used is actually absorbed by the mixture. Therefore, the absorbance of the reaction mixture is checked by using a UV-VIS spectrometer, the result of which is shown in Figure 3.2.

For the use in the model, which is worked out in the following sections, it is important to have the correct numbers. For the interval 220-240 nm, the average absorbance is 0.821 and a specific absorbance of 10.3 m^2/mol is calculated. For the

interval of 240-270 nm, the average absorbance is much lower at 0.431 and a specific absorbance of 5.39 m^2/mol.

As not every photon that's being absorbed is used for the desired reaction, the quantum efficiency is introduced (which is explained in Section 2.4.1). The quantum efficiency is basically the fraction of the amount light used for the desired reaction over the amount of absorbed light. For the reduction of Eu in the conditions described before, the quantum efficiency is equal to 0.66 ± 0.04. [52]

Other variables concerning this reaction mixture is the concentration of europium entering the reactor and the flow rate that is directly determining the residence time. The incoming concentration of $EuCl_3$ is kept at 10 mM and the flowrate is variable as it is linked to the residence time (τ).

4.1.4 Summary of all parameters

A short summary is given to indicate which parameters are used in the model and which physical meaning they have. This summary is given in table format as shown in Table 4.2.

4.2 Model equations and constraints

As reactor, a tubular reactor in plug flow will be used as it has generally a higher yield than continuous stirred reactors. A plug flow is assumed despite the low flow rates (as shown in Chapter 5), the main basis for plug flow is the formation of gas bubbles and solid particles. A tubular reactor can be divided into very small fragments perpendicular to its z-axis (axis of flow). Over such a small volume, a mass balance can be applied, herein the concentration of Eu will drop due to light absorption and reaction. This can be generally written as follows:

$$Accumulation = Input - Output + Generation - Dissipation \tag{4.4}$$

For a tubular reactor in plug flow, the mass balance can be build up using Figure 4.3 as guide. With Q the flow rate, C_A the concentration of component A and z the axis of flow. Index i stands for incoming and o for leaving fluid.

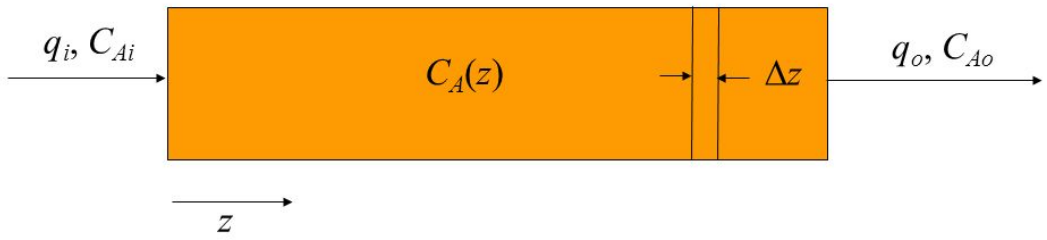

Figure 4.3: General scheme of a tubular reactor in plug flow [53]

Table 4.2: All parameters necessary for the photochemical reactor model.

Section	Parameter	Meaning	Value	Unit
Reactor	d_{out}	Outer diameter of reactor	0.003	m
	d_{in}	Inner diameter of reactor	0.0014	m
	d_{wall}	Wall-thickness of the reactor	0.0008	m
	L	Length of reactor	9.4	m
	#coils	Number of reactor coils	44	
	D_{cooler}	Outer diameter of cooler	0.068	m
	$V_{reactor}$	Volume of reactor	$14.47 \cdot 10^{-6}$	m^3
	$S_{projected}$	Projected surface area of reactor	0.0132	m^2
Tubing	$\mu_{R,220-240}$	Attenuation of reactor (220-240 nm)	270.9	m^{-1}
	$\mu_{R,240-270}$	Attenuation absorbance of reactor (240-270 nm)	514.3	m^{-1}
Lamp	$I_{in,220-240}$	Irradiation at reactor wall (220-240 nm)	9.54	W/m^2
	$I_{in,240-270}$	Irradiation at reactor wall (240-270 nm)	228.26	W/m^2
	$\lambda_{220-240}$	Wavelength at maximal intensity of 220-240 nm interval	$230 \cdot 10^{-9}$	m
	$\lambda_{240-270}$	Wavelength at maximal intensity of 240-270 nm interval	$254 \cdot 10^{-9}$	m
Mixture	$\varepsilon_{Eu,220-240}$	Specific absorbance of Eu-solution (220-240 nm)	10.3	$m^2.mol^{-1}$
	$\varepsilon_{Eu,240-270}$	Specific absorbance of Eu-solution (240-270 nm)	5.39	$m^2.mol^{-1}$
	$Q.E.$	Quantum efficiency	0.66 ± 0.04	
	c_{in}	Incoming Eu-concentration in the feed	10.0	$mol.m^{-3}$
	Q	Flow rate	variable	
	Θ	Temperature	15 - 20	℃

Using Equation 4.4 and the model for a tubular reactor in plug flow, the following mass balance is assembled:

$$\frac{\partial c}{\partial t} = Q \cdot \frac{\partial c}{\partial V} - Rc \tag{4.5}$$

With c the concentration, t time, $\frac{\partial c}{\partial t}$ the accumulation term, Q the flow rate of the medium, $\frac{\partial c}{\partial V}$, the difference in concentration (input-output) for a very small volume (dV) and Rc is the reaction term (in $mol.s^{-1}$). For this case, a photon flux limited reaction is assumed.

For a tubular reactor working at steady state, no accumulation will occur, this leads to a $\frac{\partial c}{\partial t}$ term which will become zero. Space-time is a term used in reactor technology that indicated the time that a small volume (dV) is present in the reactor from start to finish, this is the ratio of the V/Q and indicated as τ.

$$0 = \frac{\partial c}{\partial \tau} - Rc \Leftrightarrow \frac{\partial c}{\partial \tau} = Rc \tag{4.6}$$

As the reaction speed (Rc) is still unknown, a relation must be found to make express it terms of light since this is the limiting reagent, earlier experiments indicated that the reaction speed is of zeroth order which indicates the light as limiting reagent as a constant light flux was used assuming a decent light path.

When light is sent to a solution containing a component which is capable of absorbing light, not all light is absorbed. The ratio of absorbed vs. emitted light is given by the absorbance of a substance. This is shown below:

$$A = \varepsilon cl = log_{10}\frac{I_{in}}{I_{out}} \tag{4.7}$$

With A the absorbance, ϵ the specific absorptivity (different for each wavelength), c the concentration of the light absorbing component, l the path-length, I_{in} the incoming light intensity and I_{out} the outgoing intensity. This formula requires collimated light (e.g. laser), this is not completely correct for the reactor that will be built, it is a good approximation especially for thin light-path geometries. Assuming that $I_{in} = I_{out} + I_{abs}$, the relation can be rewritten in terms of absorbed light:

$$I_{abs} = I_{in} \cdot (1 - 10^{-\varepsilon \cdot c \cdot l}) \tag{4.8}$$

For I_{out}, the following relation is observed, which will be necessary to implement the light that can pass through the reactor wall. Hereby, μ is the attenuation of the material, equivalent of the combination of specific absorbance and concentration.

$$I_{out} = I_{in} \cdot 10^{-\mu \cdot l} \tag{4.9}$$

The reaction speed can be written in terms of absorbed light flux:

$$Rc[\frac{mol}{m^3 s}] = \frac{I_{abs} \cdot S \cdot QE}{h \cdot \frac{c_{light}}{\lambda} \cdot N_A \cdot V} = \frac{I_{in} \cdot 10^{-\mu_{PFA} \cdot l_{wall}} \cdot (1 - 10^{-\varepsilon \cdot c \cdot l_{fluid}}) \cdot S \cdot QE}{h \cdot \frac{c_{light}}{\lambda} \cdot N_A \cdot V} \tag{4.10}$$

with I_{abs} the absorbed intensity ($W.m^{-2}$), I_{in} the incoming intensity produced by the UV-lamp ($W.m^{-2}$), $(\mu)_{PFA}$ the attenuation of of PFA tubings (m^{-1}), l_{wall}, the path-length of the light through the reactor wall (m), ε the specific absorptivity (different for each wavelength) (m^2/mol), c the concentration of the light absorbing component [Eu^{3+}−SO_4^{2-}] ($mol.m^{-3}$), l the path-length in the reactor (m), QE quantum efficiency (ratio of efficiently used photons to absorbed photons), h Planck constant ($J.s$), c_{light} the speed of light ($m.s^{-1}$), λ the wavelength (m), N_A the number of Avogadro (mol^{-1}), S the projected surface area of the reactor available for light (m^2) and V the volume of the reactor (m^3). Part of the denominator is used to convert the intensity to the amount of photons (in mol) that is absorbed by the solution.

A scheme of the reactor with all appropriate symbols is shown in Figure 4.4, it can give a better idea of how the light travels trough the reactor and which part of it is absorbed.

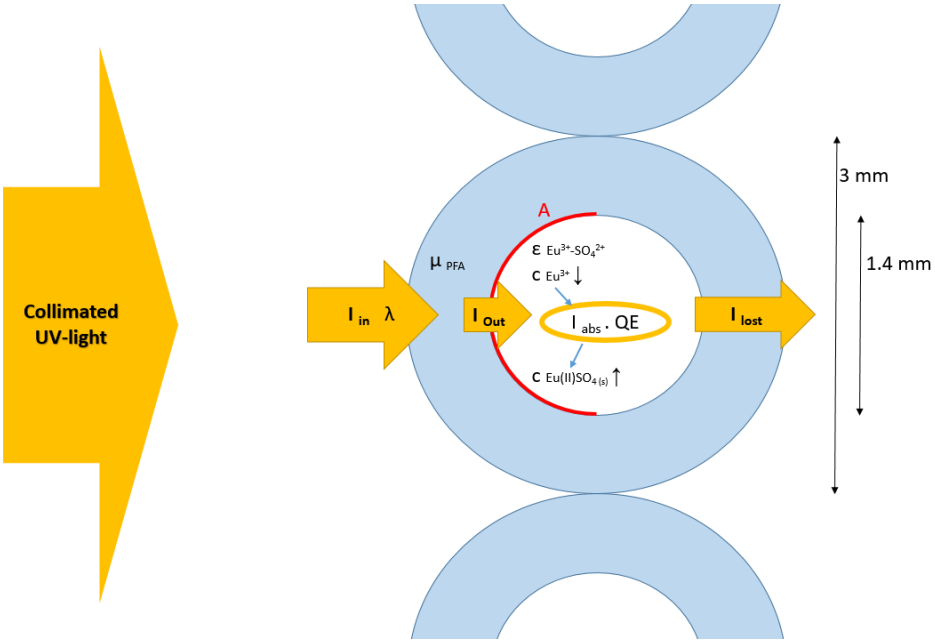

Figure 4.4: Cross-section of the reactor wall. The wall is portrayed in light blue. Light enters from the left side (lamp) and is assumed to be collimated. The incoming light passes through the reactor wall which absorbs a fraction of the light. A fraction of the remaining light is absorbed and used for the reduction of Eu^{3+}.

Inserting the reaction speed into the mass balance of the tubular reactor, yields the following result:

$$\frac{\partial c}{\partial \tau}\left[\frac{mol}{m^3 s}\right] = \frac{I_{in} \cdot 10^{-\mu_{PFA} \cdot l_{wall}} \cdot (1 - 10^{-\varepsilon \cdot c \cdot l_{fluid}}) \cdot S \cdot QE}{h \cdot \frac{c_{light}}{\lambda} \cdot N_A \cdot V} \tag{4.11}$$

It can be observed that the reaction speed also contains the concentration, making

it more difficult to integrate the formula. Secondly, when different wavelengths are used, the equation splits up for each wavelength.

In the case of the Eu-reduction, 2 absorptivities will be used for the range of 220-240 nm and for the range of 240-270 nm. The LPML has its largest output at 254 nm as such, it will be used for the reduction of Eu as well, but with a different absorptivity and in most cases a different quantum efficiency. The concentration refers to the concentration of the $[Eu^{3+}-SO_4^{2-}]$-complex as this is the light absorbing species, it is assumed that all Eu^{3+} is surrounded by the excess SO_4^{2-} in solution thus this value is the same as the concentration of Eu^{3+}. For this situation, the equation becomes:

$$\frac{\partial c}{\partial \tau}[\frac{mol}{m^3 s}] = \sum_{i=1}^{2} \frac{I_{in,i} \cdot 10^{-\mu_{PFA,i} \cdot l_{wall}} \cdot (1 - 10^{-\varepsilon_i \cdot c \cdot l_{fluid}}) \cdot A \cdot QE_i}{h \cdot \frac{c_{light}}{\lambda_i} \cdot N_A \cdot V} \tag{4.12}$$

With the index 1 referring to the region of 220 to 240 nm and index 2 referring to 240 to 270 nm. The path-length that the light travels through isn't just the diameter of the reactor tube, instead it will be an average since light can also pass along the sides. The average path-length is determined by an area integral and determined to be:

$$\frac{\pi \cdot r^2}{2} = 2 \cdot r \cdot \frac{l}{2} \leftrightarrow l = \frac{\pi \cdot r}{2} \tag{4.13}$$

This equation will also be used to determine the average wall thickness the light travels through.

Fitting all of them together leads to:

$$\begin{aligned} \int_{c_{out}}^{c_{in}} \frac{1}{\sum_{i=1}^{2} I_{in,i} \cdot 10^{-\mu_{PFA,i} \cdot l_{wall}} \cdot (1 - 10^{-\varepsilon_i \cdot c \cdot l_{fluid}}) \cdot QE_i \cdot \lambda_i} \partial c \\ = \int_{\tau_{ind}}^{\tau} \frac{S}{h \cdot c_{light} \cdot N_A \cdot V} \partial \tau \end{aligned} \tag{4.14}$$

The integral boundaries at the left hand side refer to the in- and outgoing concentration of Eu in solution, the integral on the right hand side only integrates from the induction time towards the residence time as this is the time in which solid particles are formed. In the time between entrance of the reactor and the induction time, no solids are produced due to a build-up of Eu^{2+} to reach supersaturation and this possibly competes against side reaction that oxidise Eu^{2+} when concentration are high. This integral can be filled in to determine the outgoing reactant concentration if the incoming concentration is decided upon. All other parameters are known, the intensities are determined by a COMSOL simulation, the quantum efficiency is known in literature, the wavelength intervals are known, the absorptivity is measured, the path-length is known and the area for light absorption can be calculated.

The integral was solved numerically using Matlab and will give an approximate outgoing concentration for a chosen incoming concentration of Eu^{3+} and a chosen residence time. The assumptions used to build up the model are shown below:

- The light intensity is uniform along the reactor and is determined by a COMSOL model.
- The absorptivity (ε) is constant for the wavelength interval.
- The quantum efficiency is constant in the wavelength interval.
- The wavelength is chosen to be the most intense peak in the interval: 230 nm for 220-240 nm and 254 nm for 240-270 nm.
- The light is mostly collimated since the reactor is relatively close to the lamp and more important, it has no large path-length (order of a few mm's in this case), thus the law of Lambert-Beer is assumed to be valid.
- The area is chosen to be the projected internal area of the helix reactor (but only the inner side which touches the fluid) (r = 0.7 mm)
- This kinetics does include the induction time in which supersaturation has to be build up, but it has to be put in manually through experiments as it cannot be calculated since not all factors are known (supersaturation concentration, and other influencing factors).
- The kinetics only include the forward reaction of the reduction of Eu^{3+}. Reverse reactions are not included but will be discussed later.
- The formation of gasses is neglected. They can have a great influence on the actual residence time as less volume of the reactor is available for the liquid.
- The formation of solids is neglected. They have the potential to absorb, refract or reflect light coming into the reactor, thus reducing the intensity.

4.3 Model results

The reaction rate and mass balance equations are derived in Section 4.2, all parameters from Table 4.2 are filled in, as well as the induction time which is experimentally determined and found in Section 5.2. The reaction rate for each concentration will be determined as well as the outlet concentration, conversion and photochemical space time yield (PSTY).

4.3.1 Reaction rate

Firstly, there is the reaction rate. The equation for this is given below;

$$\frac{\partial c}{\partial \tau}[\frac{mol}{m^3 s}] = \sum_{i=1}^{2} \frac{I_{in,i} \cdot 10^{-\mu_{PFA,i} \cdot l_{wall}} \cdot (1 - 10^{-\varepsilon_i \cdot c \cdot l_{fluid}}) \cdot S \cdot QE_i}{h \cdot \frac{c_{light}}{\lambda_i} \cdot N_A \cdot V} \tag{4.15}$$

Equation 4.15 is filled in and shown in the Figure 4.5. On the x-axis, which is logarithmic, the concentration of Eu^{3+} (absorbing species) is plotted. On the left y-axis, which is logarithmic as well, the reaction rate is plotted. And on the right y-axis, the absorbed light fraction is plotted.

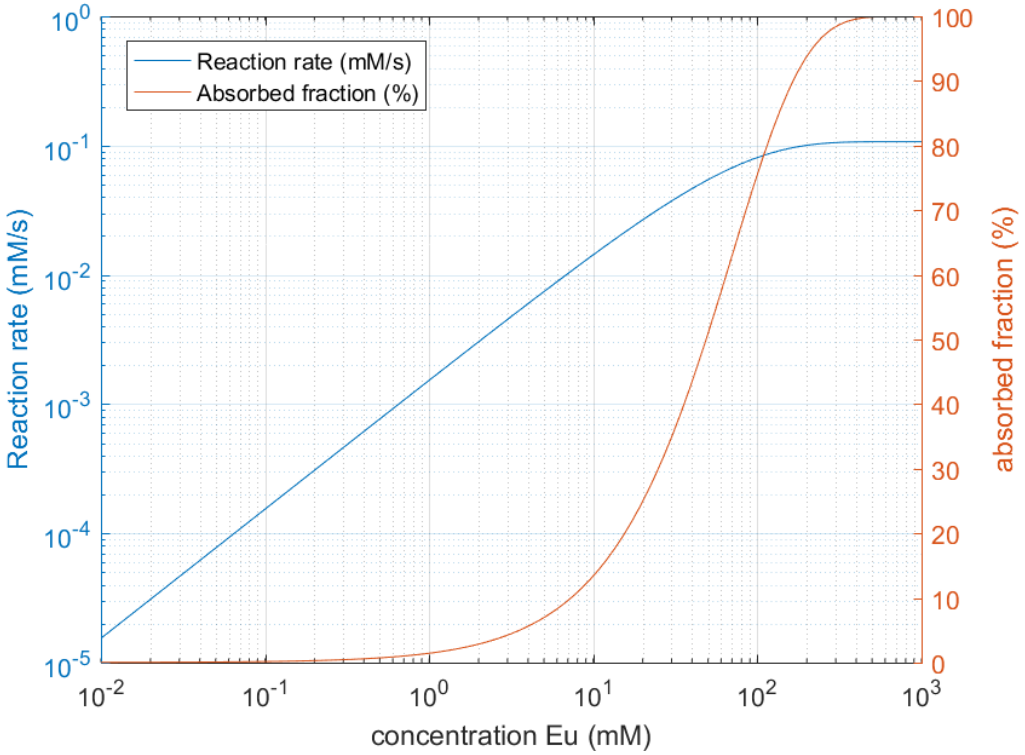

Figure 4.5: Reaction rate for a photon limited reactor of the removal of $EuSO_4$

Figure 4.15 shows that the reaction rate (in blue) is linear and rising in a log-log graph from a low concentration up to 10^2 mM. This rate is very specific for the geometry of the reactor and the reaction which is used. Above 10^2 mM, the reaction rate levels of to a constant value. This behaviour can be explained by the physics behind it. At low concentrations, the light absorption is dependent on the concentration of the absorbent species (Eu^{3+}–SO_4^{2-}), but at these concentrations, more than 50% of the incoming light is not absorbed (10^{-2} up to $10^{1.5}$ mM), hence in this region, the reaction rate scales with the concentration of absorbent

species. Above $10^{1.5}$ mM, the fraction of light that is absorbed exceeds 50% and from then on, the absorbed light doesn't scale with concentration any more since most of the light is already absorbed. It must be noted that this reaction rate is calculated without concerning the solids which can reflect, absorb or scatter UV light.

In the planned experiments, the reactor will be fed with 10 mM Eu^{3+}, therefore this is situated in the concentration limited region. This has as a downside that the reaction rate will drop as the reaction progresses when less light is absorbed. It drops from $2 \cdot 10^{-2}$ $mM.s^{-1}$ for 10 mM to $2 \cdot 10^{-3}$ $mM.s^{-1}$ for 10 mM, which is a factor of 10. Thus as concentration decreases, more light is lost and efficiency will drop.

Both curves on Figure 4.15 can be manipulated by several factors. To influence the absorbed fraction curve, there are two options. Either the path-length can be increased, which means that the diameter of the tube should increase. Either the specific absorbance of the substance must increase to absorb more light which is used usefully, but this is too difficult to achieve. These conclusions were obtained based on Equation 4.7 and 4.8.

To increase the reaction rate, a few options are possible. Either the lamp is changed to a lamp with a higher intensity, as such the absorbed fraction remains the same with the exact same geometry, but net more light is absorbed, thus a higher reaction rate is achieved. Secondly, a different geometry can be used whereby a higher surface to volume ratio is achieved (i.e. thinner tubes), this will positively influence the reaction rate. But this change is prone to clogging the reactor with the formed solids. Lastly, since a PFA tube is used, it is also absorbing a rather large amount of light, if this can be changed to e.g. quartz, a lot of light will remain available for the reaction, hence a higher reaction rate. These conclusions can be drawn from Equation 4.15. Other options, such as altering the quantum efficiency of the reaction or changing the absorbing wavelength are less interesting to do due to their higher difficulty.

Influence of reaction rate As described before, the reaction rate can be influenced by the ratio of the area over volume, the intensity and the transparency of the tube. The absorbed fraction can be influenced by the diameter of the tubing (more path-length for the light). To give an idea these parameters are altered as compared to the reference situation (which is the reactor set-up).

By altering the diameter of the tube from 1.4 mm up to 10 times higher and 10 times lower, Figure 4.6 is obtained. As the diameter increases by 10-fold, the A/V ratio decreases by 10-fold and vice versa with a reference A/V of 909 m^2/m^3.

Looking at the absorbed fraction curve, it can be seen that the S-shaped part switches about a decade to lower concentration when the diameter is increased by 10-fold. As the diameter is decreased, the opposite happens. Looking at the reaction rate, it is shown that that does not change a lot in this configuration, it is only useful to shift to a higher A/V ratio if a high concentration of reagents ($> 10^2$) is present in the reactor. The main difference is that the plateau shifts to a lower concentration

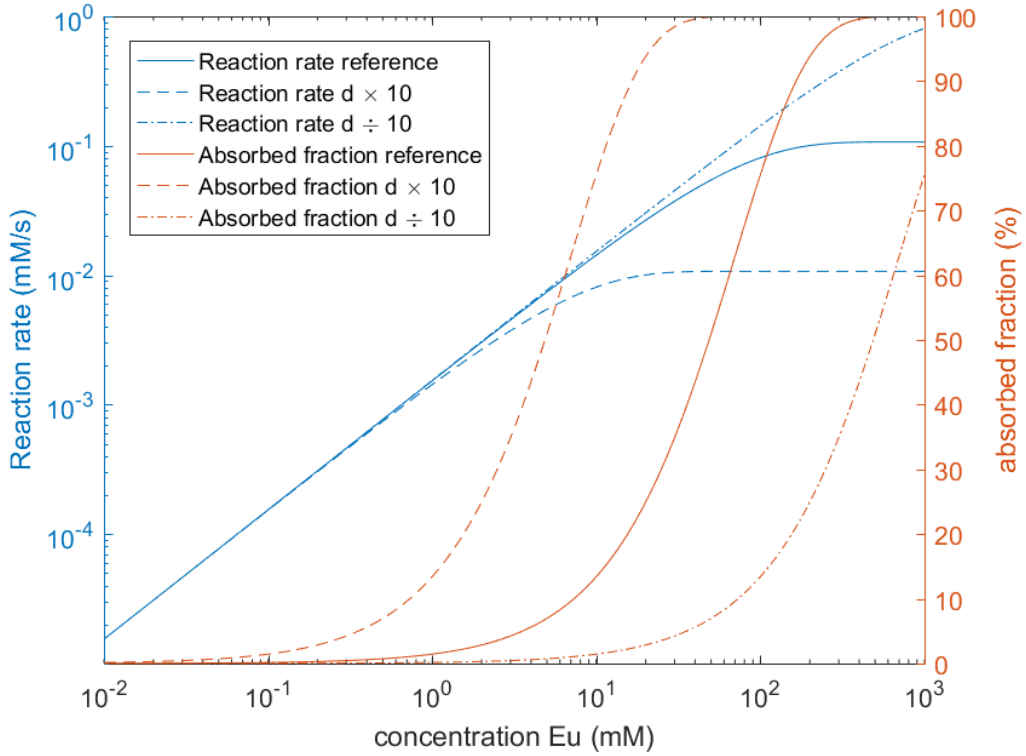

Figure 4.6: Influence of diameter and area over volume on reaction rate and absorption fraction.

with increasing path-length, this is normal as the plateau is linked to the absorbed fraction. The physical meaning of the plateau is in fact the point onto which nearly all incoming light is absorbed and the reaction rate can no longer increase with increasing absorbance (linked to concentration). When the tube diameter decreases, the plateau shifts indicating that a higher reaction rate can be obtained for higher concentration (100 up to 1000 mM) compared to the reference. This can be explained by its higher area to volume ratio, which is exploited at those high concentrations.

Secondly, the irradiance linked to the intensity of the lamp can be altered as well. This leads to Figure 4.7. As the intensity is increased by 10-fold, the reaction rate increases by 10-fold at each concentration. When the intensity is decreased by 10-fold, the reaction rate decreases at each concentration at 10-fold. This however assumes light-limiting reactions. As the reaction becomes limited tue to mass transfer, the rate will decrease compared to light-limiting reactions.

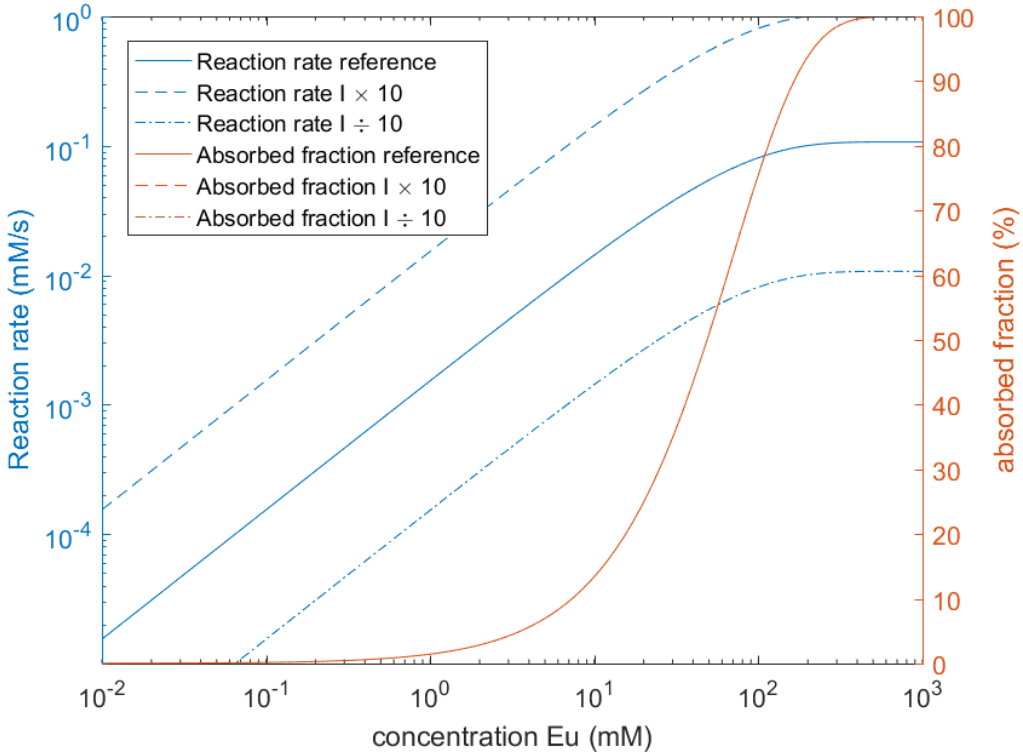

Figure 4.7: Influence of lamp intensity on reaction rate and the absorbed fraction.

4.3.2 Conversion estimation

Using the previously derived model and a numerical solver for Equation 4.16 (shown below), an estimate can be made for outlet concentration of Eu^{3+} if the inlet concentration, the 'induction' time (τ_{ind}) and a certain residence time (τ) is known or chosen. In the later graphs, the 'induction' time is taken from experiments performed in Section 5.2 and is equal to 295 seconds.

$$\int_{c_{out}}^{c_{in}} \frac{1}{\sum_{i=1}^{2} I_{in,i} \cdot 10^{-\mu_{PFA,i} \cdot l_{wall}} \cdot (1 - 10^{-\varepsilon_i \cdot c \cdot l_{fluid}}) \cdot QE_i \cdot \lambda_i} \partial c = \int_{\tau_{ind}}^{\tau} \frac{S}{h \cdot c_{light} \cdot N_A \cdot V} \partial \tau \tag{4.16}$$

In order to estimate this conversion, Equation 4.16 has to be worked out. The right hand side is easy to do as the answer is equal to;

$$rhs = \frac{S}{h \cdot c_{light} \cdot N_A \cdot V} \cdot (\tau - \tau_{ind}) \tag{4.17}$$

An analytical solution to the left hand side integral could not be provided, therefore this part is solved numerically by using the trapezoidal rule for numerical integration. The Matlab code for this is shown in Appendix B.2.

Outlet concentration Several graph types are possible, but the most interesting might be to put the residence time (τ) on the x-axis, the inlet concentration of Eu^{3+} on the y-axis and plot the outlet concentration of Eu^{3+} still left in solution. This will result in this graph:

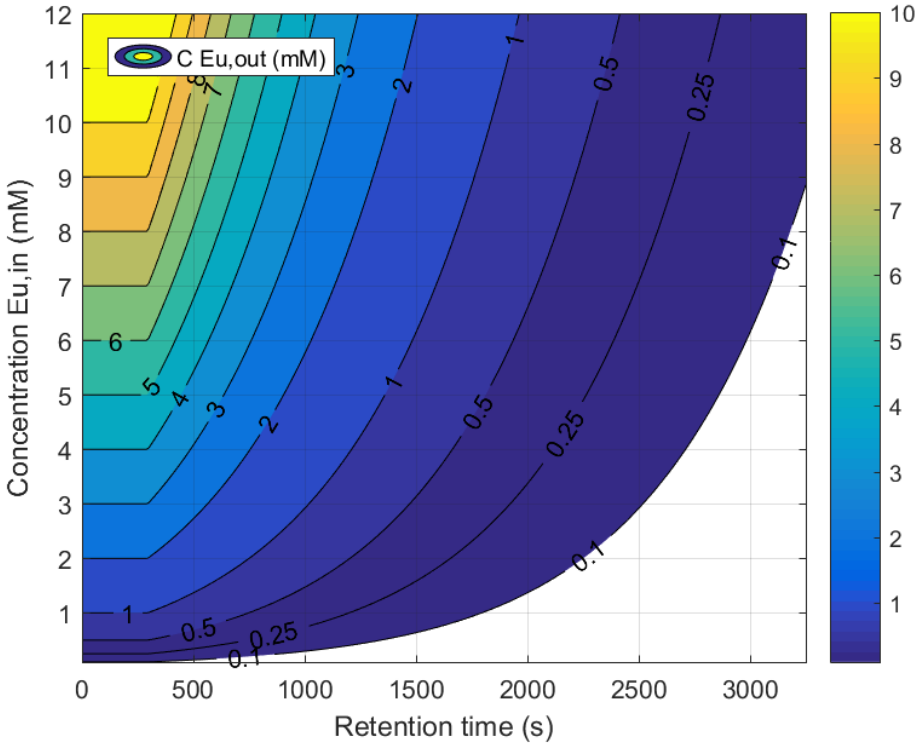

Figure 4.8: Outlet concentration of Eu^{3+} for different residence times and inlet concentration of Eu^{3+}

It is shown on Figure 4.8 that the concentration of Eu^{3+} doesn't change in the first 300 seconds. This is due to the 'induction' time which is required to build up supersaturation and initialize crystallisation. After this 'induction' time, it is shown that for a given inlet concentration, the outlet concentration lowers as function of the residence time. It must be noted that there is a 'fast' part, between 300 and roughly 1500 seconds, whereby the concentration is lowered rather fast and there is also a 'slow' part, starting from 1500 and beyond. In this 'slow' part, the remaining Eu^{3+} is so low as such that light absorption drops significantly and so does the reaction rate as is shown on Figure 4.5

However, this outlet concentration is for ideal conditions (without the presence of solids and gas) as indicated before, the main deviation that will occur is that in the higher residence times, the outlet concentration will be higher due to light blockage by solids and back reaction due to pH.

Conversion In the same manner, another plot can be made which shows the conversion as function of the inlet concentration and residence time. This graph is less special, as indicated below.

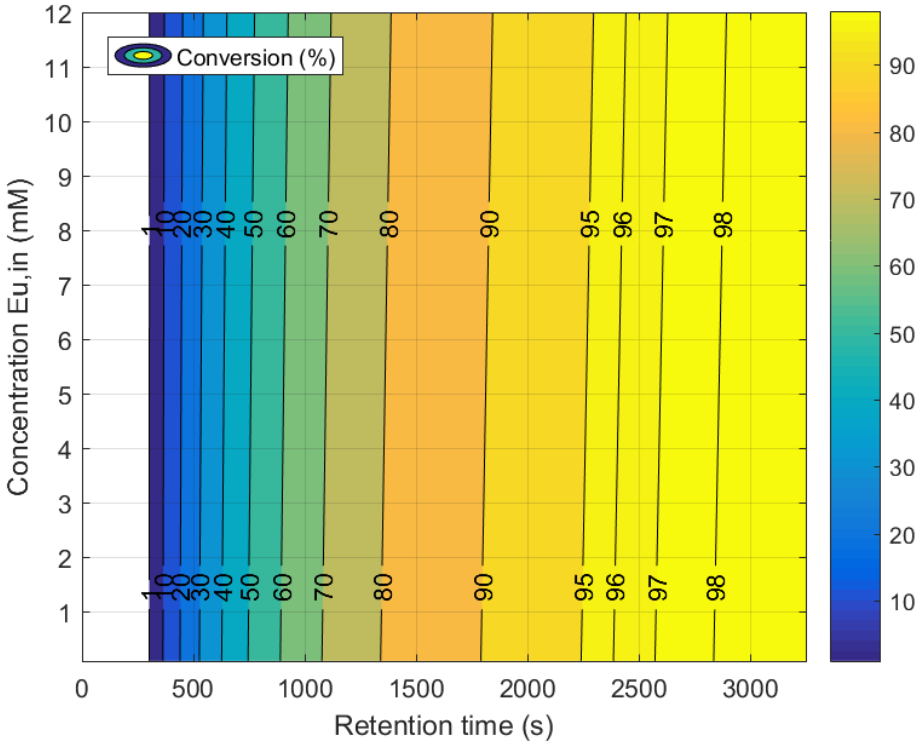

Figure 4.9: Conversion of Eu^{3+} for different residence times and inlet concentration of Eu^{3+}

In Figure 4.9, the conversion in % is given as function of residence time and inlet concentration. The most prominent factor is that the conversion increases with residence time, fast between 300 and 1500 seconds and slower towards the end. It can also be noted that the conversion is less at a given time for a low compared to a high inlet concentration due to the slower reaction rate (lower absorbance of light).

Photochemical space time yield (PSTY) And lastly, a performance indicator, the PSTY (photochemical space time yield) can be calculated and plotted as well. The PSTY is explained in papers by Leblebici et al. [36] and is the ratio of space-time

yield over the scaled lamp power. For a reactor (with volume (V)) with a certain in- and output over a residence time (τ) and a certain lamp (with a power drawn (P) for the volume of reactor (V)) the PSTY becomes:

$$PSTY\,[mol \cdot s^{-1} \cdot m^{-3} \cdot W^{-1}] = \frac{c_{in} - c_{out}}{\tau \cdot \frac{P \cdot 1m^3}{V}} \tag{4.18}$$

Calculating Equation 4.18 for each couple of points (c_{in}, c_{out}, τ) of the data that is plotted in Figure 4.8, the lamp power (60 W) and the reactor volume of $14.47 \cdot 10^{-6} m^3$, the following is obtained:

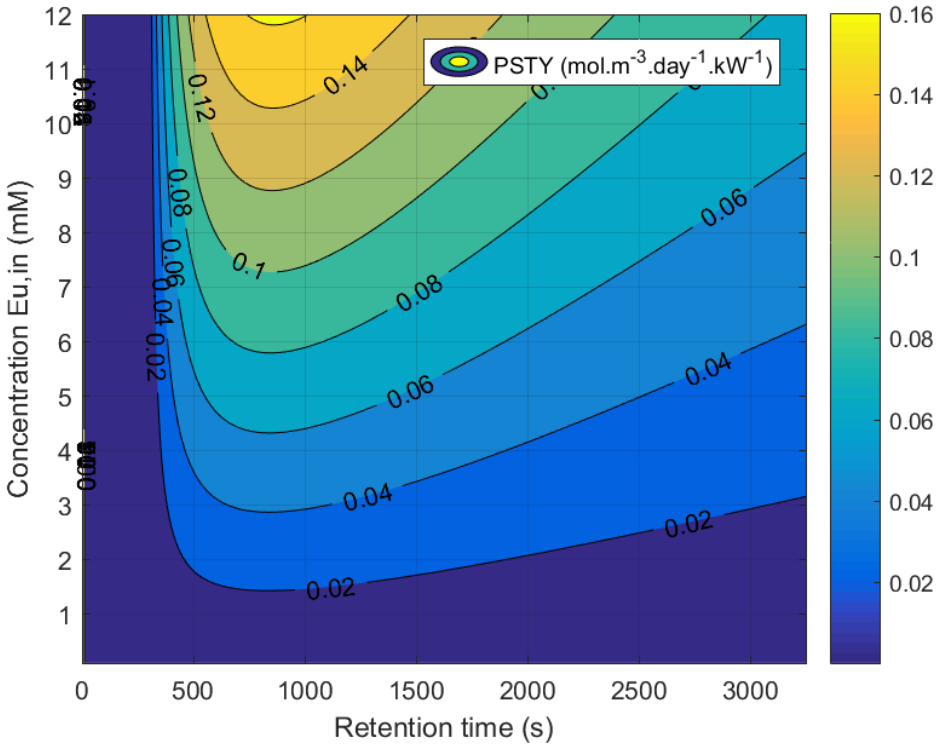

Figure 4.10: PSTY of the reactor for Eu^{3+} recovery for different residence times and inlet concentration of Eu^{3+}

Figure 4.10 for the PSTY is slightly more interesting as before. It can be seen that there is an optimal residence time for each inlet concentration, these are roughly in the neighbourhood of 900 seconds except for an inlet concentration of 1 mM (700 seconds). This optimum can be explained using the previous 2 graphs. It could be seen that the outlet concentration lowers in 2 different rates, it has a fast and a slow part. This fast part, as previously discussed is more favourable as more light is used efficiently compared to the slow part, where the last remaining Eu^{3+} ions are being removed. This effect is visible on the graph of the PSTY.

The reason for the rise in PSTY (between 300 and 500 seconds) is due to the induction time. Product is only formed started from the induction time, but the ratio of formed product over residence time (and the formed product rises faster than the residence time in that area) is taken which has this peculiar effect.

These models provide a good estimate for the conversion and efficiency of the process, in reality, these two parameters will be slightly different due to light blockage by solids formed in the reactor. Nonetheless, these models provide the maximum conversion possible, thus a goal to reach for.

4.4 Conclusion

A model which predicts the outflow of the reactor based on its feed and dimension has been developed in this chapter. Via this outflow, feed, residence time, lamp power and the dimensions of the reactor, it can determine the efficiency as well, also know as photochemical space time yield [36]. It assumes a light absorption by the solution following the law of Lambert-Beer and ignores the effects of gas or solid formation in the reactor. As it is a general model, it can be used for reactors with different geometries and reactions as long as all variables are known in terms of geometry and reaction details (e.g. absorption, quantum efficiency). In the next chapter, this model is put to the test by fitting it with the data for the Eu-reduction and precipitation in a tubular photochemical reactor.

Chapter 5

Separation of europium and yttrium in aqueous medium

As the separation of europium from yttrium failed in methanolic media, a different approach was needed. This approach was explored before by Van den Bogaert. [8, 7] The separation of the two elements was done via a charge transfer between Eu^{3+} and SO_4^{2-} to yield Eu^{2+} which immediately precipitates as $EuSO_4$. The exact details can be found in Section 2.3.2.

A simplified process flow diagram can be found in Figure 5.1. Herein for simplicity an equimolar mixture of Eu and Y is presented. The reactions, as mentioned before, are found in Section 2.3.2. The most important point to note here, is that solid $EuSO_4$ is formed directly after the reduction of Eu^{3+} has taken place. Thus, the reactor has to be designed in such a way that it won't be clogged. Several types (in size) of tubular reactors can be used, but in order to reduce the risk of clogging a meso type (millimetre range) will be used.

One of the important parameters in chemical reactors is the residence time, or the time the reactants spend inside the reactor. The reactor is a tubular reactor, comparable to a tube, thus the residence time can be calculated as the ratio of the volume of the reactor (V) over the flow (Q) as given in the following equation:

$$\tau = \frac{V_{reactor}[m^3]}{Q[m^3/s]} \tag{5.1}$$

As the set-up consisting of a plug flow reactor will be used as described in Section 3.3.2, it is important to know the residence time provided by the peristaltic pump in the set-up.

5.1 Determination of the flow rate and residence time

The reactor volume has been calculated before to be equal to 14.47 mL. The flow rate (and consequently the flow (Q)) is governed by a peristaltic pump which had to be calibrated before the experiments could take place. The pump uses a tube over which rollers turn at a certain rate. This pushes the fluid through the tube. The

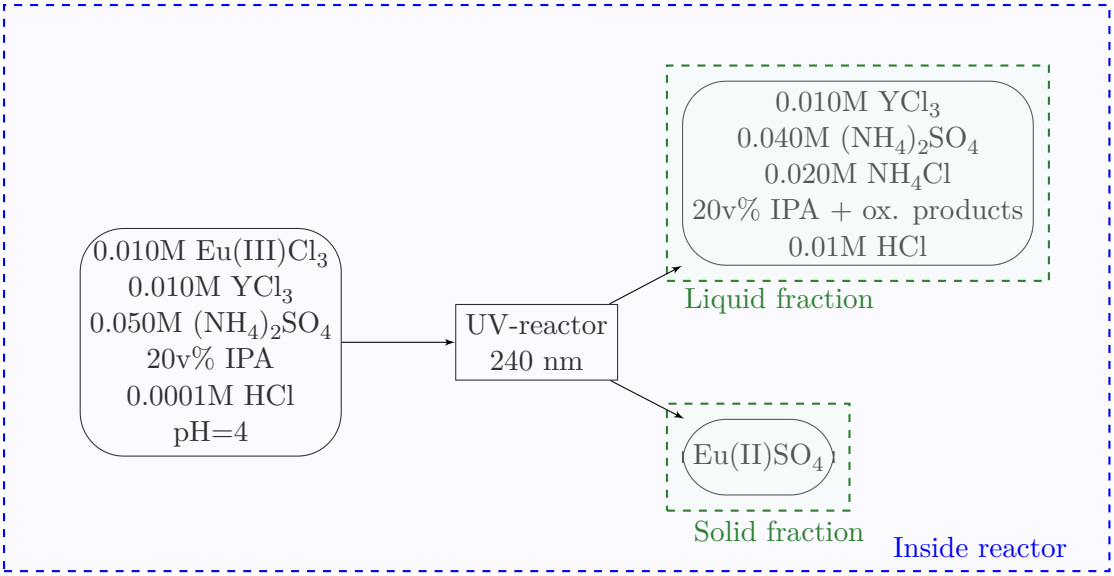

Figure 5.1: Diagram of the separation of Eu and Y by charge transfer of Eu to SO_4^{2-}. All reactions happen in the reactor, meaning that solid $EuSO_4$ is formed in situ after the reduction of Eu has taken place, IPA (radical scavenger) is oxidised to substances such as acetone.

rate at which the rollers turn can be adjusted via a setting knob on the device. The relation between this setting and the flow rate has to be determined. This was done by determining the volume (weight by balance) displaced after a certain measured time. The error on this measurement was determined by a calibration line as the flow rate scales linear with the setting on the pump.

For this pump, two types of tubes where used which were in contact with the rollers. The difference between them was their internal diameter, one was 3.17 mm in diameter and the other has a diameter of 1.3 mm. Therefore, the flow rate will be different inside the reactor with each these tubes are connected to the reactor. The calibration was done for each tube for which the results are shown in Figures 5.2 and 5.3.

If the flow rate is divided by the volume of the tubular reactor, the residence time is obtained. Using the data from Figure 5.2 the residence time for each pump setting could be plotted in Figure 5.3.

The data of which residence time corresponds with which pump setting is shown in the table found in Appendix C.1 in Table C.2 and C.3. The error on the flow rate as seen in figures 5.2 and 5.3 can be found in Appendix C.1.

For this type of reactor at these flow rates, laminar flow is expected as the Reynolds number is ranging from 4.3 (τ = 3054 s) up to 487 (τ = 27 s), calculated using a $\rho_{water} = 1000 kg/m^3$ and a viscosity of water of $10^{-3} Pa.s$. Most of the time a residence time of 3054 s up to 481 s will be used, thus the range is reduced from Re = 4.3 to 27. The Reynolds number varies and experiments will show that gas is

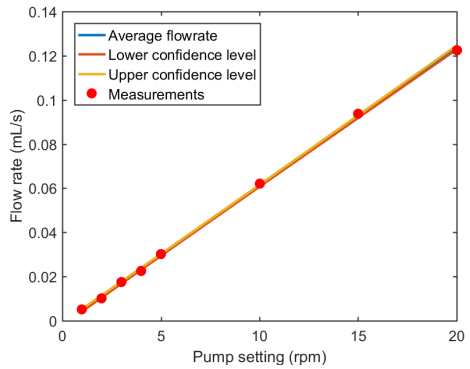

(a) Flow rate using small tubings 1.3 mm diameter in the peristaltic pump. The calibration line is equal to $Flowrate(mL/s) = 0.0063(mL/s) \cdot RPM - 0.0015(mL/s)$

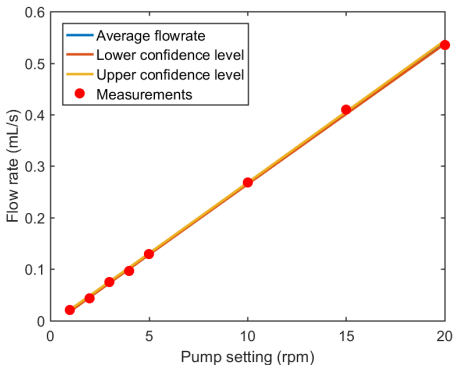

(b) Flow rate using big tubings 3.17 mm diameter in the peristaltic pump. The calibration line is equal to $Flowrate(mL/s) = 0.0274(mL/s) \cdot RPM - 0.0082(mL/s)$

Figure 5.2: Flow rate of the peristaltic pump at different pump settings with two different tubings.

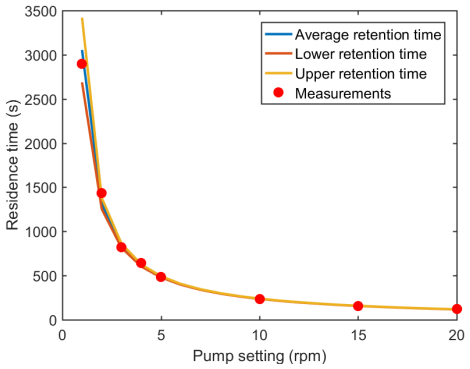

(a) Residence time obtained by using small tubings 1.3 mm diameter in the peristaltic pump.

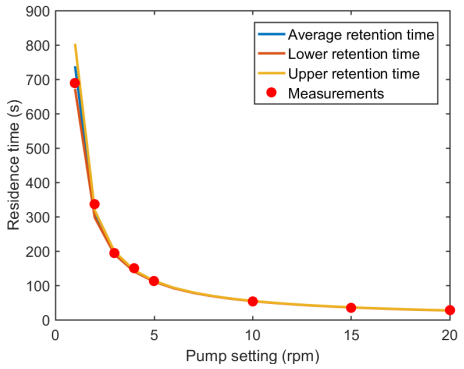

(b) residence time obtained by using big tubings 3.17 mm diameter in the peristaltic pump.

Figure 5.3: Residence time for the tubular reactor provided by the peristaltic pump at different pump settings with two different tubings.

formed inside the reactor, this makes it rather useless to calculate a residence time distribution for several cases as it will be completely different in the experiments.

5.2 Eu recovery from Eu solution without Y

In order to determine whether this method works for separation of YOX, the principle is tested using a solution only containing Eu^{3+} to have a look at its performance. The principle is displayed in the scheme in Figure 5.1 but without the Y^{3+}. Herein, $EuCl_3$ is introduced with all nescessary additives (see Section 2.3.2) into the reactor (with a volume of 14.47 mL) whereby the Eu^{3+} is reduced and precipitated as $EuSO_4$.

Once the correct residence time can be calculated, this pump was used to determine the conversion of Eu^{3+} in solution to precipitated $EuSO_4$ which is the final product. This is done by measuring the concentration still left in solution and calculating the conversion by measuring the inlet concentration as well. The conversion is determined as follows:

$$conversion = \frac{C_{in} - C_{out}}{C_{in}} \cdot 100\% \tag{5.2}$$

The conversion is dependent on the inlet concentration (as this determines the absorbency of the solution by the law of Lambert-Beer). Therefore a solution of 10 mM of $EuCl_3$ is used for each experiment to keep this parameter constant. The remainder of the solution contained 50 mM of $(NH_4)_2SO_4$ and 20 v/v% isopropanol dissolved in milli-Q water. How this solution is made can be found in Section 3.2.

Set-up The solution is sent through the reactor with a 60 W LPML (spectrum found in 4.1.2. The pump used is described before and manages the residence time by varying the flow rate, the reactor itself is not changed between experiments. This implies that clogging might be a possibility at very high residence times (low flow rates). But this is indicated clearly if this occurred. The experiments were done in order of rising residence times (from high to low flow rates) to prevent clogging the system from the beginning. The results can be found in the Figure 5.4 and in the table in Appendix C.2.

Results In Figure 5.4 several observations could be made. In the beginning of the graph, it can be seen that there is a certain induction time is present, this has been described before by Van den Bogaert and it is the time in which supersaturation of Eu^{2+} has to be build up and no product is formed [7]. In these results, the induction time is equal to 295 seconds (4.9 minutes).

Secondly, the shape of the curve is linear in the first part from 300 up to 1000 seconds of residence time, but this shape is not maintained with higher residence times. Thus for the first part, a zeroth order reaction rate (light flux limited) can be assumed. For higher residence times, more factors are involved. As residence time increases, pH lowers which becomes a problem as time increases. As pH decreases, Eu^{2+} will oxidise to Eu^{3+} due to a difference in redox potential (between Eu^{2+}/Eu^{3+} and H_2/H^+) increases and produce H_2 in the process. This H_2 has two effects, it reduces the actual residence time as it occupies space in the reactor and it reduces conversion as it is formed due to oxidation of Eu^{2+}. Therefore, as residence time increases and conversion increases, conditions are less favourable for the conversion

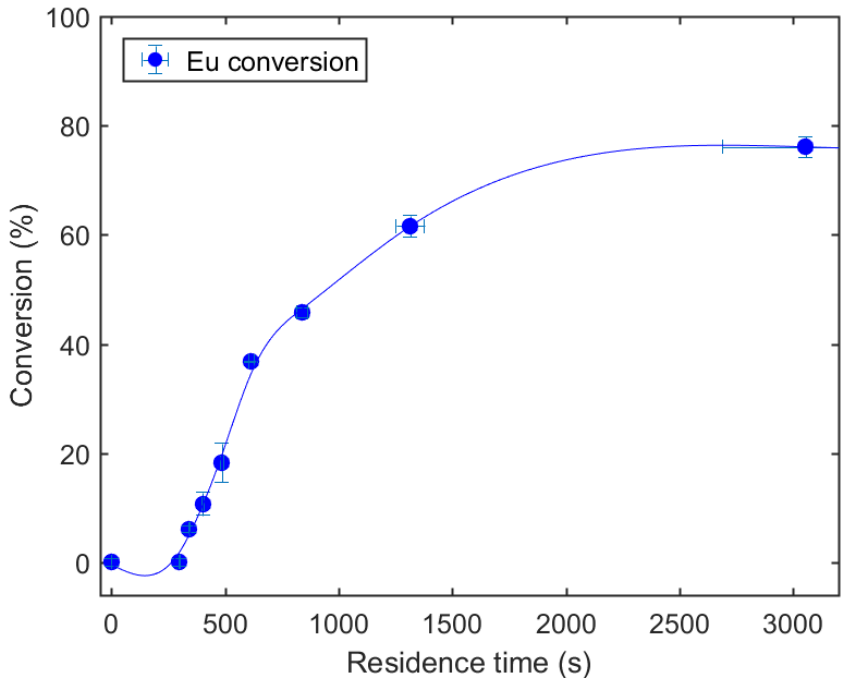

Figure 5.4: Conversion vs. residence time using the LPML tubular setup with a Eu-solution as feed.

of Eu^{3+} to Eu^{2+} and deviations from this zeroth order reaction rate are observed as reverse reaction are involved.

It can also be observed that 100% conversion is not reached in the experiments, the maximum observed conversion in this type of reactor with 10 mM of starting concentration of Eu^{3+} is 75%. There are four reasons why a sort of flattened curve is observed. Firstly, as the concentration of Eu^{3+} drops, the absorbance drops as well, thus the reaction rate is lowered, making it more difficult to produce $EuSO_4$. Secondly, as the reaction progresses, more and more $EuSO_4$ is formed which also implies that more and more acid is formed as explained above (see reaction scheme in Section 2.3.2), this acid has the potential to oxidise Eu^{2+} and as the pH lowers, the reaction rate of the back-reaction (oxidation) increases. As the back-reaction occurs, more and more gas is formed, which lowers the actual residence time as explained above. Lastly, as more and more solids are formed, more light can be reflected, absorbed or scattered by the solids which reduces the amount of photons received by the Eu^{3+} still in solution thus limiting the reaction speed for the reduction of Eu^{3+} and formation of the product. The solids can even create dark spots in the reactor by completely blocking UV-light, this hypothesis will be explored in Chapter 6. The combination of these aspects might explain why the measured curve flattens out and will never reach 100% conversion. Due to the gas formation in this reactor which is not desired, a certain loss of space of reactor volume is observed which is not the

case in a batch reactor whereby the formed gas can escape freely in the atmosphere.

The solids are dragged along the tube and clump together at very low flow rates, at higher flow rates they didn't seem to clump together (as the turbulence increases and so does the Re number) that much and be more dispersed. One can predict that at very low flow rates (high residence times) very dense plugs of solids are being formed. These very dense plugs will block the light to the inside of the plugs such that these dense plugs act as dark spots in the reactor which favour the oxidation of Eu^{2+} as a limited amount of light and a local high concentration of Eu^{2+} is present.

Leblebici et all. already proved that dark spots in a reactor for this particular reaction is not at all desired since it stimulates the back reaction, i.e. the oxidation of Eu^{2+} [52]. These dark spots might occur inside the plugs of solid particles as the particles shield the inside of the slug from any light thus promoting the back reaction to occur. As these solid particles tend to clump together more with lower flow rates (higher residence times) this phenomena occurs more in that case.

Mass transfer could also be a limitation in this set-up with long residence times. As the solids gather in dense plugs, the remainder of the Eu^{3+} must be brought to the crystals to grow which is hindered when all solids are closely together. Disabling the solids to cluster together might increase mass transfer of Eu^{3+} from the bulk to the solid particles.

Model Results In previous chapter (Chapter 4), a model was developed to estimate the reactor outflow, it needed only one extra factor to work, which was the induction time. Using the previous data, the induction time can be estimated to be 295 seconds. This leads to the prediction as seen in Figure 5.5 with the measurements as dots in red and the prediction in blue. It can be seen that the reactor follows the model until 700-800 seconds up to a conversion of 40-50%, after this point, deviations start to occur due to acidification, light blockage and less absorbance. Eventually a plateau is reached at around 75% conversion whereas the model doesn't identify the existence of the plateau (considering that the model doesn't account for solids and acidity), but the model indicates a decrease in reaction rate starting at a residence time of 1000 seconds as seen in the results as well. The model is useful to identify the maximal conversion determined by the light absorption and provides an point to aim for when optimizing this reactor by implementing different strategies as seen in Chapter 6 whereas the flow is pulsed to reduce dark spots in the reactor. This technique will reduce the slug formation and thus eliminating spots which are ideal for oxidation of Eu^{2+} which needs to be avoided.

As seen in the model chapter, a performance parameter, PSTY, was introduced to describe the productivity of the reactor and its efficiency compared in terms of lamp power. This PSTY can be determined for every measurement by the equation as seen in Section 4.3.2 in equation 4.18. The PSTY is basically the amount of product formed per unit of reactor per time per kW of standardised lamp power.

From Figure 5.6, it can be seen that the PSTY from the experiments do seem to fit the PSTY predicted by the model in the range between 300 and 800 seconds of residence time. After 800 seconds a deviation starts to occur which might be

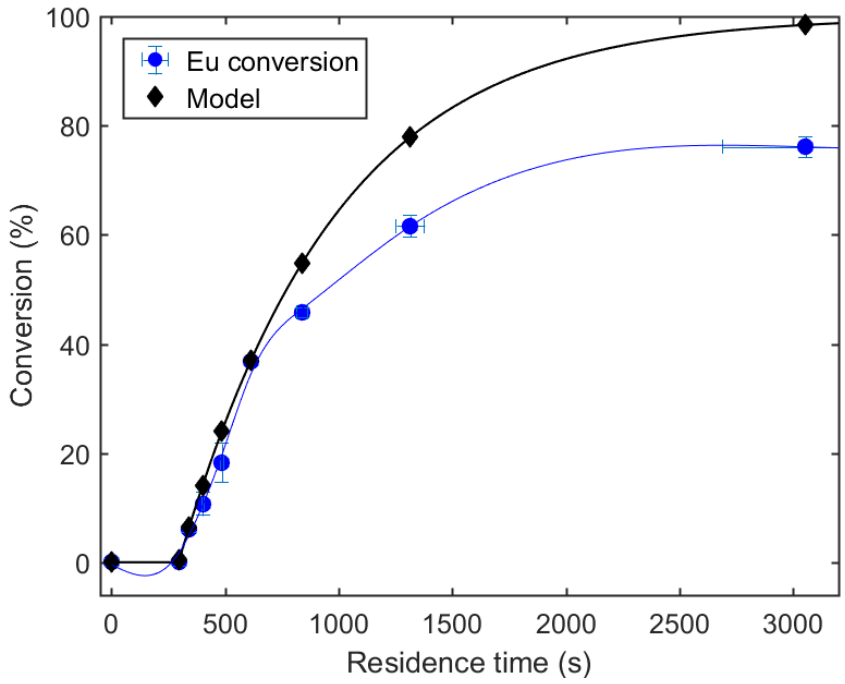

Figure 5.5: Conversion vs. residence time using the LPML tubular setup compared to the model predictions.

linked to a more favourable environment for the reverse reactions that reduce the conversion. It can also be seen that an optimum is present in the model as well as in the measurements. These 2 optima are at a slightly different residence time. The model predicts the optimum at 900 seconds whereby the measurements indicate that this is present at 700 seconds. The deviation can be explained by the increased rate of the reverse reactions as conversion increased. Theoretically, working at a residence time of 700 seconds will yield the largest amount of product per time, but this indicates that for a residence time of 700 seconds, still more than 60% of the initial Eu is present in the outlet of the reactor. Based on an economic point of view, this operation point is not the way to go, unless a recycle stream can be used, which cannot be done when actual YOX is used as Y in solution will become more and more concentrated and eventually precipitate.

Determining losses for highest residence time Some of the losses (difference in model and measurements) as described before can be determined. As mentioned before gas is produced in the reactor. The reason is the oxidation of Eu^{2+} to Eu^{3+} due to a difference in redox potential to form H_2 in the progress. The couple of redox

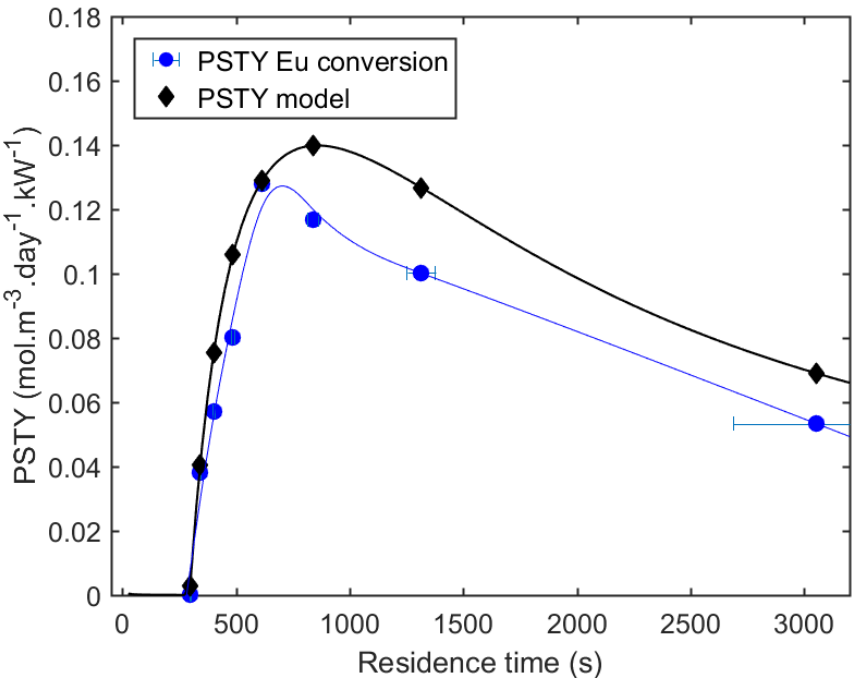

Figure 5.6: PSTY vs. residence time using the LPML tubular setup with a Eu-solution compared to the model predictions. No vertical error bars were placed due to the multiple variables in the PSTY formula.

reactions is the following:

$$Eu^{3+} + e^- \rightleftharpoons Eu^{2+} \quad E_0 = -0.35V \tag{5.3}$$

$$2\,H^+ + 2\,e^- \rightleftharpoons H_{2(g)} \quad E_0 = 0.00V \tag{5.4}$$

The redox potential of Eu^{2+}/Eu^{3+} is slightly lower than -0.35 V due to the ionic strenght of the solution (explained later). The redox potential of Eu^{2+}/Eu^{3+} is equal to -0.236 V at pH 4 (initial pH) and -0.118 V at pH 2 (final pH). Thus, when the conversion increases, the difference between the redox potentials increases and the gas production rate increases.

This results in two losses, firstly a loss of volume available for the liquid, thus a lower actual residence time and secondly the loss of actual product (Eu^{2+}) that is converted to starting product (Eu^{3+}). To estimate the gas content of the reactor, the velocity of the liquid at an interface (gas-liquid or liquid-solid) is measured at the outlet of the reactor, this is done by timing the time it took to travel a certain distance (100 mm) in the last part of the reactor and comparing it to the expected velocity (reactor length divided by residence time). The results are shown in Table 5.1.

It can be seen that the actual flow rate is substantially higher than the expected flow rate based on a reactor filled with liquid from which the data is found in

Table 5.1: Measured versus expected flow rates for a residence time of 3054 seconds.

Nr.	$v_{measured}$ (mm/s)	$Q_{measured}$ (mL/s)	$Q_{expected}$ (mL/s)	v_{gas} (mm/s)	Q_{gas} (mL/s)
1	3.44	0.00530	0.00473	0.36	0.00056
2	3.46	0.00533	0.00473	0.38	0.00059
3	3.50	0.00539	0.00473	0.42	0.00065
4	3.40	0.00523	0.00473	0.32	0.00050
Average	3.45	0.00531	0.00473	0.37	0.00058

Appendix C.1 in Table C.2 (the first entry). The gas flow and velocity is derived by subtracting the measured flow from the expected flow rate and velocity respectively. Using this information the actual residence time is calculated

$$V_{reactor}/Q_{average} = \frac{14.47\,mL}{\frac{0.00531+0.00473}{2} mL/s} = 2882s \tag{5.5}$$

This actual residence time (2882 s) is shorter than the predicted residence time (3054 s) based on a reactor full of liquid, with a difference of 5.7%. This indicates that the measurement point will shift towards the left on Figure 5.5. The gas volume present in the reactor is 5.7% if a constant gas production is assumed (linear increase as function of time) (determined by $Q_{gas,average}/Q_{average}$). Assuming a pressure of 1 bar, the amount of gas in the reactor can be determined by the ideal gas law:

$$n_{H_2} = \frac{p \cdot V}{R \cdot \Theta} = \frac{101300Pa \cdot 0.057 \cdot 14.47 \cdot 10^{-6} \cdot m^3}{8.31J \cdot mol^{-1} \cdot K^{-1} \cdot 298K} = 3.37 \cdot 10^{-5} mol \tag{5.6}$$

$$n_{Eu^{2+},oxidised} = 2 \cdot n_{H_2} = 6.75 \cdot 10^{-5} mol \tag{5.7}$$

$$c_{Eu^{2+},oxidised} = \frac{n_{Eu^{2+},oxidised}}{V_{liquid}} = \frac{6.75 \cdot 10^{-5} mol}{(1-0.057) \cdot 14.47 \cdot 10^{-3} L} = 0.00498 mol/L \tag{5.8}$$

It is determined that 0.00498 M, which is 4.98 mM oxidised to form H_2 gas. As the inlet concentration of Eu^{3+} is equal to 10 mM, this is not possible based upon the model since only 2 mM (20% of 10 mM) is the difference between the model and measurements, which is the amount that is lost. But in this reasoning, one remark must be made, a lower conversion is eventually reached (75%). This indicates that a higher concentration was present in the reactor than seen in the model, thus a higher light absorption and reaction rate (for the reduction of Eu^{3+} was possible. As this reduction was counteracted by the oxidation of Eu^{2+}, it is possible that this amount is formed. The amount of 'lost conversion' which is the difference between theoretical conversion (integral of reaction rate to residence time and actual conversion) can be

estimated based upon the measurements, but this will not be done here due to its complexity.

Thus the losses by the oxidation of Eu^{2+} are difficult to link to the amount of gas produced in the reactor. As it was not possible to put a number onto these losses, it is not possible to determine the loss by solids blocking UV light as this is too difficult to determine the area taken in by solids on a picture of the reactor as it is not known if they block all UV light or just a small fraction.

Comparison to batch results of Van den Bogaert et al.

Batch reactor by Van den Bogaert Van den Bogaert et al. used a cylindrical batch reactor with a volume of 100 mL, a diameter of 4 cm and covert with a quartz plate to prevent evaporation. 80 mL of 10 mM $EuCl_3$ with 50 mM of $(NH_4)_2SO_4$ is poured in the reactor and 16 mL of isopropanol (20v/v%) is added to the solution. This results in a height of 7.64 cm in the reactor. The mixture is stirred for the duration of the reaction. The results of this experiment are seen in literature in Section 2.3.2 in Figure 2.10. The comparison will be made against the one with highest intensity of 11.6 $mW.cm^{-2}$ with a lamp source of 160 W as the average intensity in the tubular reactor is 23.8 $mW.cm^{-2}$, which is slightly more than double. As seen in the previously mentioned graph, the batch results indicate an induction time of 6 hours, a time of 10.7 hours to remove 50% of the available Eu, and 13 hours to remove nearly 100%. [7]

Induction time The induction time is a lot lower as compared to the results in a batch type reactor of Van den Bogaert et all. He measured induction time of 6 hours for a reactor with halve of the intensity. Scaling to a batch reactor with similar irradiation relates to an induction time of 2.77 hours as the product of the induction time and intensity is constant in his results. Comparing an induction time of 295 seconds (tubular reactor) to 9980 seconds (batch), the induction time is 34 times shorter, which is a large reduction in time.

Removal rate The removal rate in the experiments of Van den Bogaert is constant (pseudo zeroth order) since its path-length for the incoming light is very high, thus nearly all incoming light can be absorbed at every moment in time. The tubular reactor with a very short path-length results in the absorption of just a few percent of the incoming light, but with a more uniform light distribution. Van den Bogaert reported a removal rate of 1.11 mM/h, scaling this to the same intensity as the tubular results in 2.28 mM/h. For the tubular reactor, the removal rate is split up in three parts, between 300-600 seconds the rate is 43 mM/h, between 600-1300 seconds the rate is 13 mM/h and between 1300-3050 seconds the rate is 2.9 mM/h. Thus even in the last part of the removal rate in the tubular reactor is larger than in the batch type with increases ranging from 27% up to 18 times faster. These results are estimated based upon the results described in Appendix C.2. The removal rate in the tubular reactor is not constant as seen in the batch reactor.

Comparing PSTY The PSTY, as described before can be calculated to describe the productivity of the reactor compared to its light input. If the PSTY is split into its components (STY and LP), the results will become more easy to comprehend. Two points are taken to compare the batch reactor to the tubular reactor, these are at 50% removal and at 75% removal (since the tubular reactor didn't approach 100% removal. The results of this comparison are seen in Table 5.2.

Table 5.2: Comparison of batch vs tubular reactor for recovery of Eu from Eu-solution without Y. With all specifications to determine the values in text.

	Factors	Batch	Tubular	Improvement
PSTY (50% Removal)	τ (h)	10.7	0.264	41
	STY ($mol.m^{-3}.day^{-1}$)	9.35	455	49
	LP (kW)	1667	4147	
	PSTY ($mol.m^{-3}.day^{-1}.kW^{-1}$)	0.00561	0.110	20
PSTY (75% Removal)	τ (h)	10.7	0.847	13
	STY ($mol.m^{-3}.day^{-1}$)	16.82	212	13
	LP (kW)	1667	4147	
	PSTY ($mol.m^{-3}.day^{-1}.kW^{-1}$)	0.0101	0.0512	5

It is shown in Table 5.2 that the PSTY of the tubular reactor is a lot better compared to the batch reactor. It excels at 50% removal of Eu with an improvement of 20. Also the space time yield is improved in a tubular reactor, the reactor is capable of producing up to 49 times more product in the same time and space as compared to the batch reactor. Thus in terms of efficiency, the tubular reactor is definitely an improvement over the batch reactor

Advantages and disadvantages of tubular compared to batch. The advantages of the tubular reactor for this type of reaction is seen above, it is more efficient in its light distribution up to a certain point. It can also be operated in continuous mode, which is more favourable for reproducible production.

But the tubular reactor has some disadvantages as well. As conversion increased and pH drops, the amount of gas in the reactor increased as well, which is not desired as a certain volume of the reactor is used by the gas. It is better to use a batch reactor in the last part of conversion from 50% conversion and up as this is more convenient for the gas pockets to escape rather than filling up the reactor.

In this case, a tubular reactor in combination with a batch reactor can be used. The batch reactor is required to efficiently remove the remaining Eu and provide an easy way for the gas to escape. It might be better to use an immersed lamp set-up as batch reactor as these tend to be more efficient than a batch reactor with a lamp placed above it.

5.3 Separation of artificial YOX

In previous experiments, the performance of the reactor was tested using a solution which only contained europium and additives, but no yttrium. In order to check whether this method is viable for separating YOX, an artificial sample is produced. This contains the correct ratio of Eu/Y, if both are converted to their oxides around 8 m/m% of Eu_2O_3 is the ratio to aim for. This results in a solution containing 10 mM of $EuCl_3$, 220 mM of YCl_3, 50 mM of $(NH_4)_2SO_4$ and 20 v/v% of isopropanol dissolved in water and the pH is adjusted to 4. How this solution is made can be found in Section 3.2. The amount of YCl_3 turned out to be 190 mM due to the hygroscopic nature of the salt, but it is still sufficient to test the performance of the reactor with the influence of large amounts of Y^{3+}.

This solution containing Eu^{3+} and Y^{3+} is fed into the reactor in the same way as in the previous experiments. It is expected from literature that the conversion will be less in time compared to previous experiment (without Y) [8]. The results from this experiment can be found in Figure 5.7 and in Appendix C.3 for the measurements.

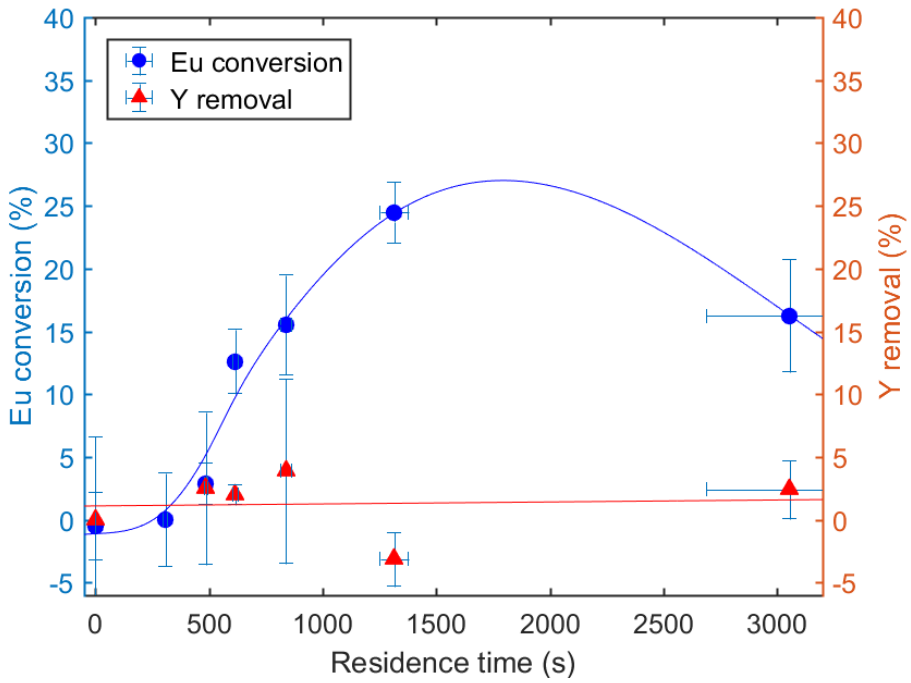

Figure 5.7: Conversion vs. residence time using the LPML tubular setup with artificial YOX as input.

Results As seen before by Van den Bogaert et al. [8], the conversion is less compared to previous experiment (without Y in solution). This deviation can be explained by an increase in induction time and a lower concentration of SO_4^{2-} in

the vicinity of Eu^{3+}. The induction time is higher (around 400 seconds, which is 100 seconds longer as before), this is explained by the fact that less SO_4^{2-} is present in the coordination sphere of Eu^{3+} as Y^{3+} attracts SO_4^{2-} in its surroundings when dissolved in water. This lowers the chance for Eu^{3+} to be reduced as less Eu^{3+} in solution will be surrounded by SO_4^{2-} which enables the charge transfer reaction to occur. This explains why it takes longer to reach supersaturation (induction time). This same mechanism will contribute to a lower reaction speed as before as the actual concentration of Eu^{3+}−SO_4^{2-} decreases.

The reaction rate is equal to 9 mM/h in the first part (300 to 1300 seconds). This rate is a lot lower as compared to the solution containing no Y (43 mM/h). The conversion decreased after a residence time of 1300 s was achieved, contrary to normal behaviour. It was observed that the reactor clogged up slightly at this low flow rate, it did not do this without the presence of Y, but as the ionic concentration in solution increases, the chance of clogging increases as well. As the electrostatic barrier is decreasing by the large concentration of introduced ions, the chance of solids being deposited on the wall and forming aggregates is higher [54]. Clogging of the walls increases the available $EuSO_4$ in the reactor which can break off the walls and redissolve and oxidise again to enrich the Eu^{3+} concentration again. A measurement was only taken after 3 residence times, thus some clogs could be forming in the reactor that have accumulated $EuSO_4$. This issue can be solved by introducing more turbulence, either by pulsing the flow or by reducing the diameter of the tube for a given flow rate and increasing reactor length or increasing reactor length, keeping the diameter constant and increasing flow rate.

On the same Figure 5.7, it is shown that the amount of Y^{3+} stays relatively the same at 0% removal with some large measurement errors, proving that this separation is usable.

Thus using the method of photochemical separation, it is possible to separate YOX in a millichannel reactor without clogging the reactor, but the efficiency is a lot lower compared to the experiments without Y^{3+} in solution.

Comparison to earlier batch results Van den Bogaert et all. in his batch-experiments also experienced a more difficult separation with the presence of large amounts of Y^{3+} (Y/Eu = 20/1) in solution. He indicated an induction time of 10 hours and a nearly full conversion time of 20 hours using an 11 W lamp submerged in a batch reactor with a volume of 300 mL which is stirred for the duration of the reaction. The intensity of the lamp at the closest point to the solution is not known however. A similar reaction rate was seen, but the efficiency is better as more product was removed in that case, only 5-10% Eu was left in solution. [8]

Determining losses for highest residence time As seen before in the experiments with the Eu-solution, an attempt will be made to estimate the losses due to gas formation. As every step is explained in paragraph 5.2, not every detail will be

explained. As before, the rate of exiting gas is estimated. The data is seen in Table 5.3.

Table 5.3: Measured versus expected flow rates for a residence time of 3054 seconds with artificial YOX as reactant in the reactor.

Nr.	$v_{measured}$ (mm/s)	$Q_{measured}$ (mL/s)	$Q_{expected}$ (mL/s)	v_{gas} (mm/s)	Q_{gas} (mL/s)
1	5.00	0.00770	0.00473	1.92	0.00296
2	4.76	0.00733	0.00473	1.69	0.00260
Average	4.88	0.00751	0.00473	1.80	0.00278

More gas is present in the reactor compared to the Eu-solutions. This reduces the actual residence time substantially to 2363 s instead of 3054 s, which is a reduction of 23%. The gas content is equal to 23%, which is substantial as this amount of gas is unwanted. By doing the same calculation as in paragraph 5.2, a loss of 24.4 mM of Eu^{2+} is calculated which is more than the inlet concentration. But just as before, a lower conversion as expected is seen which has increased the amount of total absorbed light, therefore this value can be true. A rough estimation can be made by assuming an average concentration of 8.5 mM (corresponds with 15% conversion). Reffering to graph 4.5, a reaction rate of 0.012 mM/s can be read. Using this average reaction rate and the actual residence time, a hypothetical conversion of 28.3 mM ($0.012 mM/s \cdot 2363 s$) is calculated which is in the neighbourhood of what is calculated. Of this 28.3 mM, only 1.6 mM (16% conversion) is converted into useful product.

Influence of Y^{3+} on separation of Eu^{3+} Why more gas is present compared to the Eu-solutions can only have one explanation, the only difference in both feeds is the Y in solution (which makes up 220 mM). As the introduced Y is in the form of YCl_3 which produces Y^{3+} and Cl^- in solution, this alters the activities for the other species in solution (Eu^{3+} and Eu^{2+}). An overview of the content of the solution is given in Table 5.4. The ionic strength is calculated by the following formula [55]:

$$I_s = \frac{1}{2} \sum_{\mathrm{i}=1}^{n} c_{\mathrm{i}} z_{\mathrm{i}}^2 \tag{5.9}$$

with I_s the ionic strenght, c the concentration and z the charge of the ions in solution.

The initial ionic strength in the Eu-solutions is equal to 0.21 M, when Y is added in, the ionic strength changes to 1.53 M. The ionic strength in the YOX-solutions is even higher (1.81 M).

To determine the activity coefficient, the Debye-H*ü*ckeltheory can be used. This theory is valid for aqueous solutions up to ionic strengths up to 0.1M. As these solutions don't comply to either of both solutions, only the principle will be explained, but figures will be left out for their inaccuracy, more complex theories might be able to give the exact figures. The formula of Debye-H*ü*uckel is the following, with A a

Table 5.4: Composition of Eu-solution, artificial YOX and real YOX solutions. The Cl^- and Na^+ (latter 2 columns) are coming from the dissolution of YOX and the neutralisation of HCl respectively. The ionic strength is determined at the beginning of the reaction and decreases by a small bit as Eu^{2+} is formed and ions are removed from the solution.

Ion	Eu^{3+}	Cl^-	NH_4^+	SO_4^{2-}	Y^{3+}	Cl^-	Na^+	Cl^-	I_s (M)
charge	3	-1	1	-2	3	-1	1	-1	
Eu-solution (M)	0.01	0.03	0.1	0.05	0	0	0	0	0.21
Artificial YOX (M)	0.01	0.03	0.1	0.05	0.22	0.66	0	0	1.53
YOX (M)	0.01	0.03	0.1	0.05	0.22	0.66	0.28	0.28	1.81

constant (0.5085 at 25℃ in water) and B a constant as well (0.3281 at 25℃ in water) and a_0 the ionic radius and z the charge of the ion for which the ionic strength is required:

$$\gamma = \exp_{10}(-A \cdot z^2 \frac{\sqrt{I}}{1 + B \cdot a_0 \sqrt{I}}) \tag{5.10}$$

It can be easily seen that as the charge increases, the ionic strength increases or the ion radius increases, this will have the same effect; the activity coefficient decreases. If Eu^{3+} is compared to Eu^{2+}, it can be seen that the charge is higher for the 3+ variant and it has a smaller ionic radius [56]. This leads to a decreased activity coefficient of Eu^{3+} compared to Eu^{2+}. As the ionic strength is increased the difference enlarges even more.

When using activities instead of concentration to determine the 'standard' redox potential of Eu (assuming Eu^{2+}/Eu^{3+} of 1/1), the following is obtained:

$$E_{Eu^{3+}/Eu^{2+}} = E_0 - \frac{0.0591}{n} \cdot \log \frac{a_{Eu^{3+}}}{a_{Eu^{2+}}} \quad E_0 = -0.35\ V \tag{5.11}$$

comparing this to the hydrogen potential, which acts as oxidator:

$$E_{H^+/H_2} = E_0 - \frac{0.0591}{n} \cdot \log \frac{a_{H^+}}{a_{H_2}} \quad E_0 = 0.00\ V \tag{5.12}$$

This means that the redox potential of Eu^{3+}/Eu^{2+} shifts to a more negative one, which favours the oxidation of Eu^{2+}, thus reducing the stability of the formed $EuSO_4$ in solution. This theory indicates that with the addition of more salts in the real YOX-solution, this problem becomes even worse.

As the reaction progresses, the pH becomes more acidic; it shifts from pH 4 to pH 2 (as seen by [8]). As the redox potential of H_2/H^+ is equal to -0.236 V at pH 4 (initially) and -0.118 V at pH 2 (end of reactor), the oxidation of Eu^{2+} is favoured even more as the reaction progresses.

The reduced activity coefficients have an additional effect; it increases the solubility of Eu^{2+}. This makes it more difficult to achieve crystallisation of $EuSO_4$

(increased induction time) and an increased solubility leads to a potential increased rate of oxidation of Eu^{2+}. The solubility is written below:

$$K_{sp} = 1.5 \cdot 10^{-9} = a_{Eu^{2+}} \cdot a_{SO_4{}^{2-}} = \gamma_{Eu^{2+}} \cdot c_{Eu^{2+}} \cdot \gamma_{SO_4{}^{2-}} \cdot c_{SO_4{}^{2-}} \tag{5.13}$$

5.4 Separation of YOX

It was already observed that with the introduction of Y^{3+} into the system, the productivity of the system drops significantly. Separation is more difficult to achieve. It is expected from results by Van den Bogaert et al. that the separation of real YOX-mixtures will be even more difficult.

Set-up To test the performance of the reactor with YOX, the YOX-mixture as described in Section 3.2 is introduced into the reactor. This mixture consists of dissolved Eu^{3+} and Y^{3+} with a very high ion concentration due to the neutralisation (by NaOH) of the used HCl that was used to dissolve the YOX. The same setup, that is used for the separation of artificial YOX and the Eu-solution, is also used for this experiment.

Results The separation is shown in Figure 5.8 for the 2 highest residence times. It is shown that no separation occurs, this was confirmed visually, no solids came out of the reactor. The Eu-concentration was constant at zero percent conversion, with a relatively high margin of error. The same is seen for the Y-concentration in the reactor outflow. A very high gas content was seen in the reactor which will be explained more into detail in the next paragraph.

It can be assumed that by irradiating the solution for a much longer period, some product might be formed in the end, but with the cost of even more gas in the reactor, which makes it not efficient.

Losses of the highest residence time Similar as in the chapter of artificial YOX, the amount of gas in the reactor is estimated by determining the velocity of the outgoing fluid. The results is shown in Table 5.5.

Table 5.5: Measured versus expected flow rates for a residence time of 3054 seconds with YOX as reactant in the reactor.

Nr.	$v_{measured}$ (mm/s)	$Q_{measured}$ (mL/s)	$Q_{expected}$ (mL/s)	v_{gas} (mm/s)	Q_{gas} (mL/s)
1	5.02	0.00772	0.00473	1.94	0.00299
2	5.52	0.00850	0.00473	2.44	0.00376
3	5.69	0.00876	0.00473	2.61	0.00402
4	5.31	0.00818	0.00473	2.24	0.00344
average	5.38	0.00829	0.00473	2.31	0.00355

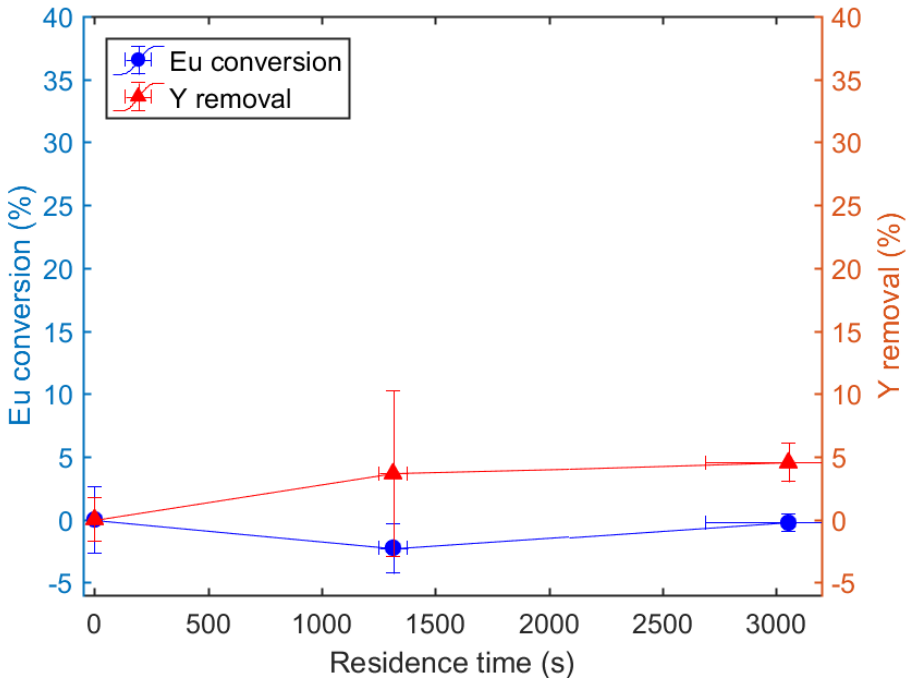

Figure 5.8: Conversion vs. residence time using the LPML tubular setup with YOX as input.

It is shown that the gas content is more than in the case of artificial YOX, which is indeed expected as previous results by Van den Bogaert indicate a more difficult separation. Using the same calculations as in the section of artificial YOX, an actual residence time of 2222 seconds is observed, which is a reduction of 27% (4% more than with artificial YOX). The gas content of the reactor is 27% leading to a loss of 30.3 mM which is also higher than the total amount of Eu^{3+} in the system. Also here, a rough estimate can be made on whether this is possible. As no conversion has occurred, but the incoming concentration is lower (8 mM), a different reaction rate is read from Figure 4.5 of 0.12 mM/s, doing the same calcution as before leads to a hypothetical conversion of 25.7 mM ($0.012 mM/s \cdot 2222 s$) which is all converted into H_2.

It can also be assumed that the redox potential of the Eu^{3+}/Eu^{2+} will become even more negative as in the case with artificial YOX, resulting in a higher chemical potential for oxidation of Eu^{2+} as seen by the higher gas content. This is caused by the increase in ionic strength by the HCl for dissolution of YOX and the added NaOH to neutralize it again.

Comparison to batch Van den Bogaert et al. did some batch experiments with actual YOX, but didn't achieve a good result by doing so. He used the same setup as described in the artificial YOX comparison which is an immersed lamp in a

large beaker of solution. He didn't achieve full conversion at all. After 50 hours of irradiating the solution, only half of the Eu in solution did precipitate as $EuSO_4$. The tubular reactor didn't achieve any better results at all.

5.5 Conclusion

Photochemical recovery of Eu is certainly possible in a tubular reactor set-up, although the separation becomes more difficult when Y is introduced in the system. The tubular reactor achieved to drastically reduce the induction time from a couple of hours to a few minutes for solutions and it was possible to remove 76% of the introduced Eu in less than 1 hour of residence time in solutions without Y. It was able to vastly reducing the residence time compared to the batch reactor for similar conversion. The model, derived in the previous chapter, matched well with the results seen in the experiments but started to deviate at a conversion of roughly 50%. At high residence times, more gas was present in the reactor hindering the reaction by reducing the actual residence time. It is possible that by extending the residence time, a higher conversion of Eu can be achieved but this reduces the efficiency of the reactor.

When Y was introduced in the form of artificial YOX (Y/Eu = 22/1), separation became more difficult as seen by the experimental results. A maximum of 25 % conversion was achieved at the second highest residence time and a decreasing conversion was seen at higher residence times, the reason for this is unknown. It is estimated that the conversion of Eu in mixtures of Eu and Y is more difficult by the increased ionic strength of the reaction which influences the redox potential in favour of Eu^{3+}, thus reducing the stability of Eu^{2+}.

Experiments on actual YOX didn't produce any solids by the reactor. A lot of gas was produced, indicating that a reaction was occurring, but not the desired one. Batch results already predicted a difficult conversion of Eu in the case of YOX. For the separation of YOX, it might be better to use either a modified tubular reactor (able to remove the formed gas) or an immersed lamp set-up as the latter one produced a reasonable result in the past.

Chapter 6

Process intensification of Eu recovery

In the previous chapter, it was clear that solid $EuSO_4$ can be made using a tubular reactor, but when the performance was compared towards the model predictions, a deviation was seen. Less product was formed than expected.

6.1 Pulsed flow experiments

As seen in the previous section, it is important to keep the flow of the fluid high enough to prevent particles from settling which can form plugs or even clog the system. In the experiments in Chapter 5 a special type flow was seen in the experiments with very long residence time (1400 seconds and up). The observed flow consisted of solid particles that were densely aggregated together with gas slugs (H_2) that divided up the flow. As the amount of aggregated solids is one of the factors which might influence the conversion, this might be an opportunity to increase conversion by operating the reactor in a saltation flow regime, where the particles are more dispersed instead of a densely agregated regime. The idea is that when these plugs are present, they act as dark spots which inhibit the forward reaction (formation of $EuSO_4$). Only the oxidation of Eu^{2+} might occur in these plugs which might even be going faster by the high local concentration of solid $EuSO_4$. Therefore, by breaking up the slugs, more light can reach the solids and preventing dark spots and reducing the change of high local concentrations of solids.

Set-up The set-up to perform these experiments is described in Section 3.3.3 and consists of a tubular reactor which is fed by a peristaltic pump that is controlled by arduino.

The aim of this experiment is to investigate whether the solid behaviour (as seen in Figure 2.11) can be influenced by manipulating the duty cycle and secondly to investigate whether dark spots (formed inside the plugs) have a large influence on the conversion. It is hypothesised that these plugs will shield off all UV-radiation, blocking the formation of more solid $EuSO_4$. Thus in these dark spots, only the

oxidation of Eu^{2+} is able to occur which lowers the conversion. By breaking up these plugs, more light is able to reach these solids, which stimulates the remaining of the Eu^{3+} (trapped in the liquid in the solids or formed due to oxidation of the solids) to be reduced as well.

Thus to check this theory, a test is composed in which the flow rate is pulsed instead of being continuous which will in theory influence the way in which the particles move in the tube. Due to limitation of the pump, the smallest pulse that can be given is 0.5 seconds long. And for consistency, the pulse width is kept constant at 5 seconds. A few duty cycles will be tested, each with their characteristic pulse flow rate, these are shown in Table 6.1. Several duty cycles are tested, ranging from 10 up to 100% of the cycle time as seen in the table. 100% duty time refers to continuous flow with the lowest flow rate, 10% duty time refers to the highest pulsed flow with short pulses with a high flow rate (10x higher than continuous flow).

Table 6.1: Pulsed flow experiments with different duty cycles for a constant residence time. The duty time refers to the percentage of time the pump was active in the cycle time. The cycle time is constant at 5 seconds. The residence time and maximal flow rate is shown as well together with its effects on the conversion.

Duty time (%)	Residence time (s)	Maximal flow rate (mL/s)	Maximal flow rate (m/s)	Eu conversion (%)	σ_{Eu} (%)
100%	2919	0.00496	0.00329	78.7	1.4
49%	2916	0.0101	0.00668	79.3	1.7
28%	2929	0.0176	0.0117	80.1	2.0
22%	2959	0.0226	0.0150	79.5	0.5
10%	2967	0.0486	0.0322	79.3	3.1

Results As is shown in Table 6.1 and on Figure 6.1, no real effect is seen. The conversion is the same comparable with different solid behaviour. To indicate how well the solids are dispersed, some pictures of the reactor are shown in Figures C.1 in Appendix C.5 to indicate the solid distribution in the reactor. It is important to look at the bottom of the reactor (last 10 coils) as the difference is remarkable. In that region, the highest concentration of solids is observed (conversion increases from top to bottom in this reactor). It can be seen that all the solids agglomerated in the regions with higher duty time (thus lower maximal flow rate), but when the duty time decreases, a more dispersed solid distribution in the reactor coils is seen, the solids do not agglomerate, certainly not at 10% duty time (which has a 10 times higher maximal flow rate compared to the reference).

Quantifying the dense solids As Figure C.1 in Appendix C.5 is rather vague to quantify the difference in flow, an attempt was made to quantify the difference. This was done by placing a spectrometer probe onto the last loop of the reactor where the difference in plugs was the largest. The reactor was started and the spectrometer

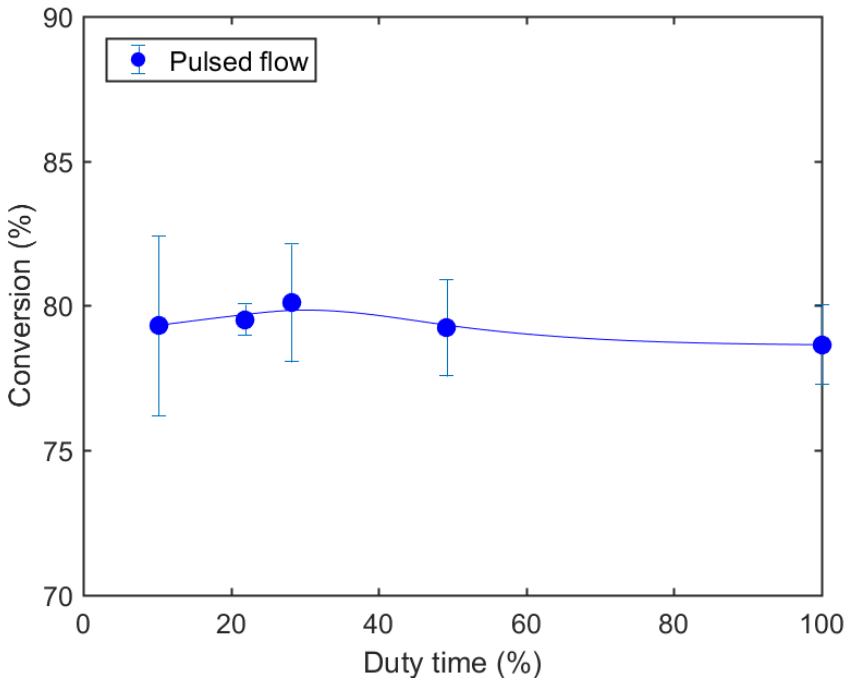

Figure 6.1: Pulsed flow experiments with different duty cycles with a constant residence time (2916-2967 seconds) and a constant pulse time of 5 seconds.

measured the intensity of the light passing through the reactor wall for two hours, but only the last part of it is useful and is shown in Appendix C.5 in Figures C.2a and C.2b (for Visible light) and Figures C.2c and C.2d (for UV light). Only the intensity of the visible spectrum is used (400 up to 600 nm) as the UV spectrum (220 up to 270 nm) was not usable but shown as well to indicate no dark spots were formed at the back of the reactor. The idea behind this set-up is that the intensity drops as a solid plug passes in front of the spectrometer and as the plug is denser, less light goes through. This method can give an indication of the amount of very dense plugs in solution. It cannot determine the volume fraction of solids as it will overestimate them as it will also take the volume of liquid into account which is in between the dense solids as they pass along the spectrometer. Thus the volume fraction will be estimated higher compared to a centrifuged sample.

The spectrometer measures an intensity between 900 $W.cm^{-2}$ (very dense plugs) up to 1600 $W.cm^{-2}$ (liquid or gas without solids). Everything in between is a solution containing liquid and small solid particles, therefore a solid fraction cannot be determined. The main difference between figures C.2a and C.2b is that more peaks are seen in Figure C.2a which extend to lower intensities, thus denser plugs are formed in the reference situation (100% duty time). To quantify this, a 'cut-off intensity' is selected. Below this intensity everything is classified as solid and above this intensity, everything is regarded as liquid or gas. This is done using a comparing

function in Matlab (script in Appendix C.5). When this data is plotted, the difference as explained before can be seen.

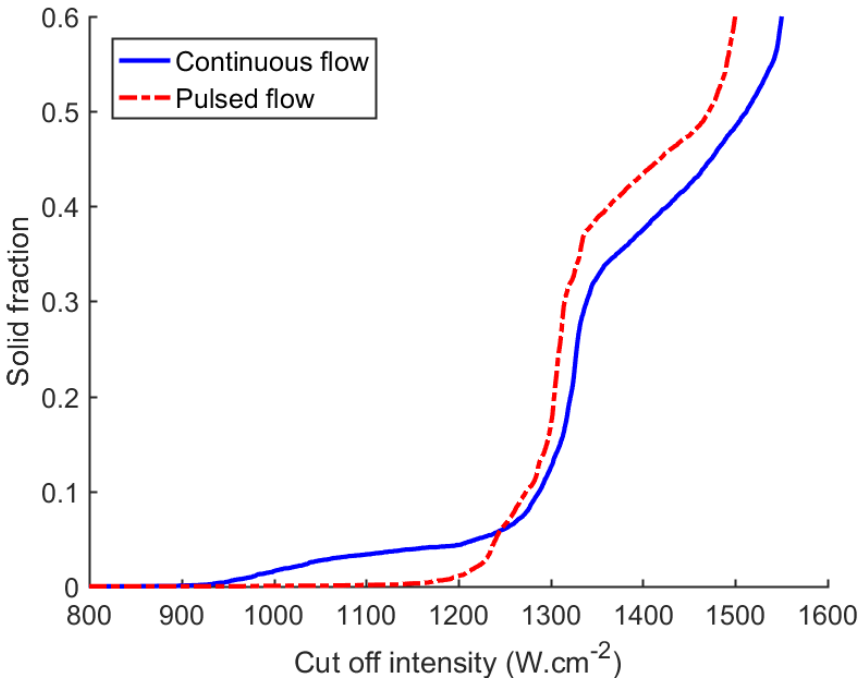

Figure 6.2: Influence of 'cut-off intensity' (explained in text) on the solid fraction calculation in continuous mode (low flow rate) compared to high pulse mode (10% duty cycle, high flow rate).

Figure 6.2 quantifies the denser solids. The reference (100% duty time) has a solid fraction of 5% at a 'cut-off intensity' of 1200 $W.cm^{-2}$ compared to < 1 % in the pulsed regime, this indicates a relatively high fraction of dense solids in the reference state which are not present in the highly pulsed mode. Thus increasing the flow rate by pulsing does break up the dense solid slugs. The total solid fraction is estimated at 35% for both modes since the graph makes a kink at that point. This is only the solid fraction in the last coil of the reactor, the total solid fraction in the reactor will be lower. A slightly higher solid fraction is seen in the pulsed mode, which is logical since the solids are more dispersed, hence they take up more space.

Determining the critical velocity for slurry flow Referring back to Figure 2.11, it is shown that by pulsing the flow, the same behaviour can be seen as if the flow rate increases. The solid distribution shifts from a high portion of solids packed in the cross-section of the tube up to a more dispersed flow (reference compared to 10% duty time). Based upon Figure C.1 an estimation can be done concerning the critical velocity for the particles when they start to settle. A sharp difference is seen between a duty time of 49% and 28%, where the particles in a 28% duty time

(and shorter) are more dispersed compared to 49% duty time and higher. Thus the critical flow rate is situated between 0.00668 and 0.0117 m/s.

Based upon the theory, the critical flow rate can be determined by the following formula by Durand as seen in Section 2.4.2: A formula was obtained to calculate the settling velocity of particles. The formula by Durand and the modified Durand equation is the following:

$$v_C = F_L\sqrt{2 \cdot g \cdot d \cdot (S_g - 1)} \tag{6.1}$$

$$v_C = F_L\sqrt{2 \cdot g \cdot d \cdot (S_g - 1) \cdot (\frac{d_p}{d})^{1/6}} \tag{6.2}$$

Some parameters are required to fill in this formula; F_L the limiting settling velocity factor is still unknown and is dependent on the particle size, g the gravity constant is equal to 9.81 $m \cdot s^{-2}$, d the diameter of the tube which is equal to 1.4 mm, d_p the diameter of the solid particles and S_g the specific gravity of dry solids ($\rho_{solids}/\rho_{water}$) which is equal to 4.98 [38].

The particle diameter is still unknown, but estimated to be in the neighbourhood of 30 μm, based upon sedimentation. Assuming Stokes' law, the following equation can be deduced;

$$d_{sphere} = \sqrt{\frac{18\mu}{(\rho_p - \rho_f) \cdot g} \cdot \frac{x}{t}} \tag{6.3}$$

with d_{sphere} the diameter of the particle, μ the viscosity of the fluid (assuming water; 10^{-3} $Pa.s$, ρ_p the density of the particle (4.98 $g.cm^{-3}$ [38]), ρ_f the density of the fluid (1.00 $g.cm^{-3}$), g the gravity constant (9.81 $m.s^{-2}$), x the distance the particle has travelled and t the time it took.

Assuming a test-tube containing a dilute dispersion of $EuSO_4$, when the test-tube was shaken to make it homogeneous, it took 4 minutes for the solution to settle again for a distance of 5 cm.

This method provides a particle size in the neighbourhood of 31 μm, despite this number is not validated by scanning electron microscopy (SEM) or another more accurate technique, it provides enough information to make an estimate using Durands equation for the limiting velocity. Using this particle size, a F_L-factor can be read from graph 2.12, which is very inaccurate for this particle size since it was developed for course particles, a factor of 0.1 can be estimated. C_v is estimated to be 0.04% for a solution with a conversion of 80% which results in 8 mM of $EuSO_4$ (1.98 $g.L^{-1}$) in solution with a solid density of 4.98 $g.cm^{-3}$.

Using this information, a limiting velocity can by caluclated by the equation of Durand (first equation) and the modified Durand (second equation) equation as shown below:

$$v_C = F_L\sqrt{2 \cdot g \cdot d \cdot (S_g - 1)} = \\ 0.1 \cdot \sqrt{2 \cdot 9.81\ (m.s^{-2})\ \cdot 0.0014\ (m) \cdot (4.98 - 1)} = 0.033\ m.s^{-1} \tag{6.4}$$

$$v_C = F_L\sqrt{2 \cdot g \cdot d \cdot (S_g - 1) \cdot (\frac{d_p}{d})^{1/6}} =$$
$$0.1 \cdot \sqrt{2 \cdot 9.81\ (m.s^{-2})\ \cdot 0.0014\ (m) \cdot (4.98 - 1) \cdot (\frac{50 \cdot 10^{-6}}{0.0014})^{1/6}} = 0.017\ m.s^{-1} \tag{6.5}$$

Durand approximates the critical velocity to be 0.033 $m.s^{-1}$ which is a slight overestimate but this formula is made for course particles, the modified formula estimates the critical velocity to be at 0.017 $m.s^{-1}$, which is a better estimate of the observed critical velocity.

Table 6.2: Pulsed flow experiments with different duty cycles for a constant residence time. The duty time refers to the percentage of time the pump was active in the cycle time. The cycle time is constant at 5 seconds. The tube Reynolds number and the particle Reynolds number are shown which are determined by Equation 2.31 by the data provided in Table 6.1.

Duty time (%)	Residence time (s)	Maximal flow rate (mL/s)	Maximal flow rate (m/s)	Re	Rep
100%	2919	0,00496	0,00322	4,5	0,3
49%	2916	0,0101	0,00654	9,2	0,7
28%	2929	0,0176	0,0114	16	1,1
22%	2959	0,0226	0,0147	21	1,5
10%	2967	0,0486	0,0316	44	3,2

To finish, the Reynolds numbers of the tube and the particles for all duty times is provided in Table 6.2 based upon the maximal flow rate provided by the peristaltic pump. As expected the Reynolds number increases with increasing flow rate. It can be seen that the particle Reynolds number is in the neighbourhood of 2 which indicated pseudo-homogeneous to heterogeneous, therefore turbulence is needed and provided by increasing maximal flow rate to disperse the solids which is seen in the experiments. This turbulence is achieved by pulsing the flow and artificially creating higher turbulence during the pulses.

The cycle time is not optimized, it is taken as short as possible for restricted by the setup (arduino and pump). An optimisation could happen, but it is unlikely that a better conversion will be achieved as no difference was seen in this experiment.

Why this experiment didn't lead to improved conversion is difficult to determine. The only explanation that can be given is that in the reference case, without pulsing the flow, light was able to be used as efficiently as in the pulsed mode, thus the amount of losses due to scattering, reflection and absorption by solids is equal in both cases.

6.2 Seeding experiments

In terms of process intensification, another possibility is to reduce the induction time. The induction time is the time needed to achieve crystal growth in the solution. This crystal growth is started when over-saturation is acquired. Skipping this step could lead to an increase in performance of the reactor since it means that no time is wasted to oversaturate the solution as this is already done by introducing crystals.

Set-up For this experiment, the same set-up is used as before, which is the tubular reactor set-up using the LPML. In the normal case, the output of the reactor is separated from the input of the reactor. In this case, 3.4% (limitation by the type of tubing available) is sent back to the input of the reactor. This is done by mixing (with a magnetic stirrer) the input (feed) and the recycle (3.4% of output) in a very small beaker (volume 10 mL) before it is pumped into the reactor. To have a steady state, the outflow is mixed as well in a small beaker (10 mL) before it is pumped to the inlet (3.4%) and to the outflow (96.6%). For this experiment, the residence time is chosen to be 615 s, which is twice the induction time (295 s). Thus when the induction time is reduced, a significant effect will be seen in the results.

Results The results from this experiment, found in Figure 6.3 and Table C.7 in Appendix C.6, indicate that seeding the feed of the reactor does increase conversion. The conversion went up from 33% for the reference to 47% conversion, which is an increase of 14 percentage points or 42% compared to the reference. The model points as indicated on the graph are calculated for an induction time of 295 s (37% conversion) for the reference and 0 s (60% conversion) for the seeding experiment. It can be seen that seeding surpasses the mode for an induction time of 295 s, but doesn't come as close as the reference to its model. When the model is tweaked to fit the data, an induction time of 170 s (47%), this is a reduction of the induction time of 125 s.

Thus seeding reduces the induction time, but doesn't reduce it to zero seconds. The PSTY, or productivity for photochemical reactors, is plotted. The same observations can be made as with the conversion, PSTY increases by seeding the solutions, since more time is available for the reaction rather than over-saturating the solution.

Other percentages of back-flow couldn't be performed due to the limitations of the available tubing. Thus it might be possible that increasing the percentage of output pumped back into the inlet can have larger effect on the PSTY and the conversion.

6.3 Conclusion

Dark spots produced by very dense plugs didn't seem to affect conversion of Eu as the results with and without pulsing to break up these plugs are very similar. Using the results from the pulsing experiments, it was possible to establish the

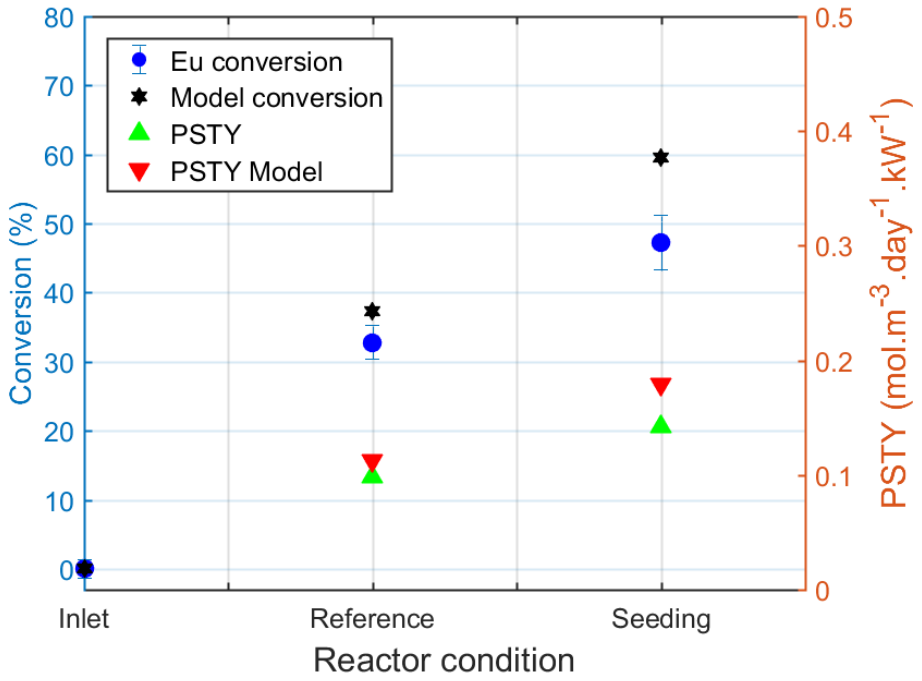

Figure 6.3: Influence of seeding on the conversion and PSTY at a residence time of 615 seconds.

critical velocity for which the solids ($EuSO_4$) form these plugs. This velocity was theoretically confirmed by the equation by Durand.

Seeding the feed of the reactor with a recycle stream of the output of the same reactor did yield better conversion. Although a part of the outlet has to be sacrificed to recycle to the reactor, it is worth the investment as the increase in conversion is significant. Conversion went up from 33% up to 47% with the same residence time but in the second case a recycle stream of 3.4% was introduced.

Chapter 7

Future work

7.1 Complete removal of europium from the solution

A complete removal or near complete removal has not been achieved in the tubular reactor set-up. In the batch set-up, described by Van den Bogaert et al., near complete removal was possible (up to 2-3% of [8, 7]. Using longer retention times, it could be determined in the future if this can also be achieved using the tubular reactor set-up. On the downside, it is very likely, especially with artificial YOX and recycled YOX, that a large amount of gas will be produced in the reactor which will decrease its performance drastically. Once near complete removal is achieved in the tubular set-up, a comparison can be made between batch and plug flow and it can be determined which type is best for which regime.

7.2 Gas removal in tubular reactors

As mentioned before gas (H_2) is formed in the reactor by the oxidation of Eu^{2+}. This gas is unwanted as it reduces the conversion and shortens the retention time as it claims valuable space in the reactor. Two methods can be thought of to remove this gas, either physically by venting off gas at various points in the reactor, either chemically by reducing the difference in redox potential between Eu^{3+}/Eu^{2+} and H^+/H_2.

Physically implementing venting in the reactor will be rather complex and eventually less efficient in terms of productivity as conversion is lost by the formation of H_2.

Chemically solving this problem can be done by reducing the ionic strength of the solution by removing a large amount of Y^{3+} from the solution by selective extraction of selective precipitation. This reduced ionic strength will vastly reduce the gas formation. Another route can be taken as well, by setting the solution to pH 4 at every point of the reactor, the difference in both redox potentials is reduced as well since in normal conditions the pH drops to 2 which increases the redox potential of H^+/H_2. This setting of pH can be done by introducing small amounts of OH^- at

several points along the reactor or by using a buffer solution, the buffer must have a pKa in the neighbourhood of 4 and be non-absorbent in the UV-area.

7.3 Seeding and influence on particle size

Only one recycle ratio was tested in the seeding experiments due to material constraints. By varying the recycle ratio, the amount of seeds can be varied and the effect on the conversion can be determined. An optimization might be possible by finding the minimal ratio for which the effect is largest.

It is likely that particle size is larger than without seeding as the introduced crystals are more likely to grow rather than more crystals to be developed. Thus by varying the recycle ratio, there is a possibility that the average crystal size can be manipulated but this hasn't yet been researched.

7.4 Reactor design with monochromatic light

Lastly, to make the reactor even more efficient, the light source can be changed to one emitting only the wavelength used in the reaction. This not only makes it more efficient, but more selective as well since side reactions based upon light can be stopped entirely if the correct type of light is not introduced into the system. LEDs lend themselves for this idea, they are capable of emitting light in a very narrow wavelength band. Secondly, lasers can be used as well as they are monochromatic, however the design of the reactor must be changed when lasers are considered to make use of their light in a more efficient way.

Chapter 8

Conclusion

The rare earth elements (REEs) play an important role in the current society. They can be found in common appliances such as magnets, (compact) fluorescent lamps, catalytic converters, etc and play a role towards a greener economy. Nowadays, the majority of the REEs are mined in China which led to disputes and price surges in the past. As a result, REEs are classified by the European Commission as a critical material due to a supply risk because of China's export quotas and of course due to their economic value. Due to this classification of the REEs and its difficult mining conditions, it becomes important to recycle REEs from end of life products that yield a fairly high amount of REEs. One of these waste streams are end-of-life fluorescent lamps.

Lamp phosphors are an important source to be considered for recycling REEs. Lamp phosphors are found on the inside of a fluorescent lamp to convert UV-light produced by the mercury vapour to visible light. Several types of lamp phosphors were developed, each with their characteristic color. The red lamp phosphor, YOX, yttria doped with europium oxide Y_2O_3:Eu^{3+} only contains 2 elements that are of economic importance is an opportunity to recycle.

The separation of YOX is commonly done by solvent extraction, but this process is expensive and inefficient. Photochemistry is upcoming concerning green chemistry. It is greener in the fact that it is more selective as it only targets specific molecules to activate them and perform specific reactions and greener as it generally can be done in mild operating conditions. The recovery of europium from YOX is one of the processes that can be performed by photochemistry due to the special redox nature of europium. Europium has 2 redox potentials that are stable, this is the +III which is the most stable form and the +II form which is targeted to perform the separation from the yttrium found in YOX. The photochemical reduction targets the +II state of europium by selectively activating a charge transfer between europium and a specific species in solution.

The separation of YOX was approached in two different ways. The first part was

based on a charge transfer reaction between Eu^{3+} and Cl^- that enabled the reduction of Eu^{3+} to occur. The reaction was performed in methanolic environment which enables the reduction step and the separation step to be done at a different time as the reaction product ($Eu(II)Cl_2$) is soluble in methanol. This principle has the benefit that these two steps can be performed in two different reactors optimized for its specific task. The separation of Eu^{2+} from Y^{3+} wasn't a success story as it could not be performed by precipitating Y^{3+} with dibutylphosphate (DBP), nor in its acidic form, nor in its salt-form was DBP selective enough. This method was based upon work performed by the previous master student. The limited stability of Eu^{2+} was the greatest issue in this separation process, although its redox potential is useful in the separation of the elements, it's instability makes the separation difficult.

As different separation procedures based upon the use of dibutylphosphate did not achieve separation of the two species (Eu and Y), different mechanisms were looked into based upon exploiting a variety of chemical properties. The first alternative separation mechanism is based upon the extraction of Eu^{2+} (produced in the photochemical reactor by the use of crown-ethers. This method had a lot of parameters to be checked with limited chance of success, therefore no attempt was made to check the principle. Secondly, a separation based on the anti-solvent approach was tried without success. Lastly, it is known that $EuSO_4$ is sparsely soluble, using this knowledge in a separation procedure in methanol-aqueous environment resulted in the fact that the Y-salt in a sulphate mixture is not soluble enough to use this method. As a suitable separation method in methanol environment could not be found, experiments in this environment were stopped and the advantage of splitting the reduction and separation step of europium was lost.

As a photochemical reactor will be build and several benchmarks are present such as the photochemical space time yield, a model was established to predict the performance of a certain geometry of reactor performing a specific reaction. This model is based upon the law of Lambert-Beer for light absorption by the absorbing species and requires information about the path-length, area available for absorption and the specific absorptivity of the species. The model has some limitations, it does not take solids into account which can reduce the available area for light absorption, also gas formation is not taken into account which can reduce the actual retention time. This model is capable of predicting the outflow of the reactor based upon the inflow and retention time. Using the previous information, the efficiency and optimal point of operation can be predicted, thus making it a tool to dimensionalise the photochemical reactor. The photochemical reactor model will be checked by experiments concerning the recovery of Eu from Eu-solutions up to artificial YOX solutions.

As the separation in methanolic environment was not possible, a separation mechanism based upon the same mechanism (reduction of Eu followed by the separation from Y) was used. The separation takes place in aqueous environment and exploits the sparse solubility of $EuSO_4$. The mechanism is well described by the work of Van den Bogaert with experiments done in batch set-up. Although separation was well, the performance of the reactor is rather poor. Times of hours

up to days are required to separate a small batch of Eu-Y mixtures.

In order to reduce the time necessary for the separation of Eu from Eu-Y mixtures, experiments were performed in a continuous process via a plug flow reactor. Continuous processes are not only more more desired by industry, but they also tend to be more efficient as plug flow reactors are commonly used. The reactor used in the experiments is a plug flow type of reactor placed as close to a low pressure mercury lamp (LPML) as possible to have the highest intensity possible.

Experiments on solutions containing Eu (and additives) results in an increased rate of removal compared to the batch results as mentioned before and a shortened 'induction time'. The 'induction time' is the time lost in the beginning of the reactor when supersaturation of Eu^{2+} has to be build up before crystallisation of $EuSO_4$ can start. The induction time is shortened from several hours to 5 minutes, which is a huge improvement. The reactor was also capable of increasing the reaction rate as explained by its improved design whereby light has more access to the reagents.

The model, as derived before, fits the experiments using Eu-solutions well, as long as no Y is present. A difference in conversion between model and measurement was seen at higher retention times as the inverse reaction (oxidation of Eu^{2+} is expected as pH decreases which is inherent to the reaction mechanism). The biggest difference of 25% between model and measurements was seen at a retention time of 3000 s.

When the performance of the reactor was tested with solutions of artificial YOX (lab grade chemicals to mimic the composition of YOX) and real YOX a different result occurred. Performance dropped from 75% conversion at 3000 seconds retention time to only 16% with a spike at 25% conversion at a shorter retention time. YOX performed even worse, no conversion was seen after 3000 seconds of retention time. This oxidation of Eu^{2+} is accompanied by the formation of H_2 which is well observed in the reactor with concentration of gas up to 27v/v%. This, of course, is far from optimal as this actual retention time is shortened by the limited availability of liquid in the reactor.

It is speculated that increasing the Y-concentration (and the overall ion concentration) in solution yields a more negative redox potential for Eu as the activity coefficients are affected, enabling the oxidation of Eu^{2+} to speed up as the difference in redox potential compared to the H^+/H_2 couple increases.

It was hypothesised that conversion was lower than expected in the reaction at high retention times by the formation of dense solid plugs that stimulate the oxidation of Eu^{2+} by blocking light. Experiments using pulsed flow to break up solid plugs by creating more turbulence did not increase conversion and no positive addition effects except the reduced chance of clogging was observed in this pulsed regime.

Seeding of the feed solution or introducing seed-crystals of $EuSO_4$ resulted in the reduction of the 'induction time', thus increasing the efficiency of the reactor. These results are still premature, but promising.

This thesis has improved the knowledge in terms of the stability of Eu^{2+} in methanolic environments concerning the separation from yttrium. Addition knowl-

edge on the kinetics of photo-reactors has led to the development of a model that can be used to develop reactors to achieve maximal performance. The model is valid for the recovery of europium from solutions without yttrium and could be useful for other photochemical processes, that can be used for the development of green processes.

Appendices

Appendix A

Recycling figures

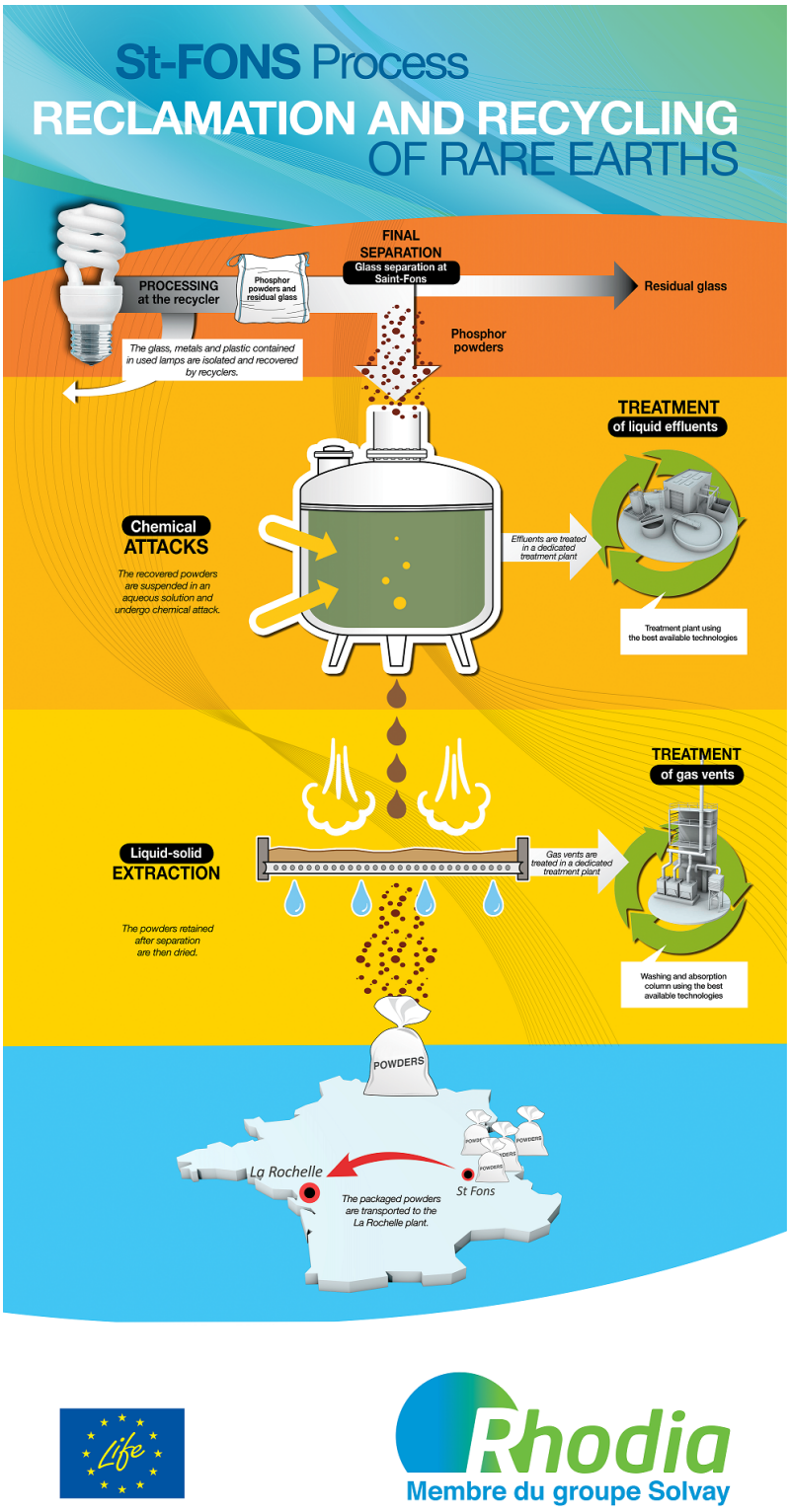

Figure A.1: Recycling lamp phosphors in Saint-Fons (Rhodia)[27]

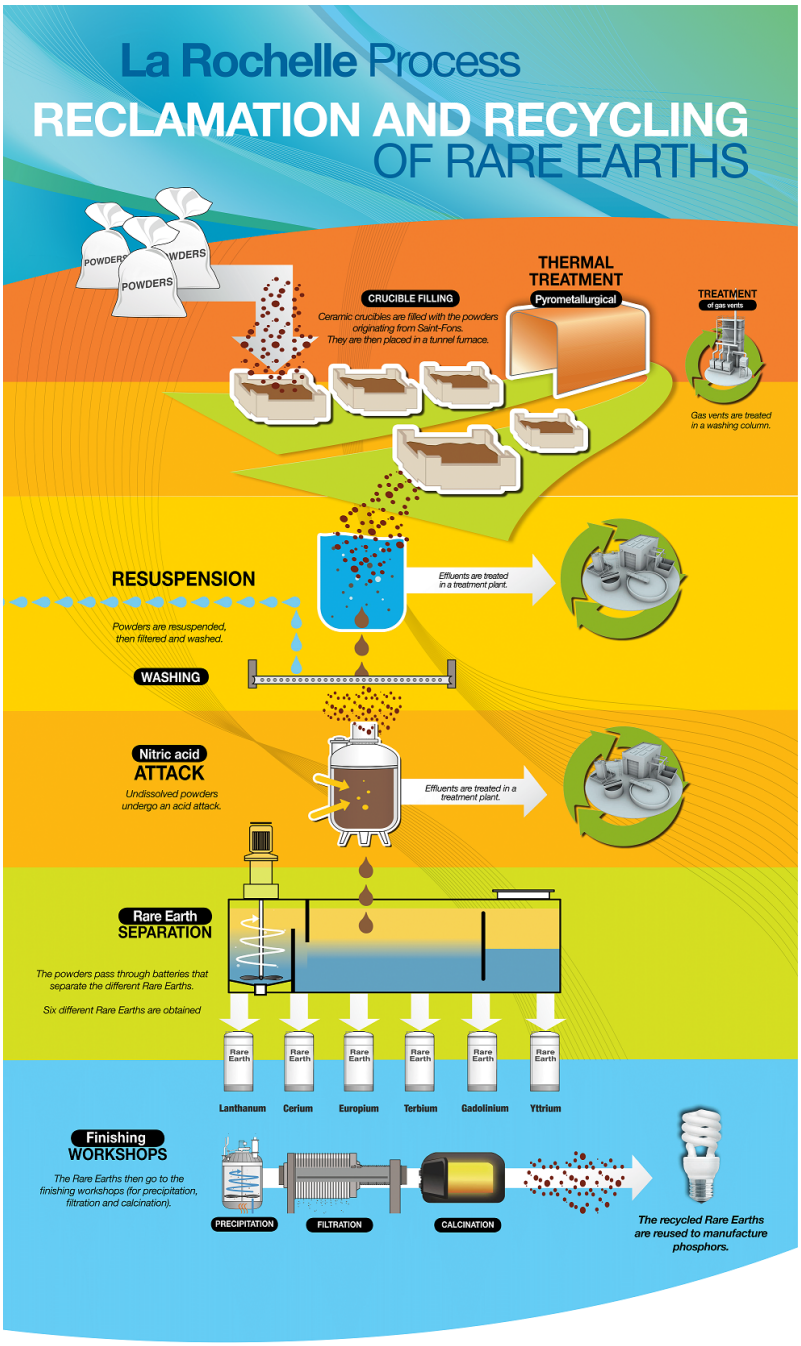

Life

Rhodia
Member of the Solvay group

Figure A.2: Recycling lamp phosphors in La Rochelle (Rhodia)[28]

Appendix B

Code

B.1 Arduino Code for pulsed flow operation

Arduino code to run peristaltic pump in pulse mode.

```
// the setup function runs once when you press reset or power the board
void setup() {
  // initialize digital pin LED_BUILTIN as an output.
  pinMode(LED_BUILTIN, OUTPUT);
}

// the loop function runs over and over again forever
void loop() {
  digitalWrite(LED_BUILTIN, HIGH);   // turn the LED on (HIGH is the
    voltage level)
  delay(1000);                       // wait for a second %TimeOn
  digitalWrite(LED_BUILTIN, LOW);    // turn the LED off by making the
    voltage LOW
  delay(1000);                       // wait for a second %TimeOff
}
```

B.2 Matlab code for photo-reactor model

Numerical solution to left hand side of reaction rate equation of model for light reactors:

$$\int_{c_{out}}^{c_{in}} \frac{1}{\sum_{i=1}^{2} I_{in,i} \cdot 10^{-\mu_{PFA,i} \cdot l_{wall}} \cdot (1 - 10^{-\epsilon_i \cdot c \cdot l_{fluid}}) \cdot QE_i \cdot \lambda_i} \partial c = \int_{\tau_{ind}}^{\tau} \frac{A}{h \cdot c_{light} \cdot N_A \cdot V} \partial \tau \tag{B.1}$$

```
%% VARIABLES
r = 0.7*10^-3; %m %Radius liquid part of tube
R = 34*10^-3; %m %Radius of cooler (reactor is wrapped around this)
dwall = 0.8*10^-3; %m %Thickness of wall (PFA)
```

```
wallpath = 0.89385*10^-3; %m %Average length light travels trough wall
    (PFA), thicker due to curve

Pi = 3.141592;
Iin1 = 9.5375; %W/m^2 %Intensity 220-240 nm
Iin2 = 228.26; %W/m^2 %Intensity 240-270 nm
QE1 = 0.66; %Enis % Quantum Efficiency
QE2 = 0.66;
lambda1 = 230*10^-9; %m %Wavelength 1 (220-240 nm)
lambda2 = 254*10^-9; %m %Wavelength 2 (240-270 nm)
E1 = 10.26127475; %1/(m^2/mol) %Average molar absorptivity (220-240 nm)
E2 = 5.38375; %1/(m^2/mol) %Average molar absorptivity (240-270 nm)
lc1 = 270.9140144; %1/m %Absorbance tube (220-240 nm)
lc2 = 514.3211394; %1/m %Absorbance tube (240-270 nm)
l = Pi*r/2; %m %Average path-length of light trough liquid
h = 6.626*10^-34; %J s %Cte Planck
cl = 299792458; %m/s %Speed of light
NA = 6.022*10^23; %1/mol %Cte Avogadro
A = 44*2*r*2*Pi*R; %m^2 %Area available for absorption in reactor
V = 44 * 2*Pi*R*Pi*r^2; %m^2 %Volume of reactor
Tind = 295.1136; %s %Induction time (via experiments)

RTD = [0:25:3250];  %s %Retention time vector
COUT = 0.1:0.1:12; %mM %Outlet concentration vector
CIN = 0.1:0.1:12; %mM %Inlet concentration vector
RTDE = max( RTD-Tind, 0.001); %s %Cut off induction time, 0.001s for no
     errors on graphs
i = 0; %Counter
j = 0; %Counter

TMES = xavg %s
CINMES = IN %mol/m^3 %Inlet concentration of reactor


%For 1 value or list of values
for i=1:1:length(tMES) %Choose retention time
t=tMES(i);

rhs = A.*t./(h*cl*NA*V); %s^2/(kg*mol) %solve rhs
lhs = 0; %set lhs to 0

ca2 = CINMES; %Choose C_in

while lhs<rhs %Calculate from C_in up to C_out
    ca1 = ca2;
    ca2 = ca2*0.9999; %stepsize
    fa1 = 1./((Iin1.*10^(-lc1*wallpath).*QE1.*lambda1.*(1-10.^(-E1.*ca1
     .*l))+Iin2.*10^(-lc2*wallpath).*QE2.*lambda2.*(1-10.^(-E2.*ca1.*l)))
     );
    fa2 = 1./((Iin1.*10^(-lc1*wallpath).*QE1.*lambda1.*(1-10.^(-E1.*ca2
     .*l))+Iin2.*10^(-lc2*wallpath).*QE2.*lambda2.*(1-10.^(-E2.*ca2.*l)))
     );
    smallIntegral = (ca1-ca2)*(fa1+fa2)/2;
    lhs = lhs + smallIntegral;
end
```

```
lhs = 0;
COUTMODEL(i) = (ca1+ca2)/2; %mM %average the error
Conversion(i) = (CINMES-COUTMODEL(i))/CINMES*100;
end

PSTYModel = ((IN-COUTMODEL)./RTD.*3600.*24)./(60./V./1000); %mol/m^3/
    day/kW



%%For a line plot
for i=1:1:length(RTDE)
t=RTDE(i);

rhs = A.*t./(h*cl*NA*V); %s^2/(kg*mol)
lhs = 0;

cinvar = CINMES;
ca2 = cinvar;

while lhs<rhs
    ca1 = ca2;
    ca2 = ca2*0.9999;
    fa1 = 1./((Iin1.*10^(-lc1*wallpath).*QE1.*lambda1.*(1-10.^(-E1.*ca1
    .*l))+Iin2.*10^(-lc2*wallpath).*QE2.*lambda2.*(1-10.^(-E2.*ca1.*l)))
    );
    fa2 = 1./((Iin1.*10^(-lc1*wallpath).*QE1.*lambda1.*(1-10.^(-E1.*ca2
    .*l))+Iin2.*10^(-lc2*wallpath).*QE2.*lambda2.*(1-10.^(-E2.*ca2.*l)))
    );
    smallIntegral = (ca1-ca2)*(fa1+fa2)/2;
    lhs = lhs + smallIntegral;
end
lhs = 0;
COUTMODEL1(i) = (ca1+ca2)/2; %mM
Conversion1(i) = (CINMES-COUTMODEL1(i))/CINMES*100;
end

PSTYModel = ((IN-COUTMODEL1)./RTD.*3600.*24)./(60./V./1000); %mol/m^3/
    day/kW

plot(RTD,PSTYMODEL,'k','Linewidth',1);


%%For a contour plot
for i=1:1:length(RTDE)
t=RTDE(i);

rhs = A*t./(h*cl*NA*V); %s^2/(kg*mol)
lhs = 0;

for j= 1:1:length(CIN) %mM
cinvar = CIN(j);
ca2 = cinvar;
```

```
103 while lhs<rhs
        ca1 = ca2;
105     ca2 = ca2*0.9999;
        fa1 = 1./((Iin1.*10^(-lc1*wallpath).*QE1.*lambda1.*(1-10.^(-E1.*ca1
         .*l))+Iin2.*10^(-lc2*wallpath).*QE2.*lambda2.*(1-10.^(-E2.*ca1.*l)))
         );
107     fa2 = 1./((Iin1.*10^(-lc1*wallpath).*QE1.*lambda1.*(1-10.^(-E1.*ca2
         .*l))+Iin2.*10^(-lc2*wallpath).*QE2.*lambda2.*(1-10.^(-E2.*ca2.*l)))
         );
        smallIntegral = (ca1-ca2)*(fa1+fa2)/2;
109     lhs = lhs + smallIntegral;
    end
111 lhs = 0;
    coutvar(j,i) = (ca1+ca2)/2; %mM
113 end
    end
115


117 [m,n] = size(coutvar); %Determining STY, LP and PSTY
    Tuss1 = repmat(RTD,m,1);
119 STY = (Tuss-coutvar)./(Tuss1).*3600.*24; %mol/m^3/day
    LP = 60/V./1000; %kW/m^3
121 PSTY = STY/LP;

123 contourf(RTD,CIN,coutvar,v,'ShowText','on')
    contourf(RTD,CIN,PSTY,'ShowText','on')
```

Appendix C

Experimental results

C.1 Pump calibration

Measurements done by determining the mass of water transferred in a container after a certain known amount of time.

Table C.1: Calibration of peristaltic pump using tubing with internal diameter of 1.3 mm and 3.17 mm.

1.3 mm ID			3.17 mm ID		
RPM	Flowrate (mL/s)	RT (s)	RPM	Flowrate (mL/s)	RT (s)
20	0.122	118	20	0.535	27.0
15	0.0938	154	15	0.410	35.3
10	0.0620	234	10	0.269	53.8
5	0.0301	481	5	0.129	112
4	0.0226	642	4	0.0969	149
3	0.0176	824	3	0.0746	194
2	0.0101	1438	2	0.0431	336
1	0.00496	2919	1	0.0210	690
			1	0.0210	690
			1	0.0214	678

The pumps are calibrated using linear regression with a confidence level of 68.2% to determine the standard deviation around each setting. This involves the use of the following equations being implemented in excel.

$$y = \hat{y} \pm t_{crit} s.e. \tag{C.1}$$

with y representing the flowrate, $\hat{y}$ the flow rate determined by linear regression, t_{crit} dependent on the size of measurement and s.e. being the standard error. For 10 measurements, t_{crit} is 1.067 and for 8 measurements, it is 1.091 for a confidence interval of 68.3% which gives the size of the standard deviation. The standard error

is determined by the following equation. [57]

$$s.e. = s_{yx} \cdot \sqrt{\frac{1}{n} + \frac{(x - \bar{x})^2}{s_{xx}}} \tag{C.2}$$

with s_{yx} being the standard error of the predicted y-value (STEYX(y,x) in Excel), n the number of measurements, x the x-value (RPM), $\bar{x}$ and s_{xx} the sum of squared deviations (DEVSQ(x) in Excel).

The residence time and its error is determined by converting the standard deviation on the flow rate using the next set of equations:

$$RT = V \cdot Q^b \tag{C.3}$$

with V the volume of the reactor (14.47 mL), Q the flow rate as determined before and b equal to -1. The standard deviation will be the following [58]:

$$\sigma_{RT} \approx \left| V b {\mu_Q}^{b-1} \sigma_Q \right| = \left| \frac{RT b \sigma_Q}{\mu_Q} \right| \tag{C.4}$$

with RT the residence time (s), V the volume of the reactor (14.47 mL), b equals -1 and Q the flow rate as seen before.[58]

This results in the graphs as seen in section 5.1 and the following tables below.

Table C.2: Calibration of peristaltic pump using tubing with internal diameter of 1.3 mm.

RPM	Flow rate (mL/s)	σ (mL/s)	Residence time (s)	σ_{RT} (s)	σ_{RT} (%)
1	0.00474	0.0006	3054	366	12
2	0.0110	0.0005	1315	63	5
3	0.0173	0.0005	838	24	3
4	0.0235	0.0005	615	12	2
5	0.0298	0.0004	486	7	1
6	0.0361	0.0004	401	5	1
7	0.0423	0.0004	342	3	1
8	0.0486	0.0004	298	2	1
9	0.0548	0.0004	264	2	1
10	0.0611	0.0004	237	2	1
11	0.0674	0.0005	215	1	1
12	0.0736	0.0005	197	1	1
13	0.0799	0.0005	181	1	1
14	0.0862	0.0006	168	1	1
15	0.0924	0.0006	157	1	1
16	0.0987	0.0007	147	1	1
17	0.1050	0.0007	137.9	0.9	1
18	0.1112	0.0008	130.1	0.9	1
19	0.1175	0.0008	123.2	0.9	1
20	0.1237	0.0009	116.9	0.8	1

Table C.3: Calibration of peristaltic pump using tubing with internal diameter of 3.17 mm.

RPM	Flow rate (mL/s)	σ (mL/s)	Residence time (s)	σ_{RT} (s)	σ_{RT} (%)
1	0.0196	0.0017	738	66	9
2	0.0470	0.0016	308	11	3
3	0.0744	0.0015	194	4	2
4	0.1018	0.0014	142	2	1
5	0.1292	0.0014	112	1	1
6	0.1567	0.0013	92.4	0.8	1
7	0.1841	0.0014	78.6	0.6	1
8	0.2115	0.0014	68.4	0.5	1
9	0.2389	0.0015	60.6	0.4	1
10	0.2663	0.0016	54.3	0.3	1
11	0.2937	0.0017	49.3	0.3	1
12	0.3211	0.0018	45.1	0.3	1
13	0.3485	0.0020	41.5	0.2	1
14	0.3759	0.0021	38.5	0.2	1
15	0.4033	0.0023	35.9	0.2	1
16	0.4307	0.0025	33.6	0.2	1
17	0.4582	0.0027	31.6	0.2	1
18	0.4856	0.0029	29.8	0.2	1
19	0.5130	0.0030	28.2	0.2	1
20	0.5404	0.0032	26.8	0.2	1

C.2 Eu recovery from pure Eu solution

Table C.4: Conversion vs. residence time using the LPML tubular setup with 2 different tubings as indicated with a Eu-solution as feed.

Tubing	RT (s)	σ_{RT} (s)	Conversion Eu (%)	σ_{Eu} (%)
Small (1.3 mm)	3054	366	76.1	1.9
	1315	63	61.6	2.0
	838	24	45.8	0.9
	615	12	36.7	0.1
	486	7	18.2	3.6
	401	5	10.7	2.1
	342	3	6.1	0.5
	298	2	0.0	0.7
	0	0	0	0.7
Big (3.17 mm)	738	66	48.0	1.4
	308	11	14.3	2.4
	194	4	0.6	1.0
	142	2	-0.5	0.3

C.3 Eu recovery from artificial YOX solution

Table C.5: Conversion vs. residence time using the LPML tubular setup with 2 different tubings as indicated with artificial YOX as feed.

Tubing	RT (s)	σ_{RT} (s)	Conversion Eu (%)	σ_{Eu} (%)	Removal Y (%)	σ_Y %)
Small (1.3 mm)	3054	366	16.3	4.5	2.4	2.3
	1315	63	24.5	2.4	-3.2	2.2
	838	24	15.5	4.0	3.9	7.3
	615	12	12.6	2.6	2.0	0.8
	486	7	2.9	1.6	2.5	6.1
	0	0	0.0	3.7	0.0	6.6
Big (3.17 mm)	738	66	7.5	1.3		
	308	11	-0.5	2.7		
	194	4	-2.1	0.3		

C.4 Eu recovery from real YOX solution

Table C.6: Conversion vs. residence time using the LPML tubular setup with YOX as feed.

Tubing	RT (s)	σ_{RT} (s)	Conversion Eu (%)	σ_{Eu} (%)	Removal Y (%)	σ_Y %)
Small (1.3 mm)	3054	366	-0.2	0.7	4.6	1.5
	1315	63	-2.3	2.0	3.7	6.6
	0	0	0.0	2.7	0.0	1.7

C.5 Pulsed flow experiments

Code for determining solid fraction:

```
y1 = spectrometer data (intensity)

for VIS = 800:1600; %cut-off intensity
for i=23335:40000; %take data from 3000-5500 seconds (stable)
if y1(i)<VIS;
    y1s(i-23335+1)=1; %solid
else
    y1s(i-23335+1)=0; %liquid or gas
end
end

y1S = sum(y1s); %count total solids
FractionSolidVIS = y1S/(40000-23335+1);
Y1PF(VIS) = FractionSolidVIS;
end

Same code for pulsed experiment
```

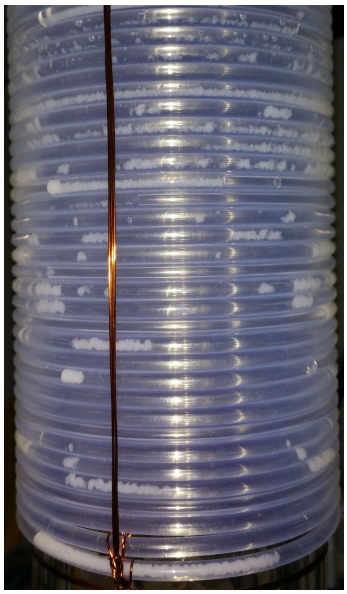

(a) Reference (100% duty time

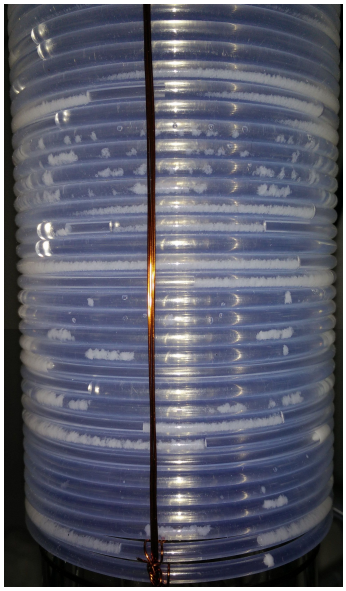

(b) 49% duty time

(c) 28% duty time

(d) 22% duty time

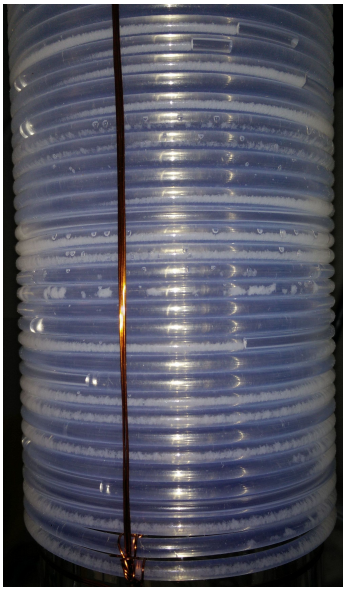

(e) 10% duty time

Figure C.1: Solid distribution at different duty times. The cycle time was set at 5 seconds and the residence time at 2916-2967 seconds. The biggest difference is seen in the last 10 coils of the reactor.

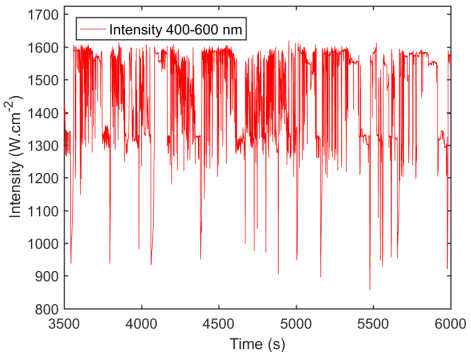

(a) Intensity of 400-600 nm for a spectrometer place behind the last loop of the reactor in reference situation (100% duty time) (2919 seconds residence time, lowest pulsation)

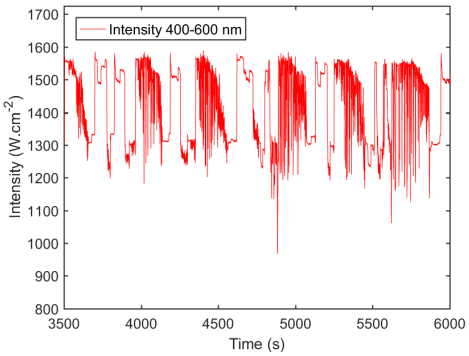

(b) Intensity of 400-600 nm for a spectrometer place behind the last loop of the reactor in 10% duty time situation (2967 seconds residence time, highest pulsation)

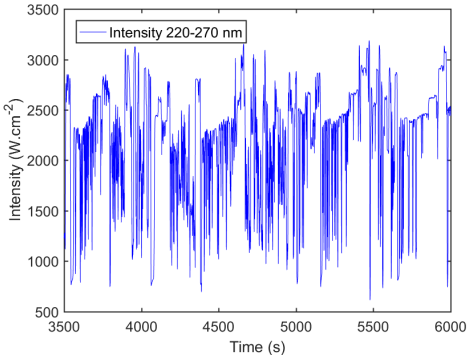

(c) Intensity of 220-270 nm for a spectrometer place behind the last loop of the reactor in reference situation (100% duty time) (2919 seconds residence time, lowest pulsation)

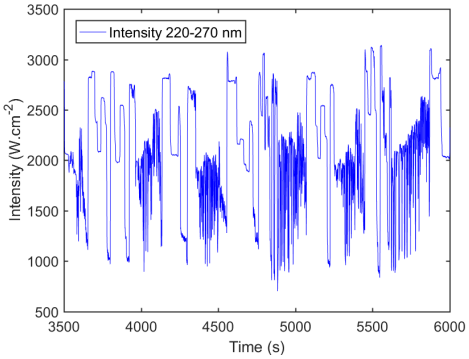

(d) Intensity of 220-270 nm for a spectrometer place behind the last loop of the reactor in 10% duty time situation (2967 seconds residence time, highest pulsation)

Figure C.2: Influence of duty time on the solid fraction and density for visible light and UV light. Low intensity indicates a solid particle passing in front of the spectrometer.

C.6 Seeding experiments

Table C.7: Conversion vs. residence time using the LPML tubular setup with seeding and with a Eu-solution as feed.

Conditions	RT (s)	σ_{RT} (s)	Conversion Eu (%)	σ_{Eu} (%)	Model (%)	PSTY ($mol.m^{-3}.day^{-1}.kW^{-1}$)	Model PSTY ($mol.m^{-3}.day^{-1}.kW^{-1}$)
Reference	615	12	32.8	2.4	37.4	0.103	0.112
Seeding	615	12	47.2	4.0	59.7	0.140	0.179
Inlet	0	0	0.00	1.4			

Appendix D

Separation of europium and yttrium in organic medium

In 2015-2016, Van Puyvelde et al. worked on a chemical essay to selectively precipitate the trivalent species of europium dissolved in methanol. It was observed that in a binary mixture of Y^{3+} and Sr^{2+}, addition of HDBP (dibutyl phosphate) selectively precipitates the trivalent ions leaving virtually all the divalent ions in the methanol. Herein, Sr^{2+} stood model for Eu^{2+}. [13]

The mechanism behind the precipitation of 3+ metals is the same as the industry reported "gel formation at high metal concentrations while using DEHPA ". The use of DEHPA in liquid-liquid extraction is already introduced in Section 2.2.6. The solids are formed by creating a metal-organic crystal, which then precipitates and can be easily separated. [59]

Using those results, an experiment was set-up to investigate this principle on divalent (Eu^{2+}) and trivalent (Eu^{3+}) europium. The idea was to irradiate the Eu^{3+} with a medium pressure lamp to photochemically reduce it by the aid of Cl^{-}-Eu^{3+} charge transfer. Van den Bogaert et all. have already observed that $EuCl_2$ (which will be formed in the reactor) would not precipitate in methanol at concentration in excess of 10 mM. [9]

Once Eu^{2+} is formed, HDBP will be added to investigate whether separation is possible by precipitation Y^{3+} (part of YOX-wastestreams) and Eu^{3+} (unreacted) and leaving the reduced Eu^{2+} in solution.

D.1 Separation process based on dibutyl phosphate

A scheme of the separation process can be found in Figure D.1; this is build up for a reactor loaded with a binary mixture of $EuCl_3$ - YCl_3 in solution to illustrate which chemicals are formed in each step. An important remark is that one HCl-molecule is formed for every Eu^{3+} that is reduced in the reactor. The entire mechanism and reactions can be found in Section 2.3.1.

As shown on Figure D.1, there are a lot of variables. First of all, the Eu^{3+}-concentration, this will be kept at 10 mM throughout all the experiments to eliminate

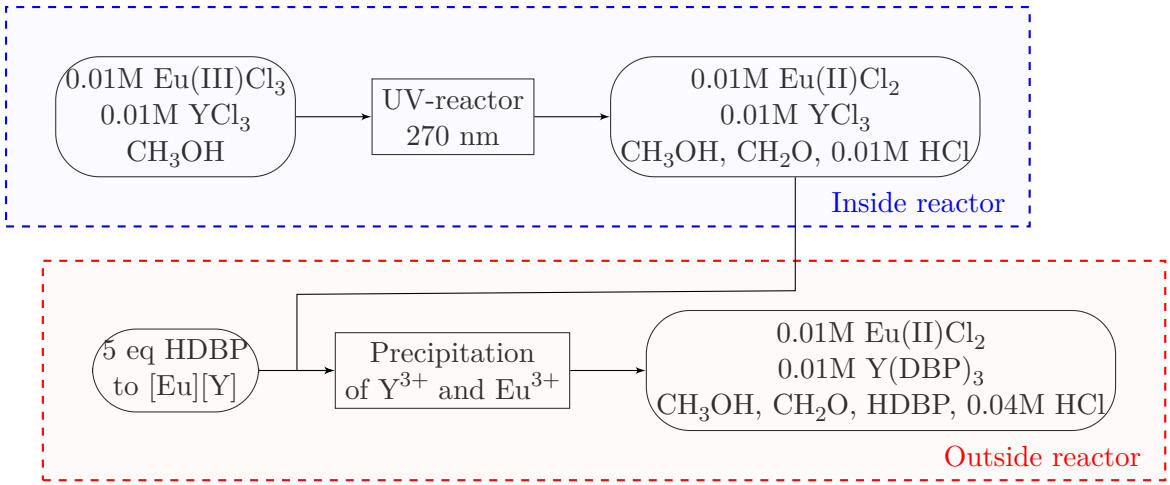

Figure D.1: Diagram of the intentional separation of Eu and Y in methanolic medium by photo-reduction of Eu and precipitation of Y. The formed $Y(DBP)_3$ is the solid precipitate.

this variable in the beginning. Secondly, it can be observed that acid is produced in the reactor (in the form of HCl) and that acid (in the form of HDBP) is introduced in the sample to precipitate Y^{3+}. In further experiments, these are 2 factors which have to be kept under control to prevent unwanted oxidation of Eu^{2+}. And lastly, the amount of Y^{3+} introduced in the system. This could influence the behaviour of the system and well be kept last to be altered.

In first instance, the main objective is to have a neat separation of Eu^{2+} from Y^{3+}. Herein, it is important to prevent precipitation of Eu^{2+} or oxidation by additives resulting in precipitation of the trivalent state of Eu.

D.2 Testing of the separation principle

In initial tests, the process flow diagram was followed as shown in Figure D.1 but without the introduction of Y in the system. This test was performed to check if europium behaves as expected (and predicted by Van Puyvelde et all).

D.2.1 Initial testing according to process flow diagram without yttrium

Principle Using the set-up described in Section 3.3.1 and the previously described principle, a batch of 10 mM Eu^{3+} was irradiated for a couple of hours. Afterwards, a large excess of HDBP (0.5 mL) was added to a 4.0 mL sample of reactor-solution. Observations were made to check if the reduced Eu (Eu^{2+} would stay in the solution. High HDBP-concentrations did not influence the Sr^{2+} (which was used in earlier tests by Van Puyvelde as a model for Eu^{2+} and never precipitated), thus a large excess was used to make sure all 3+-metals present in the solution would precipitate

(all unreacted Eu^{3+}). [13]

Results A sample containing 18.3 mL of 10 mM $EuCl_3$ was introduced in the batch reactor. The sample was irradiated for 4 hours and the spectrum of the light was monitored with the spectrometer positioned right above the reactor (spectrum not included). It was observed that the intensity of the 270 nm peak increased after a few hours of illumination. According to the law of Lambert-Beer, this results in the depletion of absorbent concentration since no liquid evaporated since the reactor was cooled to 10 °C. This observation verified the formation of $EuCl_2$ in the reactor.

After 4 hours of irradiation, the lamp was shut down and a sample was taken immediately after. The large amount of HDBP (0.5 mL) was added to the 4 mL sample. By doing this, a small amount of gas was released.

This resulted in the formation of precipitation and a small amount of gas (which is expected in the reaction scheme) when the HDBP was added to the irradiated solution. The supernatans was analysed by TXRF (method in Section 3.7.3) and the measurement revealed that only 1 ppm (10^{-5}M) of Eu remained in solution, which is more than 100 times less than the amount of Eu that was started with. It is possible that too much HDBP (here a ratio of HDBP/Eu of 62.5/1 was used) was added and a more stoichiometric amount could yield more favourable results. But nonetheless, this result doesn't verify the stated separation method in Figure D.1, the formed Eu^{2+} doesn't behave as expected as it precipitated instead of staying in solution. Another reason might be the acidity of the solution during illumination or when HDBP is added, this will be investigated later on.

D.2.2 Reduction the HDBP/Eu ratio

Principle The stoichiometric amount of HDBP that is needed to complex all trivalent metals can be derived from the equations in subSection 2.3.1. The equations indicate that $Eu(DBP)_3$ and $Y(DBP)_3$ is formed when HDBP is added to a solution containing Eu^{3+} and Y^{3+}. Therefore the stoichiometric amount of HDBP is equal to 3-times the trivalent metal concentration in solution. [60] Van Puyvelde experimentally found that the HDBP to trivalent metal ratio should be higher than 3/1. 5/1 was the minimal ratio needed to precipitate all trivalent metals in solution. [13]

$$\begin{aligned} [\text{HDBP}] &= 3 \cdot [\text{REE}^{3+}]\,(\textit{stoichiometric}) \\ [\text{HDBP}] &= 5 \cdot [\text{REE}^{3+}]\,(\textit{experimental}) \end{aligned} \tag{D.1}$$

Results The same set-up and procedure was used as before but with different HDBP concentration ranging from 30 to 50 mM and Eu-concentration of 10 mM, which represents a ratio of 3/1 up to 5/1 of HDBP to Eu.

But even these more optimized HDBP concentration resulted in the formation of a precipitate and some gas, indicating that Eu^{2+} oxidises to form $Eu(DBP)_3$ that will precipitate in this mixture.

D.2.3 Acidity problems

Extra care is needed to control the conditions of the solution. Since Eu^{3+}/Eu^{2+} is a redoxcouple with a reduction potential of -0.35 V, it can interfere with a number of chemicals that have redox potentials that are higher than -0.35 V. The main inference will be from H^+/H_2 couple which has a standard redox potential of 0.00 V. As H^+ is formed during irradiation of the $EuCl_3$ and is released when HDBP is added, both of these moments will be investigated. Consider the following redox couples:

$$Eu^{3+} + e^- \rightleftharpoons Eu^{2+} \quad E_0 = -0.35V \tag{D.2}$$

$$2\,H^+ + 2\,e^- \rightleftharpoons H_{2(g)} \quad E_0 = 0.00V \tag{D.3}$$

For both equations, the appropriate half cell potential (E_h) has to be calculated. Calculation is done using the Nernst-equation, given below for an example equation:

$$aA + bB + n(e^-) \rightleftharpoons cC + dD \tag{D.4}$$

$$E_h = E_0 - \frac{R \cdot T}{n \cdot F} \cdot \ln \frac{[C]^c \cdot [D]^d}{[A]^a \cdot [B]^b} \tag{D.5}$$

The half cell potential for Eu^{3+} and Eu^{2+} in solution considering a conversion of about 90% and a standard redox potential of -0.35 V becomes:

$$E_{Eu^{2+}/Eu^{3+}} = -0.35\,V - \frac{0.0591}{1} \cdot \log \frac{9 \cdot 10^{-3}}{10^{-3}}\,V = -0.41\ V \tag{D.6}$$

In order to keep Eu^{2+} in solution, the H^+/H_2 redox couple may not exceed -0.41 V and must be more negative. As the sample is illuminated in the reactor, HCl is formed when Eu^{3+} is reduced. Considering a conversion of 90%, 9 mM of HCl is formed. The HCl dissociates and its proton is carried in solution as $CH_3O^+H_2$. This results in the following half cell potential:

$$E_h = 0.000\,V - \frac{0.0591}{2} \cdot \log \frac{1}{(9 \cdot 10^{-3})^2}\,V = -0.12\ V \tag{D.7}$$

This value is already higher than -0.41 V (even higher than -0.35 V) resulting in oxidation of the formed Eu^{2+}. To be complete, the half cell potential is also given when HDBP would be added (30 mM), assuming the worst case scenario in which all HDBP dissociates. This leads to 39 mM of H^+ in total. Not all HDBP will dissociate as its pKa in water is 2.32 [61] which is a weak acid.

$$E_h = 0.000\,V - \frac{0.0591}{2} \cdot \log \frac{1}{(39 \cdot 10^{-3})^2}\,V = -0.08\ V \tag{D.8}$$

When the H^+ concentration increases, so does the redox potential. These potentials as calculated before are indicative since they are meant for aqueous solutions and use activities instead of concentration (but this won't give a completely different result).

In order to eliminate H^+ as an oxidiser, the concentration has to be brought back to the point where the redox potential is lower than the Europium redox potential.

This is at an H^+-concentration of 10^{-7} M, the redox potential situated at -0.4137 V which is slightly lower than the Europium redox potential for this specific situation.

The amount of OH^- can be increased to capture all the H^+ formed in the reactor and by the HDBP. This can be done by adding NaOH or another alkali to the reactor before the reaction is set-up. NaOH can also be added to HDBP in stoichiometric ratio to capture all H^+. Another option is to use NaDBP or other type of DBP^--salt (preferably without water) to eliminate H^+.

D.2.4 Introducing OH^- into the system

Principle As indicated above, the concentration of H^+ is too high in certain points of the process resulting in the oxidation of the product. To prevent this, OH^- can be added at strategic points to eliminate this problem.

The limit of $[OH^-]$ in MeOH that can be added without precipitating Eu is important in the following experiments, therefore it was determined. It was found that hydrolysis occurred at a concentration of 0.03 M of OH^- (using NaOH) with 10 mM of $EuCl_3$ (it is the same concentration for $EuCl_2$) in methanol. Thus, the maximal concentration of NaOH must be held below 0.01 M (safety margin) to avoid hydrolysis.

Result In a first experiment, NaOH was added in the reactor. The reactor was filled with 18.3 mL $EuCl_3$ (0.01 M) solution and NaOH (0.01 M). The illumination time was 4h. When samples (4.0 mL) were taken and HDBP (30 mM up to 90 mM, which is a ratio of DBP/Eu of 3/1 up to 9/1) was added, a large amount of precipitate was found in all of them. This indicates that Eu^{2+} oxidised again. The analysis by TXRF confirmed this finding, again only 10^{-5} M was measured in solution in all of them.

It can be concluded that not enough NaOH was added in the reactor since Eu^{2+} oxidised again, either in the reactor, either by the addition of HDBP. Using 10 mM of $EuCl_3$, not enough NaOH can be added to neutralize the formed HCl and the HDBP, 0.04 M is required to do so.

D.3 Investigation of the separation step by dibutyl phosphate of pure Eu/Y mixtures

In previous experiments $EuCl_2$ was synthesised in the photoreactor. As it is uncertain how much is produced and if it is stable at all once the lamp is turned off, experiments are stopped using the reactor and synthetic $EuCl_2$ is used in following experiments. This is done to optimize the separation of $EuCl_2$ from YCl_3 in the first place and deal with the stability of the formed $EuCl_2$ from the reactor in a later stage. As the problems are situated in the formation and addition of H^+ in the system, the use of synthetic $EuCl_2$ eliminates the formed HCl in the reactor. As such, the acidity of the solution can be better controlled in the next experiments.

D.3.1 HDBP as separating agent

The addition of pure HDBP (in concentrations of 5 up to 120 mM) in solution with 10 mM of $EuCl_2$ produces the same result as seen in the previous tests. Eu^{3+} as well as Eu^{2+} produce the same amount of precipitate. This indicates that Eu^{2+} oxidises in this solution to form $Eu(DBP)_3$ and precipitate, this was an expected result as it was also seen before.

It was observed that an increase in precipitate occurred up to a HDBP concentration of 50 mM (equal to a ratio of HDBP/Eu of 5/1). It was confirmed by TXRF that solutions with a HDBP concentration lower than 50 mM still contained a substantial Eu in the supernatans. This indicates that the stoichiometric amount of HDBP isn't sufficient to precipitate all trivalent metals in solutions, a ratio of 5/1 HDBP/M is required.

D.3.2 Mixture of HDBP and NaOH as separating agent

An equimolar mixture (with a slight excess of NaOH) of HDBP and NaOH (by weighing the NaOH) was produced and the required amount of DBP^- (to produce the same concentration as in the experiments before (5 mM up to 120 mM of DBP^-)) was added to solutions containing pure 10 mM $EuCl_3$ in MeOH or 10 mM $EuCl_2$ in MeOH respectively. All produced a precipitate, indicating that this method of elimination the proton of HDBP is not well controlled. Better is to use NaDBP-salt which will be used in further experiments.

D.3.3 NaDBP-salt as a better controlled separating agent

NaDBP-salt is a better alternative than adding a mixture of HDBP and NaOH, in this way the acidity is better controlled as the operation window in terms of acidity is very limited. In order to use NaDBP-salt, it must first be synthesised.

Synthesis of NaDBP-salt

NaDBP was synthesized by adding HDBP to NaOH (dissolved in H_2O) whereby the pH is monitored. The addition of HDBP was stopped at pH 7. The solution was evaporated afterwards in an oven at 110 ℃ for a day. The crystals were later dissolved in MeOH to obtain a 1 M solution/dispersion.

NaDBP-salt as separating agent

Using this 1 M NaDBP solution/dispersion, the same concentration of DBP^- (5 mM up to 120 mM) were added to pure methanolic $EuCl_3$ and $EuCl_2$ solutions. The same result was seen (even at very low amounts of NaDBP) as with the addition of pure HDBP. In both solutions, a precipitate (type $Eu(DBP)_3$) was formed immediately and in equal amounts (Eu^{3+} compared to Eu^{2+}). The precipitate was easily distinguishable by its characteristics; $Eu(DBP)_3$ aggregates easily and settles

relatively fast, whereas hydrolysed Eu forms a 'cloud' in the solution and settles slower.

The precipitate could be explained by a slight excess of HDBP that is still present in the salt solution which contributes to an H^+ concentration in methanol that is high enough to stimulate oxidation of Eu^{2+} ($[H^+]$ has to be lower than 10-7 M to eliminate oxidation of Eu^{2+}). The better option in further steps is to wash the salt with a non-polar solvent to extract excess HDBP.

De-acidifying NaDBP-salt

In order to wash the excess HDBP, a viable non-polar solvent had to be chosen. Two solvents were chosen; n-dodecane ($C_{12}H_{26}$) and n-hexane (C_6H_{14}). Washing NaDBP with hexane formed a gel phase, which wasn't seen when dodecane was used. As such, n-dodecane is chosen and in further tests the dried NaDBP-salt was washed twice with n-dodecane (about 10 mL of washing agent per 5 mL of salt).

After washing, the salt was dried, weighed and dissolved in methanol to form a 1 M dispersion which was continuously stirred when in use. The 1 M salt dispersion was added to the Eu^{2+} solution at different concentrations ranging from 4.8 mM up to 24 mM and higher, but it was already observed that hydrolysis of Eu occurs in the high concentration range (24 mM). The problem with hydrolysis in this set-up is that the hydrolysed Eu settles and mixes with the $Y(DBP)_3$ or even $Y(OH)_3$ that will form in the actual YOX-samples, making it impossible to separate Eu from Y when they both precipitated. The results of the experiment are shown in table D.1. A note must be made here, the added NaDBP to this Eu-samples is not enough to precipitate all Eu in solution as the ratio of DBP/Eu is equal to 0.5/1 up to 2.4/1 and at least 5/1 is required to precipitate all Eu in solution.

Table D.1: Addition of de-acidified NaDBP to $EuCl_2$ solutions. Higher concentrations than 24 mM showed hydrolysis as well. The concentration of Eu dropped slightly due to dilution, the stock concentration of Eu was 10 mM.

C $EuCl_2$ (mM)	C NaDBP (mM)	Result
9.95	4.8	Clear solution
9.90	12	Signs of hydrolysis
9.76	24	Hydrolysis

Although the first result from table is favourable, this results was not reproducible, therefore this method is not suitable for separation of Eu from Y.

De-acidifying and de-watering NaDBP-salt

Earlier observations indicated the hygroscopicity of NaDBP (gelling of the salt after exposing it to air for a couple of days), therefore it was hypothesised that the dried salt could include a small, but not neglectable amount of water into its structure. That tiny fraction of water can increase the OH^- concentration as it is known that

NaDBP is a weak base (pKa of HDBP is 2.32 [61]) thus a small fraction forms HDBP in water and decreases the acidity by doing so (increasing OH^- concentration). A second problem is that the included water might decrease the OH^- at which Eu hydrolyses since Eu hydrolysis at pH 6.8 in water [8].

In order to test this hypothesis, a solution of washed (with dodecane) NaDBP solution was made and Al_2O_3 for drying was added. Al_2O_3 was chosen above common drying agent such as $MgSO_4$ to avoid that DBP^- was consumed in complexing the metal ions of the drying agent, Al_2O_3 is, in contrast to common drying agents, very poorly soluble which avoids complexing by DBP^-. The solution was shaken and left standing for a few minutes to be sure that all water is pulled from solution. This solution was later added in concentration ranging from 5 mM up to 120 mM to samples containing 10 mM of Eu^{2+} but no additional effect compared to the non-dried NaDBP solution was observed. Hydrolysis happened again at 24 mM of added NaDBP. Therefore, drying is not necessary to improve results.

Separation by de-acidified NaDBP-salt followed by HCl

Hypothesizing that the hydrolysed Eu can be redissolved by slightly acidifying the solution after the NaDBP was added to get back in the correct acidity range. For this, an operability window was searched for. In this window the hydrolysed Eu redissolves but the polymeric Y-precipitate (which will eventually be present in YOX-samples) will not. This range is most likely to be in neutral environment.

To test this hypothesis, an experiment was done with the following procedure; a certain concentration of NaDBP (listed in table) was added to a solution of 10 mM $EuCl_2$. The Eu^{2+} hydrolysed and the solution was shaken well. After this, a certain amount of HCl (waterbased, 1 M) was added up to which the solution became clear again and all Eu did redissolve. The result of these experiments are found in table D.2.

One remark: when the HCl was added to the samples with 192 - 526 mM of NaDBP, immediately after that a precipitate was formed (type: $Eu(DBP)_3$). The results show that it is possible to dissolve the hydrolysed Europium again in with only small concentrations of NaDBP (24.4 mM). It seemed that larger concentrations of NaDBP result in oxidation and precipitation of the Eu in solution.

To check whether Eu^{2+} can be separated from Eu^{3+} and Y^{3+}, some solutions contain a combination of all elements are made. The solutions and composition can be found in table D.3. Experiments 1-3 contained the pure elements, 4-6 contained equimolar solutions, 7 contains all 3. And 8-9 contains a solution which comes close to the composition of YOX, containing Eu^{2+} in sample 8 and Eu^{3+} in sample 9. Experiments 10-12 are used to prove a point which is later explained using the Pourbaix diagrams, these can be compared to 1-3.

Table D.3 shows that it is possible to separate Eu from Y, but not Eu^{2+} from Eu^{3+} which was intended (exp. 1-4). This can be derived from measurement 1, 2 and 4 as they nearly indicate the same amount of Eu in the liquid fraction. The error of the measurement is relatively large as can be seen by measurement 1, 2, 4 and 10 and 11 as they all roughly should be 100% of recovery.

Table D.2: Addition of washed NaDBP to $EuCl_2$ solutions and acidifying the solution afterwards. Higher concentrations than 24.4 mM of NaDBP showed hydrolysis even with more HCl. Sample 3 which resulted in a clear solution was taken as a reference for upscaling (samples 4-8) the principle. In sample 4, the ratio of HCl/Eu was kept constant. In samples 5 to 8, the ratio of NaDBP/Eu was kept constant. The concentration of Eu dropped slightly due to dilution, the stock concentration of Eu was 10 mM. The reason why all concentrations are not whole numbers is due to dilution effects.

No.	C $EuCl_2$ (mM)	C NaDBP (mM)	C HCl (mM)	Result	Comments
1	9.76	24	7.1	Hydrolysis	
2	9.76	24	32.8	Hydrolysis	
3	9.76	24	196	Clear solution	Reference
4	9.52	47	192	Precipitate	≡ HCl/Eu
5	9.52	47	322	Precipitate	≡ NaDBP/Eu
6	9.30	70	411	Precipitate	≡ NaDBP/Eu
7	9.09	91	476	Precipitate	≡ NaDBP/Eu
8	8.89	111	526	Precipitate	≡ NaDBP/Eu

Table D.3: Addition of washed NaDBP to mixed REEs solutions and acidifying the solution afterwards. The NaDBP content was kept at 24.4 mM and the total REE concentration was kept at 4.88 mM (setting the ratio of DBP/Eu at 5/1. Above these concentration, precipitation of Eu occurs.

	REE			**DBP**	**Acid**	**Recovery in liquid**	
No.	C $EuCl_2$ (mM)	C $EuCl_3$ (mM)	C YCl_3 (mM)	C NaDBP (mM)	C HCl (M)	Eu (%)	Y (%)
1	4,88	0.00	0.00	24.4	0.20	85.7	-
2	0.00	4.88	0.00	24.4	0.20	102	-
3	0.00	0.00	4.88	24.4	0.20	-	4.50
4	2.44	2.44	0.00	24.4	0.20	93.9	
5	2.44	0.00	2.44	24.4	0.20	46.1	1.77
6	0.00	2.44	2.44	24.4	0.20	54.4	3.37
7	1.63	1.63	1.63	24.4	0.20	54.3	4.72
8	0.59	0.00	4.29	24.4	0.20	33.5	3.20
9	0.00	0.59	4.29	24.4	0.20	35.6	2.30
				C HDBP (mM)			
10	4.88	0.00	0.00	24.4	0.20	104	-
11	0.00	4.88	0.00	24.4	0.20	96.7	-
12	0.00	0.00	4.88	24.4	0.20	-	2.10

When mixtures of Eu and Y are tested by this method, different results occur. The recovery of Eu is lower when Y is added to the mixture indicating that Eu co-precipitates with Y and that the precipitate of Eu-DBP cannot be fully broken after it's mixed with Y-DBP precipitate.

Furthermore, it can be seen that NaDBP and HDBP in these acid conditions tend to selectively precipitate Y and leave Eu in solution as seen in experiments 1-3 and 10-12.

Eu^{2+} cannot be separated from Eu^{3+} due to the fact that the oxidation number of Eu^{2+} is changed when the product hydrolyses. In the Pourbaix diagram (although for water, the species in the diagram can also be used for methanolic environment), which is shown below on Figure D.2a, it can be seen that there exists only one hydrolysed species of Eu, which is $Eu(OH)_3$. Therefore, the oxidation number changes from +II to +III when the Eu hydrolyses. When in the second stage HCl is added, no Eu with oxidation number +II is present in the solution and thus the difference between +II and +III cannot be determined in this method as all Eu is oxidised again.

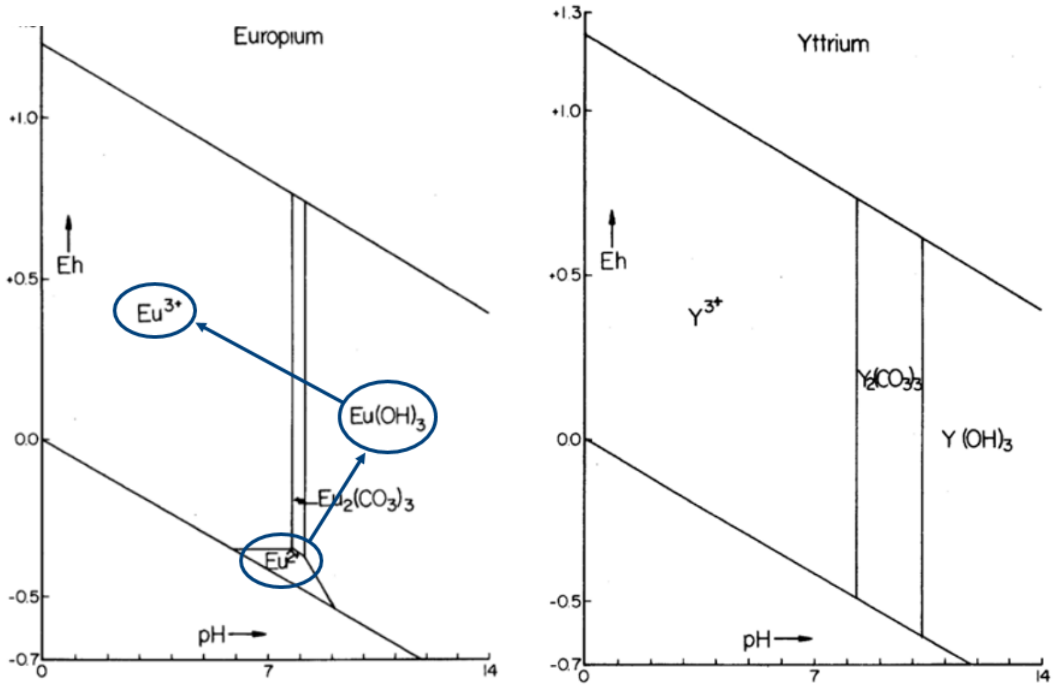

(a) Pourbaix diagram of Eu showing what happened when Eu hydrolyses and HCl is added afterwards. [35]

(b) Pourbaix diagram of Y [35]

Figure D.2: Pourbaix diagram of Eu and Y [35].

To indicate that yttrium behaves similar to europium in these conditions, the Pourbaix diagram is shown as well.

Secondly, it is peculiar why so much acid is required for the separation of Eu from Y. By calculating the pH of the solution (although not relevant in MeOH, but due to the high HCl concentration, a mixture of H_2O (20v/v%) and MeOH is obtained), it turns out to be situated at 0.7 (neglecting the influence of the formed HDBP) for the reference solution from table D.2. The two experiments above had a pH around the pKa of HDBP (pKa is 2.32 [61]) for the first and slightly more acidic than the pKa for the second.

The reason it works only in this pH range and concentration range might be due to the following reaction which only occurs in this form for Eu:

$$Eu^{3+} + 3\,DBP^-_{(l)} \longrightarrow Eu(DBP)_{3,(s)} \tag{D.9}$$

$$Y^{3+} + 3\,DBP^-_{(l)} \longrightarrow Y(DBP)_{3,(s)} \tag{D.10}$$

For Y, the following reaction could occur as well:

$$Y^{3+} + 3\,HDBP_{(l)} \longrightarrow Y(DBP)_{3,(s)} + 3\,H^+ \tag{D.11}$$

But the following will NOT occur:

$$Eu^{3+} + 3\,HDBP_{(l)} \not\longrightarrow Eu(DBP)_{3,(s)} + 3\,H^+ \tag{D.12}$$

This hypothesis is not completely certain, for this the method has to be changed slightly. For this, the acid has to be added first, followed by the NaDBP or HDBP, this might also yield better results since the precipitate of $Eu(DBP)_{3,(s)}$ cannot be formed if the hypothesis is correct, leading to fewer co-precipitation. As the concentration of Eu that can be treated this in solution is so low and the yield is not optimal as well, this is not tested further.

But as these experiments do not yield favourable results in terms of separation of Eu^{2+} from Eu^{3+} and Y^{3+}, these experiments are stopped and alternatives are being investigated.

D.4 Separation of Eu and Y using alternative methods

Since separation by selective precipitation using HDBP, NaDBP or derivative methods did not yield the intended results, alternatives were tried. A first alternative is based upon the extraction of Eu^{2+} from the reaction mixture coming from the reactor. The second alternative is based upon the use of selective crystallisation by the use of an anti-solvent. And the last method also uses selective precipitation but with a different species.

D.4.1 Separation by extraction by crown ethers

Crown ethers are mostly used to selectively extract certain elements to another phase thus separation a mixture of elements, it can also be used for the separation of Eu^{2+} from the reaction mixture.

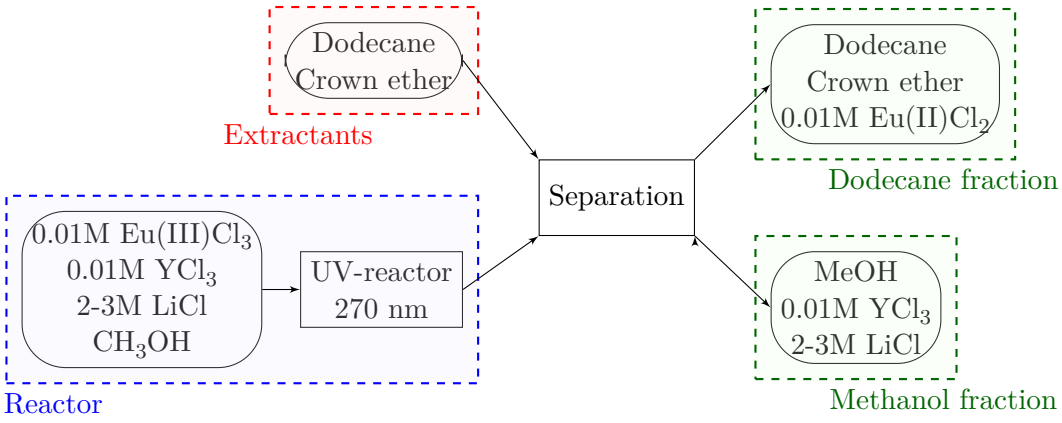

Figure D.3: Simplified diagram for the extraction approach using crown ethers to extract the formed Eu^{2+} from the reaction liquid.

The general idea is that the a mixture of $EuCl_3$ and YCl_3 together with large amounts of LiCl are dissolved in methanol enter the reactor. This reactor is a tubular reactor which will be coiled around a LPML or MPML to photochemically reduce Eu^{3+} to Eu^{2+}. The effluent of the reactor is then mixed with a solution of dodecane with a small amount of crown ether. In principle, the crown ether (which type must be determined later) should extract the Eu^{2+} from the methanolic solution to the dodecane layer. The large amount of LiCl should in theory keep the mixture of dodecane and methanol from dissolving into each other. In the end, all Eu^{2+} should be captured by the crown ethers and transferred to the dodecane layer and the YCl_3 should be kept in the methanolic layer. Thus this can create a separation of the Eu^{2+} and Y^{3+}. A scheme of the idea is given in Figure D.3.

D.4.2 Separation by anti-solvent

The use of an anti-solvent to lower the solubility of a certain species is widely used in pharmacy to crystallize medicines and purifying them at the same time. The general principle of anti-solvent use is seen in Figure D.4. [62]

By the addition of anti-solvent, the concentration of product slightly decreases, and secondly the solubility of the product decreases sharply as is shown on Figure D.4.

From the work of Bart van den Bogaert, it is known that $EuCl_2$, the product that is formed in the reactor when starting from $EuCl_3$ in methanol, is poorly soluble in ethanol (EtOH) (6.83 mM), even worse in isopropylalcohol (IPA) (0.08 mM). And Van den Bogaert deduced that the lower the dielectric constant is, the lower the solubility becomes. For EtOH, the ε is equal to 24.5 and for IPA it is 17.9. For hexane, another solvent that can be used, the ε is equal to 1.88 [63]. Deducing from the theory above, the solubility of $EuCl_2$ should be very low. [9, 12] The scheme of the is method is seen in Figure D.5.

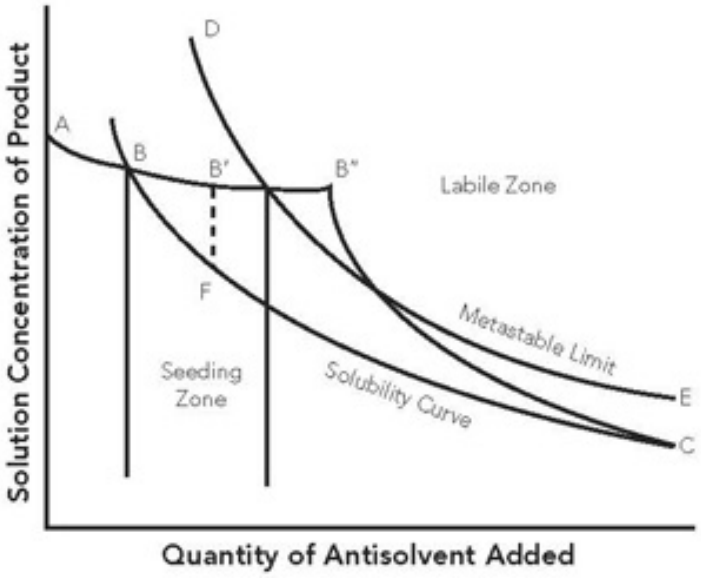

Figure D.4: Solubility of product in function of the total amount of anti-solvent added [62]

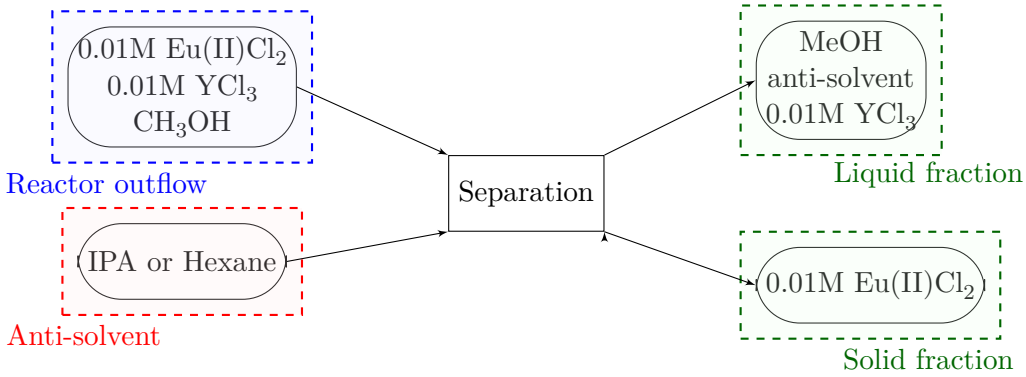

Figure D.5: Diagram for the anti-solvent approach.

The aim is to selectively precipitate $EuCl_2$ and keep YCl_3 in solution. To test whether this is possible, a few experiments are undertaken. In the first place, it must be ensured that YCl_3 is soluble in the combination of solvent/anti-solvent. Therefore several samples were measured, each with a different ratio of solvent/anti-solvent. YCl_3 was dissolved in methanol (MeOH) (the solvent) with a concentration of 10 mM, such that the concentration of YCl_3 is reduced as the amount of anti-solvent is increased. The results of this experiment are shown in the following table

It can be seen that the YCl_3 is still soluble in solutions containing up to a ratio of anti-solvent over solvent of 100/1 although the concentration of Y had dropped

Table D.4: Experiments on the separation by anti-solvent, the aim is to keep YCl_3 in solution. AS stands for anti-solvent and S for solvent. For both solvents, IPA and hexane, no precipitation occurs up to the ratio of anti-solvent over solvent of 100 (100 mL of IPA is needed for 1mL of MeOH). The concentration of Y (10 mM in the solvent) lowers due to the dilution by the anti-solvent.

YCl_3 - IPA			**YCl_3 - Hexane**		
AS/S	C YCl_3 (mM)	Result	AS/S	C YCl_3 (mM)	Result
1	5.00	No Precipitation	1	5.00	No Precipitation
2	3.33	No Precipitation	2	3.33	No Precipitation
5	1.67	No Precipitation	5	1.67	No Precipitation
10	0.91	No Precipitation	10	0.91	No Precipitation
100	0.10	No Precipitation	100	0.10	No Precipitation

in that solution to 0.1 mM. An issue occurred with hexane, because hexane and methanol don't mix very well in the region of AS/S of 1 up to 10 thus the test-tube was shaken very well to see if anything did precipitate. In the last mixture with the highest ratio of AS/S, no phase separation was observed thus if any anti-solvent effect would occur, it would be visible in this stage.

As YCl_3 does not create any crystals in these mixtures, it can be further tested on $EuCl_2$ to see if and when precipitation occurs. Therefore, the same type of experiment is done as with Y. 10 mM of $EuCl_2$ is dissolved in MeOH and mixed with anti-solvent (IPA or hexane) in a certain ratio. These results are found in table D.5.

Table D.5: Experiments on the separation by anti-solvent, the aim is to keep YCl_3 in solution. For both solvents, IPA and hexane, no precipitation occurs up to the ratio of anti-solvent over solvent of 100 (100 mL of IPA is needed for 1mL of MeOH). The concentration of Eu (10 mM in the solvent) lowers due to the dilution by the anti-solvent.

$EuCl_2$ - IPA			**$EuCl_2$ - Hexane**		
AS/S	C $EuCl_2$ (mM)	Result	AS/S	C $EuCl_2$ (mM)	Result
1	5.00	No Precipitation	1	5.00	No Precipitation
2	3.33	No Precipitation	2	3.33	No Precipitation
5	1.67	No Precipitation	5	1.67	No Precipitation
10	0.91	No Precipitation	10	0.91	No Precipitation
100	0.10	No Precipitation	100	0.10	No Precipitation

As shown in table D.5, no precipitation of $EuCl_2$ occurs even the ratio of anti-solvent over solvent went up to 100/1 for IPA and hexane. Even the very apolar and low dielectric hexane could not produce a precipitate of $EuCl_2$. The concentration of Eu in that confuguration is very low (0.1 mM) but it cannot be increased by 10-fold

since the concentration of YCl_3 may not exceed solubility in MeOH in samples with very high Y/Eu ratios (e.g. YOX-waste streams). Therefore, this method is not usable to separate $EuCl_2$ from YCl_3 after the reduction step of Eu.

D.4.3 Separation by sulphates

Van den Bogaert et al. has done some experiments on the separation of Eu from Y by precipitation Eu as $EuSO_4$. This was only possible since $EuSO_4$ is very poorly soluble in water and $Y_2(SO_4)_3$ is well soluble. For water, the solubility of $EuSO_4$ is equal to 0.001 g / 100 g H_2O, for $Eu_2(SO_4)_3$ it is 2.10 g / 100 g H_2O and for $Y_2(SO_4)_3 \cdot 8\,H_2O$ it is equal to 7.47 g / 100 g H_2O. [12] Indicating that $EuSO_4$ can be selectively precipitated in aqueous environment.

The idea was to broaden this method to use it in methanolic environment. Since sulphates require a very polar environment to be soluble, in the end it might be that a certain fraction of water has to be added to make sure the $Y_2(SO_4)_3 \cdot 8\,H_2O$ is still soluble. Otherwise, without the presence of water, a phenomenon called salting out might occur.

An article concerning the solubility of Na_2SO_4 in methanol-water environment from which the graph can be found in Figure D.6.

Although this graph is only valid for Na_2SO_4, it gives a general view of solubility of sulphates in MeOH-water. Firstly, the solubility is temperature dependent as with most salts, in this case the solubility increases with temperature, but with some sulphates the solubility will decrease with increasing temperature. And secondly, the solubility decreases sharply in the first part of the graph between 0 and 0.2 (methanol mass ratio). If this is also the case for $Y_2(SO_4)_3$, the method will not be usable.

The general idea in this separation method is to mix the effluent of the reactor (which will consist of $EuCl_2$ and YCl_3 dissolved in methanol) with an aqueous solution of sulphates (e.g. Na_2SO_4). This leads to the formation of $EuSO_4$ and $Y_2(SO_4)_3$. An arbitrary 50/50 % of MeOH-water is chosen, this means that the same flow rate of effluent is mixed with an equal flow rate of sulphate-solution. Increasing the water content will lead to a larger waste flow and the decrease of water content will probably also decrease the solubility of $Y_2(SO_4)_3$. A schematic view of this method is shown in Figure D.7.

To test if this method is viable, the solubility of $Y_2(SO_4)_3$ must be tested in a 50/50 v/v of $MeOH/H_{20}$. It was calculated that a 50/50 v/v solution of MeOH-water is equivalent to 40.35 g of MeOH mixed with 50 g of water which has a density of around 0.954 g $\cdot$ mL^{-1} and is equivalent to a mass ratio of 0.807. From the graph, a solubility of 1.79 g / 100 g solvent was calculated using the results from the article, which is a solubility of around 120 mM of Na_2SO_4.

Using this information, several samples where made with increasing concentration of YCl_3 and constant concentration of Na_2SO_4 set at 100 mM since 120 mM was difficult to achieve. The results are shown in table D.6.

It is seen that the solubility of $Y_2(SO_4)_3$ or $Y_2(SO_4)_3 \cdot Na_2SO_4 \cdot 2\,H_2O$ is quite poorly. As seen in Section 2.2.4, precipitation as double sulphate salt can occur as

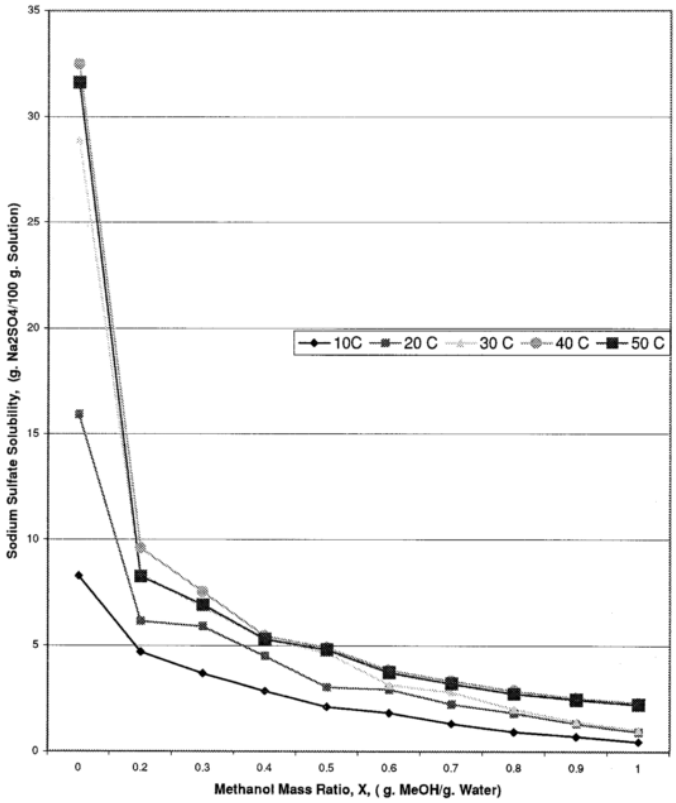

Figure D.6: Solubility, stated in g of Na_2SO_4 per 100 g of solution, in mixtures of MeOH-water in function of the mass ratio of MeOH over water [64]

the concentration of Na_2SO_4 is too high, solubility of Y-salt decreases by a factor of 4-5 once the the double salt is formed and falls to zero once a Na_2SO_4 concentration of 25 parts per 100 parts water (in mass) is reached (for the aqueous case). Based upon the theory for aqueous solutions, $Y_2(SO_4)_3 \cdot Na_2SO_4 \cdot 2\,H_2O$ will only form once a concentration of Na_2SO_4 of 8 parts per 100 parts water (in mass) is reached (80 g/L). [65] Solubility of Na_2SO_4 does not extent to that point in MeOH-water mixtures [64]. Thus the exact composition of the precipitated Y-salt is not known.

As soon as a concentration of 10 mM (possibly even lower) of Y^{3+} is reached in 100 mM of SO_4^{2-}, a precipitate is formed. Indicating that the solubility product is equal or less than $K_{sp} \leqslant 10^{-3}\,(= 10^{-1} \cdot 10^{-2})$.

Since the solubility of $Y_2(SO_4)_3$ is too low, it is not possible to use the described method. Ideally, the solubility of $Y_2(SO_4)_3$ should be equal or higher than 100 mM for it to be even viable.

The solubility of $Eu_2(SO_4)_3$ or $Eu(SO_4)$ wasn't tested since the solubility of $Y_2(SO_4)_3$ was already too low to have the method working and because the solubility of $Eu(SO_4)$ is known from previous work by Van den Bogaert et al in aqueous environments. [8]

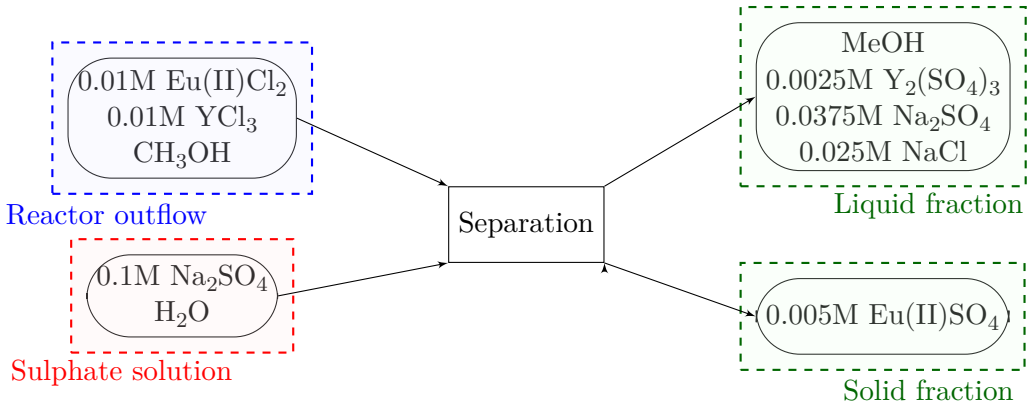

Figure D.7: Simplified diagram for the sulphate separation approach. Assume 50% reactor outflow and 50% sulphate solution by volume. An excess of sodium sulphate is displayed here, for real processes, this amount could be reduced.

Table D.6: Solubility test of $Y_2(SO_4)_3$ in 50/50 v/v % MeOH/water.

C Y^{3+} (mM)	C SO_4^{2-} (mM)	Result
0	100	Clear solution
1	100	Clear solution
10	100	Precipitate
20	100	Precipitate
40	100	Precipitate
60	100	Precipitate
80	100	Precipitate
100	100	Precipitate
120	100	Precipitate

D.5 Conclusion

It was not possible to achieve separation of Eu and Y by the process flow diagram in Figure D.1, although several adjustments were made. Most of these adjustments were aimed at adjusting the acidity level in the reaction mixture for the HDBP and NaDBP experiments, but this seemed to be too difficult as the Eu (2+ and 3+ state) has a tendency to hydrolyse as the concentration increased too much and the Eu^{2+} has a tendency to oxidise as the pH dropped too much. In either case, the Eu^{2+} which is formed is lost due to oxidation or hydrolysis (since $Eu(OH)_3$ is the only hydrolysis product that can be formed of Eu).

Other methods were tested as well, these included the addition of an anti-solvent to selectively crystallize $EuCl_2$ and the addition of an aqueous Na_2SO_4 solution to form $EuSO_4$ which would precipitate in a mixture of methanol and water. But both of these methods suffered from problems, selective crystallisation wasn't possible since

no precipitate of either $EuCl_2$ or YCl_3 (other element in YOX-waste) was formed in a solution containing ratios of 100/1 of anti-solvent to solvent. For the other method, the solubility of $Y_2(SO_4)_3$ was too low as it precipitated at a concentration of even 10 mM.

As separation of Eu from Y was positioned after the reduction step of Eu by means of selective precipitation and crystallisation, another chemistry must be reached for as will be shown in the following chapters. These methods were all aimed to separate the separation step from the reduction step. As such that no solids are formed in the reactor (reduction step), thus making operation easier.

Bibliography

[1] Eni Generalic. *Rare earth elements*. URL: http://www.periodni.com/rare%7B%5C_%7Dearth%7B%5C_%7Delements.html.

[2] J.H.L. Voncken. *The Rare Earth Elements*. 2016, pp. 1–5. ISBN: 978-3-319-26807-1. DOI: 10.1007/978-3-319-26809-5. URL: http://link.springer.com/10.1007/978-3-319-26809-5.

[3] Ismar Borges de Lima and Walter Leal Filho. *Rare earths industry*. 1st. Rio de Janeiro: Elsevier, 2015, p. 434. ISBN: 9788578110796. DOI: 10.1017/CBO9781107415324.004. arXiv: arXiv:1011.1669v3.

[4] Geology.com. *REE - Rare Earth Elements - Metals, Minerals, Mining, Uses*. URL: http://geology.com/articles/rare-earth-elements/.

[5] European Commission. "Report on critical raw materials for the EU, Report of the Ad hoc Working Group on defining critical raw materials". In: May (2014), p. 41. URL: http://ec.europa.eu/enterprise/policies/raw-materials/files/docs/crm-report-on-critical-raw-materials%7B%5C_%7Den.pdf.

[6] K. Binnemans and P.T. Jones. "Perspectives for the recovery of rare earths from end-of-life fluorescent lamps". In: *Journal of Rare Earths* 32.3 (2014), pp. 195–200. ISSN: 10020721. DOI: 10.1016/S1002-0721(14)60051-X. URL: http://linkinghub.elsevier.com/retrieve/pii/S100207211460051X.

[7] Bart Van Den Bogaert et al. "Influence of irradiance on the photochemical reduction of europium(III)". In: (2016), pp. 4198–4204. DOI: 10.1039/c6gc00541a.

[8] Bart Van den Bogaert et al. "Photochemical recycling of europium from Eu/Y mixtures in red lamp phosphor waste streams". In: *Green Chemistry* 17.4 (2015), pp. 2180–2187. ISSN: 1463-9262. DOI: 10.1039/C4GC02140A. arXiv: {_}barataMaterialsandTechniquesofpolychromewoodensculpture. URL: http://xlink.rsc.org/?DOI=C4GC02140A.

[9] Bart Van Den Bogaert et al. "Photochemical recovery of europium from non-aqueous solutions". In: Iii (), pp. 1–15.

[10] Lio Van Meerbeeck. "Influence of Irradiance on the Photochemical Separation of Europium / Yttrium Mixtures". In: (2015), p. 93.

[11] Daphné Havaux. "Photochemical Recovery of Europium from Rare Earth Mixtures". PhD thesis. KU Leuven, 2014, p. 150.

[12] Lore Gheeraert. “Photochemical Recovery of Europium from Rare Earth Mixtures in Organic Solutions”. In: (2016), p. 128.

[13] Vincent Van Puyvelde. “A new chemical platform for light-assisted recycling of YOX lamp phosphor”. PhD thesis. KU Leuven, 2016, p. 92.

[14] B Van Gosen et al. “The Rare-Earth Elements , Vital to Modern Technologies and Lifestyles”. In: *U.S. Geological Survey Fact Sheet 2014-3078* (2014), p. 4. DOI: http://dx.doi.org/10.3133/fs20143078. URL: http://dx.doi.org/10.3133/fs20143078.

[15] K. Binnemans et al. “Rare-earth economics: The balance problem”. In: *Jom* 65.7 (2013), pp. 846–848. ISSN: 10474838. DOI: 10.1007/s11837-013-0639-7.

[16] Simon Cotton. *Lanthanide and Actinide Chemistry*. West Sussex: Wiley, 2005, p. 301. ISBN: 9780470010082. DOI: 10.1002/0470010088.

[17] Abigail Walters and Paul Lusty. “Rare earth elements - Commodity Profile”. In: *British Geological Survey* November (2011), p. 54. URL: http://www.mineralsuk.com.

[18] Gordon B. Haxel, James B. Hedrick and Greta J. Orris. “Rare Earth Elements - Critical Resources for High Technology”. In: *U.S. Geological Survey Fact Sheet 087-02* (2002).

[19] ICICI Securities. *Rare earth elements: No longer rare...* URL: http://content.icicidirect.com/mailimages/RareEarth.htm.

[20] Doris Schüler et al. “Study on Rare Earths and Their Recycling”. In: *Öko-Institut eV , Abschlussbericht* 49.January (2011), pp. 30–40. URL: http://www.oeko.de/oekodoc/1112/2011-003-en.pdf.

[21] Koen Binnemans et al. “Recycling of rare earths: A critical review”. In: *Journal of Cleaner Production* 51 (2013), pp. 1–22. ISSN: 09596526. DOI: 10.1016/j.jclepro.2012.12.037. URL: http://dx.doi.org/10.1016/j.jclepro.2012.12.037.

[22] JAMES KANTER. *Europe’s Ban on Old-Style Bulbs Begins - The New York Times*. 2009. URL: http://www.nytimes.com/2009/09/01/business/energy-environment/01iht-bulb.html?%7B%5C_%7Dr=0.

[23] Osram. *LCA of a compact fluorescent lamp | OSRAM*. URL: http://www.osram.com/osram%7B%5C_%7Dcom/sustainability/environmental/product-lifecycle-management/lca-of-a-compact-fluorescent-lamp/index.jsp.

[24] EU. *3. How do fluorescent lamps work?* URL: http://ec.europa.eu/health/opinions/en/energy-saving-lamps/l-3/3-cfl-characteristics.htm.

[25] NEWMOA. *NEWMOA - Mercury Use in Lighting*. URL: http://www.newmoa.org/prevention/mercury/imerc/factsheets/lighting.cfm (visited on 05/08/2017).

[26] Yufeng Wu et al. “The recycling of rare earths from waste tricolor phosphors in fluorescent lamps: A review of processes and technologies”. In: *Resources, Conservation and Recycling* 88.100 (2014), pp. 21–31. ISSN: 18790658. DOI: 10.1016/j.resconrec.2014.04.007. URL: http://dx.doi.org/10.1016/j.resconrec.2014.04.007.

[27] Rhodia. “La Rochelle Process Reclamation and recycling of rare earths”. In: (). URL: http://www.solvay.com/en/binaries/Process-Saint-Fons-151777.pdf.

[28] Rhodia. “La Rochelle Process Reclamation and recycling of rare earths”. In: (). URL: http://www.solvay.com/en/binaries/Process-La-Rochelle-EN-151498.pdf.

[29] C.K. K. Gupta and N Krishnamurthy. *Extractive metallurgy of rare earths*. Vol. 37. 1. 1992, pp. 197–248. ISBN: 0-415-33340-7. DOI: 10.1179/imr.1992.37.1.197. URL: http://www.maneyonline.com/doi/abs/10.1179/imr.1992.37.1.197%7B%%7D5Cnhttp://www.tandfonline.com/doi/full/10.1179/imr.1992.37.1.197.

[30] Asian Metal. *Rare earth elements(REE): industrial technology, smelting process-Metalpedia*. URL: http://metalpedia.asianmetal.com/metal/rare%7B%5C_%7Dearth/extraction.shtml.

[31] T.L. Cottrell. “The Strengths of Chemical Bonds”. In: *S.W. Benson, J. Chem. Educ.* (1958). Ed. by B. deB. Darwent, A–21 to A–34.

[32] Glenn Elert. *Electromagnetic Spectrum - The Physics Hypertextbook*. 2017. URL: http://physics.info/em-spectrum/ (visited on 05/06/2017).

[33] Wolf Vielstich. “Electrochemical energy conversion: methanol fuel cell as example”. In: *Journal of the Brazilian Chemical Society* 14.4 (Aug. 2003), pp. 503–509. ISSN: 0103-5053. DOI: 10.1590/S0103-50532003000400003. URL: http://www.scielo.br/scielo.php?script=sci%7B%5C_%7Darttext%7B%5C&%7Dpid=S0103-50532003000400003%7B%5C&%7Dlng=en%7B%5C&%7Dnrm=iso%7B%5C&%7Dtlng=en.

[34] Widicus Weaver Group. *Widicus Weaver Research Group - Methanol Photolysis Reaction Dynamics*. 2016. URL: http://chemistry.emory.edu/faculty/widicusweaver/photolysis.html.

[35] Douglas G. Brookings. “Eh-pH diagrams for the rare earth elements at 25C and one bar pressure”. In: *Geochemical Journal* 17 (1983), pp. 223–229.

[36] M Enis Leblebici, Georgios D Stefanidis, and Tom Van Gerven. “Chemical Engineering and Processing : Process Intensification Comparison of photocatalytic space-time yields of 12 reactor designs for wastewater treatment”. In: *Chemical Engineering & Processing: Process Intensification* 97 (2015), pp. 106–111. ISSN: 0255-2701. DOI: 10.1016/j.cep.2015.09.009. URL: http://dx.doi.org/10.1016/j.cep.2015.09.009.

[37] M. Enis Leblebici et al. “Efficiency Vs. Productivity in Photoreactors, a Case Study on Photochemical Separation of Eu”. In: *Chemical Engineering Journal* (2016). ISSN: 13858947. DOI: 10.1016/j.cej.2016.10.112. URL: http://linkinghub.elsevier.com/retrieve/pii/S1385894716315224.

[38] M. Weber. “LIQUID-SOLID FLOW”. In: *A-to-Z Guide to Thermodynamics, Heat and Mass Transfer, and Fluids Engineering*. Begellhouse. DOI: 10.1615/AtoZ.l.liquid-solid_flow. URL: http://www.thermopedia.com/content/51/.

[39] MARIO CERDA CORTES. *Slurry conveying*. 2012. URL: https://www.slideshare.net/mariocerda/slurry-conveying (visited on 03/23/2017).

[40] Michael R. Poirier. “Minimum Velocity Required to Transport Solid Particles from the 2H-Evaporator to the Tank Farm”. Aiken. URL: http://sti.srs.gov/fulltext/tr2000263/tr2000263.html.

[41] Anthony Grzina; Aleks Roudnev; Kevin E. Burgess. “Surry Pumping Manual”. In: (2002), p. 67.

[42] *PFA Structure*. URL: https://upload.wikimedia.org/wikipedia/commons/thumb/9/91/PFA%7B%5C_%7DStructure.svg/200px-PFA%7B%5C_%7DStructure.svg.png.

[43] William Reusch. *UV-Visible Spectroscopy*. URL: https://www2.chemistry.msu.edu/faculty/reusch/virttxtjml/spectrpy/uv-vis/spectrum.htm.

[44] Jim Clark. *the Beer Lambert Law*. 2007. URL: http://www.chemguide.co.uk/analysis/uvvisible/beerlambert.html.

[45] H Sawai and L E Orgel. “Isotopomer”. In: *IUPAC Compendium of Chemical Terminology* 97.12 (1975), pp. 3532–3. ISSN: 0002-7863. DOI: 10.1351/goldbook.I03352. URL: http://goldbook.iupac.org/PDF/goldbook.pdf%7B%%7D5Cnhttp://goldbook.iupac.org/I03352.html%7B%%7D5Cnhttp://goldbook.iupac.org/I03352.html%7B%%7D5Cnhttp://www.ncbi.nlm.nih.gov/pubmed/1141584.

[46] Hannes Aiginger. “Historical development and principles of total reflection X-ray fluorescence analysis (TXRF)”. In: *Spectrochimica Acta Part B: Atomic Spectroscopy* 46.10 (1991), pp. 1313–1321. ISSN: 05848547. DOI: 10.1016/0584-8547(91)80180-B.

[47] Elements Ru, Lower Limits, and The Lld. “Lab Report XRF 426 S2 PICOFOX Total Reflection X-ray Fluorescence Spectroscopy - Working Principles”. In: *Spectroscopy* (2007).

[48] Bruker. “Introduction to X-ray Fluorescence Analysis (XRF)”. In: (2006), p. 62.

[49] NIST. *X-Ray Mass Attenuation Coefficients | NIST*. URL: https://www.nist.gov/pml/x-ray-mass-attenuation-coefficients.

[50] Bruker. *Bruker: S2 PICOFOX - Technical Details, TXRF Spectrometer for Trace Analysis*. URL: https://www.bruker.com/products/x-ray-diffraction-and-elemental-analysis/micro-xrf-and-txrf/s2-picofox/technical-details.html.

[51] Ocean Optics. *Cosine Correctors - Ocean Optics*. URL: http://oceanoptics.com/product/cosine-correctors/.

[52] M. Enis Leblebici et al. "Efficiency Vs. Productivity in Photoreactors, a Case Study on Photochemical Separation of Eu". In: *Chemical Engineering Journal* (2016). ISSN: 13858947. DOI: 10.1016/j.cej.2016.10.112. URL: http://linkinghub.elsevier.com/retrieve/pii/S1385894716315224.

[53] Edward Hoover. *Selected Differential System Examples from Lectures. - ppt download*. URL: http://slideplayer.com/slide/7626581/) (visited on 12/14/2016).

[54] Benjamin Dersoir and Jean-baptiste Salmon. "Clogging in micro-channels : from colloidal particle to clog Benjamin DERSOIR Intitulé de la thèse La physique du colmatage : de la particule colloïdale au bouchon ." In: (2015).

[55] B. Kosata M. Nic, J. Jirat. "ionic strength, I". In: *IUPAC Compendium of Chemical Terminology*. Ed. by A. D. McNaught Wilkinson and A. Oxford: Blackwell Scientific Publications. ISBN: 0-9678550-9-8. DOI: 10.1351/goldbook.I03180. URL: http://goldbook.iupac.org/I03180.html.

[56] Ingmar Persson. "Hydrated metal ions in aqueous solution: How regular are their structures?" In: *Pure and Applied Chemistry* 82.10 (2010), pp. 1901–1917. ISSN: 0033-4545. DOI: 10.1351/PAC-CON-09-10-22.

[57] Bernard Liengme. *Regression Analysis - Confidence Interval of the Line of Best Fit*. 2017. URL: http://people.stfx.ca/bliengme/exceltips/regressionanalysisconfidence2.htm (visited on 04/04/2017).

[58] Eun Sul Lee and Ronald E. Forthofer. "Strategies for Variance Estimation". In: *Analyzing Complex Servey Data* 22 (2006), pp. 22–39.

[59] E. Anticó et al. "Solvent extraction of yttrium from chloride media by di(2-ethylhexyl)phosphoric acid in kerosene. Speciation studies and gel formation". In: *Analytica Chimica Acta* 327.3 (1996), pp. 267–276. ISSN: 00032670. DOI: 10.1016/0003-2670(96)00103-1.

[60] W.H. Baldwin and C.E. Higgins. "Complexes of dibutyl phosphoric acid". In: *Journal of Inorganic and Nuclear Chemistry* 17.3-4 (1961), pp. 334–336. ISSN: 00221902. DOI: 10.1016/0022-1902(61)80159-0.

[61] Yasuhisa Kawamura. "Dibutyl Phosphate OECD SIDS". In: (1994).

[62] Wayne Genck. *Make The Most of Antisolvent Crystallization | Chemical Processing*. URL: http://www.chemicalprocessing.com/articles/2010/210/.

[63] LSU Macromolecular Studies Group. *Dielectric constant*. URL: http://macro.lsu.edu/HowTo/solvents/Dielectric%20Constant%20.htm.

[64] Ogbonnaya C. Okorafor. “Solubility and density isotherms for the sodium sulfate-water-methanol system”. In: *Journal of Chemical and Engineering Data* 44.3 (1999), pp. 488–490. ISSN: 00219568. DOI: 10.1021/je980243v.

[65] Atomistry. *Yttrium sulphate*. URL: http://yttrium.atomistry.com/yttrium%7B%5C_%7Dsulphate.html (visited on 04/19/2017).